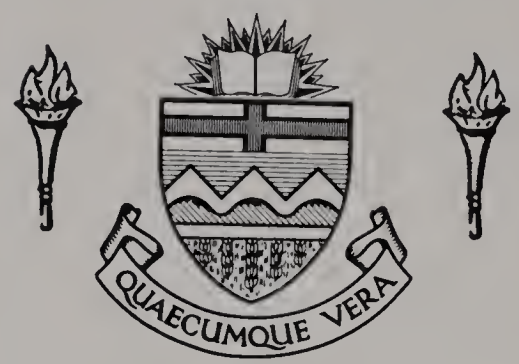

THE UNIVERSITY OF ALBERTA

RELEASE FORM

NAME OF AUTHOR Keith Donald McLeod

TITLE OF THESIS The Dynamics of the Motion of Optically Detectable Particles in Nerve Axons

DEGREE FOR WHICH THESIS WAS PRESENTED Master of Science

YEAR THIS DEGREE GRANTED 1980

THE UNIVERSITY OF ALBERTA

THE DYNAMICS OF THE MOTION OF OPTICALLY DETECTABLE PARTICLES IN NERVE AXONS

By

KEITH D. MCLEOD

A THESIS

SUBMITTED TO THE FACULTY OF GRADUATE STUDIES AND RESEARCH

IN PARTIAL FULFILMENT OF THE REQUIREMENTS FOR THE DEGREE

OF MASTER OF SCIENCE

DEPARTMENT OF ELECTRICAL ENGINEERING

EDMONTON, ALBERTA

FALL, 1980

THE UNIVERSITY OF ALBERTA

FACULTY OF GRADUATE STUDIES AND RESEARCH

The undersigned certify that they have read, and recommend to the Faculty of Graduate Studies and Research, for acceptance, a thesis entitled The Dynamics of the Motion of Optically Detectable Particles in Nerve Axons submitted by Keith Donald McLeod in partial fulfilment of the requirements for the degree of Master of Science.

ABSTRACT

Principles of discrete Fourier and spectral analysis have been applied to the motion of optically detectable particles in nerve axons. Particle positions recorded by means of cinemicrophotography were digitized from consecutive series of film frames. The trends in x and y position with time (whose values were the particle mean velocity components $\overline{Vx}$ and $\overline{Vy}$ respectively) were removed from the data and the remaining deviations Fourier analyzed. Power spectra obtained from these analyses indicated that the vast majority of the signal power in the deviations fell below .1 Hz., indicating that the filming rate (3 fps) had been sufficiently rapid to record all but the most minute details of particle motion. All power spectra contained a strong peak at low frequencies, and it was concluded that variations in the instantaneous velocities of the particles could be characterised as low frequency oscillations.

The trend-free measurements of particle x and y positions were processed with a band-limited differentiator to obtain estimates of the instantaneous velocity components. The characteristics of the differentiator and the means of implementing it were based on studies of simulated particle motion and on the power spectra of the motion of real particles.

Some of the errors inherent in the velocity estimation procedure were assessed by redigitizing the trajectory of a single particle several times. This approach yielded estimates of error in the velocity estimates which had a standard deviation of about .02 um/sec, or approximately one order of magnitude less than that of the finite difference method of estimating instantaneous velocity (as used by other workers).

One hundred seventy two particles tracked in ten axons were analyzed. The x component of velocity (longitudinal to the axon) was typically one to two orders of magnitude greater than that of the y component (radial to the axon). The estimates of the x component of instantaneous velocity were quantitatively examined, and inter-group comparisons made of a number of parameters of particle motion. The spatial characteristics of the velocity-position data were investigated with the use of the SURFACE II spatial analysis and display system. Contour plots of the x component of particle instantaneous velocity as a function of position were produced. Some correlation between particle locations and corresponding instantaneous velocities was apparent.

ACKNOWLEDGEMENTS

The author is indebted to Dr. Z.J. Koles of the Department of Electrical Engineering and Dr. R.S. Smith of the Department of Surgery for their guidance, encouragement, and assistance during the course of this work. The use of the facilities of the Neurophysiology Laboratory of the Department of Surgery was much appreciated, as was the financial assistance provided by the National Research Council of Canada, the Department of Electrical Engineering, and the Department of Biomedical Engineering and Applied Sciences.

Technical assistance provided by staff of the Department of Biomedical Engineering and Applied Sciences, in particular that of Mr. N. Ouellette and Mr. R. Labahn, is also gratefully acknowledged.

I would like to thank my parents for their continued efforts towards my education, and fellow student Paul Fisher for his friendship and support. In conclusion, I would like to express my deep appreciation to my wife Linda for her patience, encouragement, and understanding during the course of this work.

TABLE OF CONTENTS

LIST OF TABLES

LIST OF FIGURES

CHAPTER I

INTRODUCTION

Each neuron has a long cytoplasmic extension known as an axon (figure 1.1). The axon and nerve endings have essentially no means for protein synthesis, hence proteins necessary for the viability of the axon must be obtained from outside the axon (Lasek,1970). It has been shown that the neuron cell body synthesizes most of the axonal proteins, and that these are moved along the axon by a process known as axoplasmic transport (Lasek,1970; Ochs,1972; Grafstein,1975).

Normal axoplasmic transport is essential for maintenance of the axon; unusual or disturbed patterns of axoplasmic transport have been associated with a number of neurological disorders (Ochs,1975). If the motive mechanisms underlying normal axoplasmic transport could be understood, it is probable that this knowledge would contribute to treatment and possible prevention of these disorders. Researchers have proposed a number of models for the motive mechanism but to date little evidence supporting any of these has been presented (Schmitt,1969; Ochs,1971; Lasek,1970). Clearly, detailed quantitative analysis of the axoplasmic transport process is necessary to provide a basis for a model adequately reflecting the dynamics of particle motion.

To describe the direction of movement within the axon,

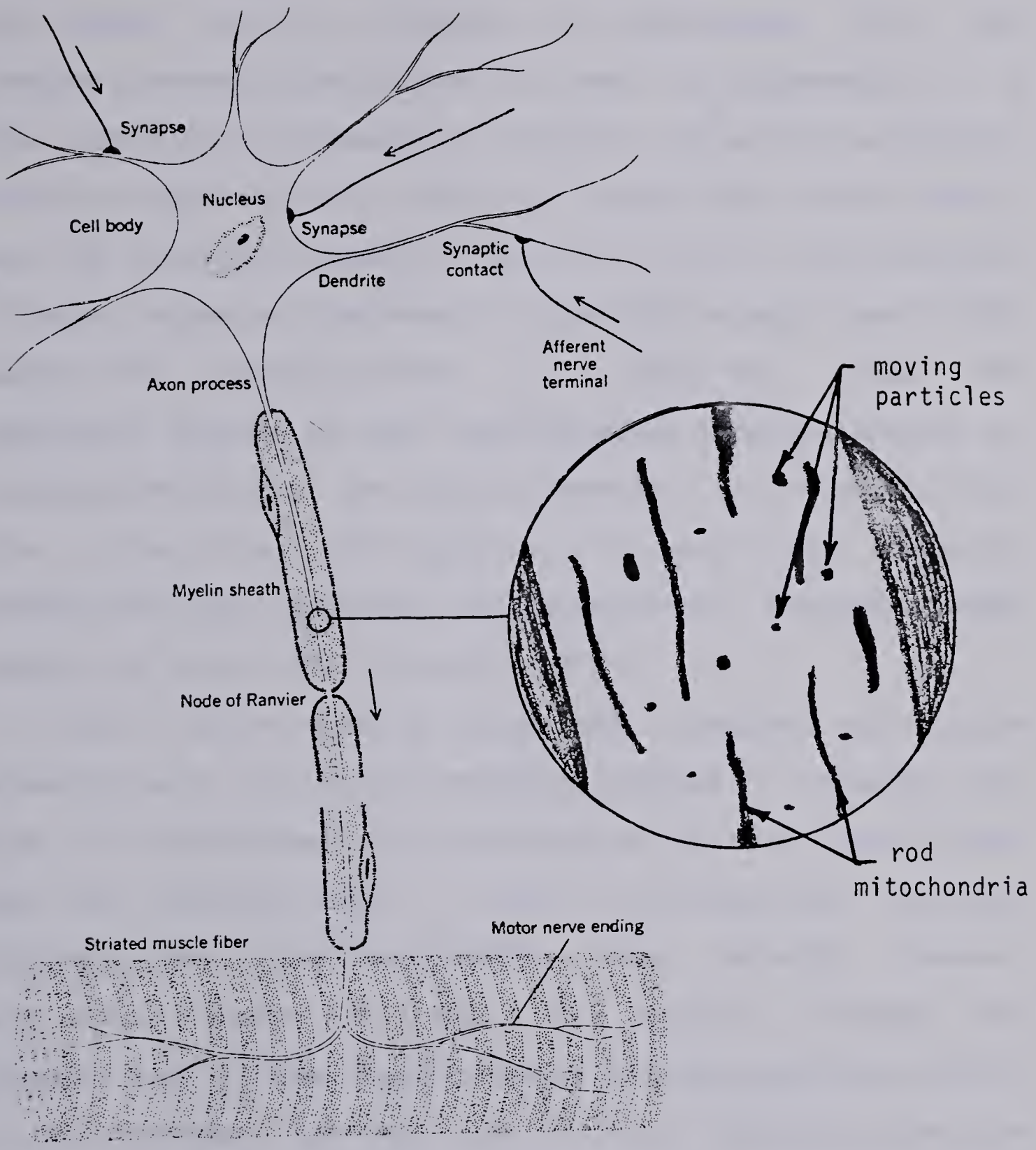

Figure 1.1 Nerve cell with some of its synaptic and neuromuscular contacts. Inset depicts microscopic view of axon. Adapted from Figure 1 of Nerve, Muscle, and Synapse (Katz,1966).

two terms shall be used: "somatopetal", which refers to motion towards the soma (cell body); and "somatofugal", which refers to motion away from the soma. Experimenters have shown, using a variety of techniques, that the transport process consists of at least two components: (1) a slow somatofugal movement of possibly the entire axoplasmic column at approximately 1 mm/day (Weiss and Hiscoe,1948), and (2) a rapid movement of materials within the axoplasmic column at rates of the order of 100-1000 mm/day (Lasek,1970; Heslop,1975; Schwartz,1979). In addition, these two components may be further distinguished from one another by the observation that the slow component is unidirectional (i.e. from the cell body out to, and along, the axon) whereas the fast component is bidirectional (Burdwood,1965; Cooper and Smith,1974; Schwartz,1979).

Until quite recently, axoplasmic transport was studied primarily with the use of indirect methods, including the rate of displacement of radioactive isotopes (Lasek,1968; Ochs and Johnson,1969) , and of cytochemical markers (Lubinska,1964; Dahlstrom,1967). These methods, however, have certain common limitations. For example, although net movement over a time frame of hours can be detected, details of the movement during much shorter intervals cannot be resolved. These methods lend themselves to the measurement of movement only in large numbers of neurons whose axons run together for an appreciable distance. They therefore do not provide data about transport in single axons.

Light microscopy of tissue-cultured neurons has revealed numerous intra-axonal particles moving both to and from the cell body (Matsumoto,1920; Hughes,1953; Pomerat et al.,1967). Although the particles moved at velocities comparable to rates of fast axoplasmic transport observed in adult neurons (Burdwood,1965), there has been some dispute as to whether conclusions concerning axoplasmic transport, reached from work on tissue-cultured neurons, can be applied to normal adult neurons (Weiss,1967). Quite recently however, rapidly moving particles with dimensions approximately that of the wavelength of light have been detected optically in living nerve fibres isolated from adult vertebrates (Smith, 1971,1972,1973; Kirkpatrick et al.,1972; Kirkpatrick and Stern,1973; Cooper and Smith,1974; Smith and Koles,1976; Hammond,1977; Forman et al.,1977a,b). These workers have shown that it is now possible to analyse the movements of optically detectable particles in adult neurons, and to relate these results to those obtained from tissue-cultured neurons, and to those results obtained from adult nerves using other techniques.

Work conducted by a number of reseachers suggests a correlation between the movement of membrane bounded bodies, among them the optically detectable organelles, and the rapid component of axoplasmic transport as determined indirectly with biochemical methods (Schwartz,1979). Assuming that such is the case, by observing and analyzing the movement of individual particles the dynamics of fast

axoplasmic transport may be be better understood.

Particle trajectories may be easily represented in the Cartesian co-ordinate system. The microscope's viewing plane can be described by the x and y co-ordinates, with the z co-ordinate in the plane perpendicular to it. Only movements in the x and y co-ordinates may be directly measured, as small movements in the z coordinate are not measureable by this method. Assuming a particle's continuous position in time; x(t),y(t); is known, the corresponding velocities Vx(t) and Vy(t) can be calculated from:

$$Vx(t) = \frac{d}{dt} x(t) \qquad Vy(t) = \frac{d}{dt} y(t) \tag{1.1}$$

The particle's radial component of velocity Vd(t) relative to its initial position is then given by:

$$Vd(t) = \frac{d}{dt} \{ \sqrt{(x(t)-x(0))^2+(y(t)-y(0))^2} \} \tag{1.2}$$

Since particle trajectories are commonly recorded on 16 mm film the position of a given particle is known only at discrete points in time (i.e. each frame). Common practice has been to orient the longitudinal axis of the axon such that on the film records it is parallel to the x coordinate axis of the position recording apparatus. The film may be viewed frame by frame, and the particle's successive x and y

positions recorded. The sampled trajectory (in two dimensions) is then represented as a series of numbers x(kT),y(kT) where k=0,1,2,..... N-1 (N is the number of readings and T is the sampling period). In other words, the particle's continuous position in time; x(t),y(t); becomes a discrete time series x(kT), y(kT), and is suitable for analysis.

Although this approach has been taken by a number of workers, the analytical techniques used to date have lacked sophistication. It has been common practice to calculate the mean velocity of a particle from the time series associated with its trajectory, according to the following:

$$V = \frac{\sqrt{\{x((N-1)T)-x((0)T)\}^2+\{y((N-1)T)-y((0)T)\}^2}}{(N-1)T} \qquad (1.3)$$

That is, the mean velocity of a particle over a given period of time is given by the total distance moved divided by the total elapsed time. Mean velocities have also been estimated from the slopes of linear regression lines calculated for particle trajectory distance-time data. Recently, some workers have attempted analysis of the small incremental movements of particles by calculating the particles' "instantaneous" velocity (Berlinrood et al.,1972; Cooper and Smith,1974; Breuer et al.,1975; Forman et al.,1975,1977a,b):

$$V((k+1)T) = \frac{\sqrt{\{x((k+1)T)-x(kT)\}^2+\{y((k+1)T)-y(kT)\}^2}}{T}$$

T=sampling period; k=0,1,2,..... N-1 (1.4)

That is, the instantaneous velocity was estimated from the distance which a particle moved between successive motion picture frames. The sign of V((k+1)T) was defined to be positive if there was a net movement between samples in the positive x direction. However, experience has shown that repeated tracking and analysis of the same particle trajectory using this method yields instantaneous velocity estimates which widely differ. Absent from the literature is any appreciation of such errors and the limitations inherent in the method.

Equation 1.4 is a first order approximation to an ideal differentiator. Two major problems are encountered in the use of this approximation which make it unsuitable for estimation of particle instantaneous velocities: (a) this approximation uses only the first two terms of an infinite series of terms describing an ideal differentiator, and is therefore quite inaccurate; and (b) this approximation is inordinately sensitive to random components in the particles' position-time data, and hence the more orderly and interesting components may be obscured. In view of the foregoing, it is suggested that the use of a more

appropriate approximation would yield more accurate and more consistent results, and could therefore shed far more light on the mechanisms of axoplasmic transport than currently exists. Improvement in the instantaneous velocity estimation technique could consist of the following procedures: (a) the use of spectral estimation techniques to examine the frequency components of particle motion; (b) the design of a more suitable approximation of an ideal differentiator, based on the results of (a); and (c) optimization of the technique through analysis of simulated and actual trajectories.

This thesis outlines the development of an improved technique for the estimation of particle instantaneous velocities through implementation of these ideas. The improved technique was used to estimate the instantaneous velocity of a number of somatofugally and somatopetally moving particles in amphibian axons. The results thus obtained were examined with a variety of methods, including correlation and regression analysis, and contour plotting, in an effort to identify patterns in particle movement.

CHAPTER II

FOURIER ANALYSIS

2.1 Introduction

Fourier analysis of a continuous function of time is a decomposition of the function, using the Fourier transform, into a sum of sinusoidal components. By using various properties of the Fourier transform, it is possible to estimate the power spectra of such functions and perform operations such as convolution.

The principles of Fourier analysis may be applied in a number of ways, depending on the nature of the function encountered. A function may describe a consistent, non-random mechanism which acts in an "orderly" manner. It is sometimes possible to derive a model, based on physical laws, which permits exact calculation of the value of the function at any instant in time. If exact calculation is possible, such a model is said to be deterministic. Principles of Fourier analysis may be used to filter and convolve such functions.

Alternatively, a function may act in an unpredictable manner, randomly varying. Nevertheless, it may be possible to derive a model which can be used to calculate the probability of a future value lying between two specified limits. Such a model is known as a stochastic model. The Fourier transform is a valuable tool in the estimation of the power spectra of such functions.

Most physically-occurring functions have both deterministic and random components, in varying proportions. The movement of particles in nerve axoplasm is such a case. The particles are moved by some orderly motive forces, and by random forces which result in a superimposed component to the motion. Random effects caused by microscope, camera, nerve, and projector movement, digitizer noise and observer error all probably contribute to the apparent random component observed in the movement of the particles. Therefore, complete analysis of the movement of particles in nerve axoplasm requires consideration of techniques of Fourier analysis used in spectral estimation, and in filtering (convolution).

2.2 The Fourier Transform

The Fourier transform $X(f)$ of a continuous function of time $x(t)$ is given by:

$$X(f) = \int_{-\infty}^{+\infty} x(t) e^{-j2\pi ft} \, dt \tag{2.1}$$

The inverse Fourier tranform of $X(f)$ is given by:

$$x(t) = \int_{-\infty}^{+\infty} X(f) e^{j2\pi ft} \, df \tag{2.2}$$

It is well known that the output $c(t)$, of a linear system whose impulse response is $h(t)$, to an input $x(t)$, is

given by:

$$c(t)=\int_{-\infty}^{+\infty} x(T)h(t-T)dT \tag{2.3}$$

This operation between x(t) and h(t) is termed convolution.

In the frequency domain, the Fourier transforms of c(t), x(t), and h(t) can be shown to be related by:

$$C(f)=X(f)H(f) \tag{2.4}$$

and the output in the time domain given by:

$$c(t)=\int_{-\infty}^{+\infty} X(f)H(f)e^{j2\pi ft}\,df \tag{2.5}$$

Hence, if a system frequency response H(f) is known, the output c(t) to any input x(t) may be calculated by Fourier transforming x(t), multiplying the result by H(f), and then inverse Fourier transforming the resultant product. Using this procedure it is possible to perform a variety of filtering tasks, including differentiation and low pass filtering.

2.3 The Discrete Fourier Transform and the FFT algorithm

2.3.1 Introduction

The movement of optically detectable particles in axons

is usually recorded on film by means of cinemicrophotography. The framing rate determines the number of "samples" of particle position taken in a given period of time and should be sufficiently rapid to sample the major characteristics of particle motion. The frame exposure period determines the length of time over which each sample is taken. It must be short enough to allow the recorded image to be considered representative of the particle's position at an instant in time. Trajectories are recorded by digitizing the x and y coordinate positions of particles over series of consecutive frames. The series of coordinate readings thus obtained are discrete rather than continuous functions of time, and are known as discrete-time signals.

In light of the foregoing, the Fourier analysis described in the previous section must be modified to accomodate the discrete nature of the data. The Discrete Fourier Transform (DFT) of a set of N numbers x(kT), k=0,1,2...N-1, is given by:

$$X(mF) = 1/N \sum_{k=0}^{N-1} x(kT) e^{-j2\pi mFkT} \qquad (2.6)$$

and the inverse transform :

$$x(kT) = \sum_{m=0}^{N-1} X(mF)e^{j2\pi mFkT} \qquad (2.7)$$

F=1/NT; T=sampling period

for k=0,1...N-1; m=0,1...N-1.

If equation (2.6) were evaluated in the obvious manner, N^2 complex multiplications and additions would be required. Although more efficient algorithms for evaluating the transform had been developed as early as 1942 (Danielson and Lanczos,1942), it was not until the now classic paper by Cooley and Tukey (Cooley and Tukey,1965) describing a computationally very efficient algorithm for evaluating the DFT, that the DFT has found widespread application. This algorithm has come to be known as the Fast Fourier Transform (FFT). For the very favourable situation when N is equal to an integer power of 2, the FFT algorithm requires only $N \text{ Log}_2 N$ operations. Obviously, computation time is considerably reduced with the result that the DFT (implemented via the FFT) has become one of the most important tools in the digital computer analysis of signals.

The FFT algorithm has been widely applied to: (1) the estimation of the power spectra of signals, and (2) the convolution of two signals, specific examples of which are auto and crosscorrelation. In both applications, however, two major problems associated with sampled discrete-time signals and the use of the DFT appear:

(1) If the sampling rate is not sufficiently high, high frequency components in the continuous signal will masquerade as low frequency ones in the sampled, discrete time series representation. This phenomenon is known as aliasing.

(2) In general, the data being analyzed is composed of arbitrary frequencies. However, the DFT only calculates the Fourier coefficients at integer multiples of 1/NT Hz. This gives rise to the problem known as the picket fence effect.

2.3.2 Aliasing

In the analysis of discrete time representations of continuous signals, aliasing describes the process by which high frequency components of a signal can be confounded with low frequencies if the sampling rate is not sufficiently high (fig. 2.1). The sampling theorem of Shannon (Shannon and Weaver,1963) states that a continuous bandlimited signal containing power from 0 to P Hz may be uniquely represented by discrete samples spaced at T second intervals if $1/2T \geq P$. That is, the sampling frequency (1/T Hz) must be equal to or greater than twice the highest frequency component in the original signal. 1/2T Hz is known as the folding frequency, since frequencies above this limit are folded (or aliased) into the frequency interval below the folding frequency.

In practice, it may be necessary to sample at a frequency below this desired minimum sampling rate. If the sampling rate is chosen such that the percentage of signal

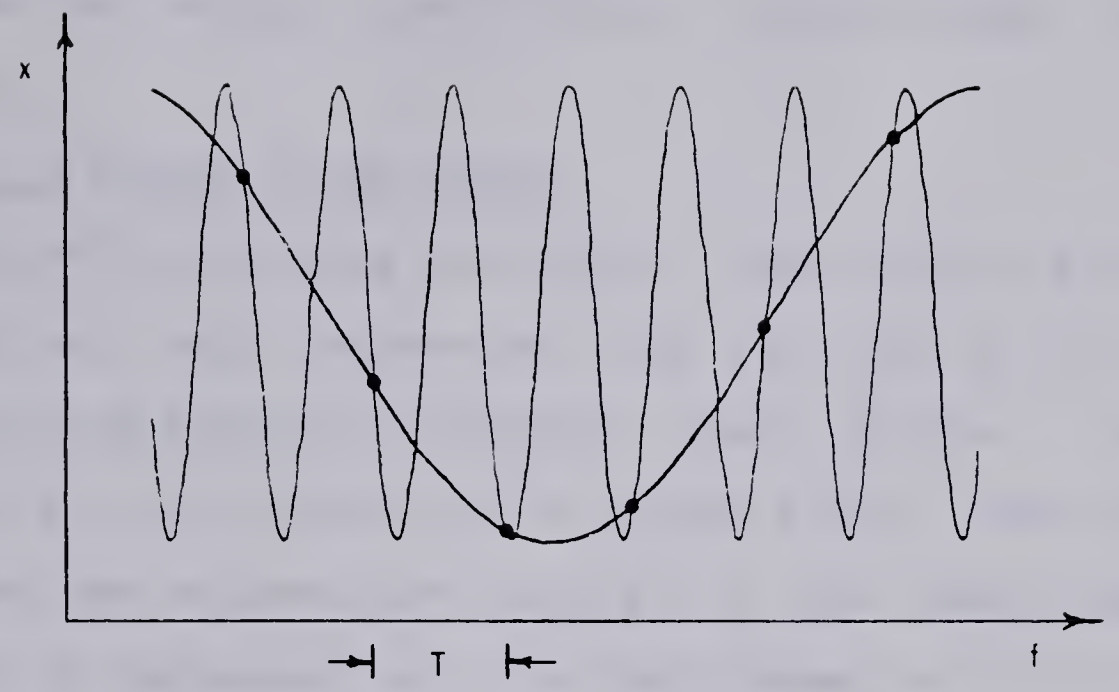

(a) Example of a sinusoid of frequency F_h Hz masquerading as one of lower frequency F_l Hz when the sampling frequency F_s (1/T Hz) has not been sufficiently rapid.

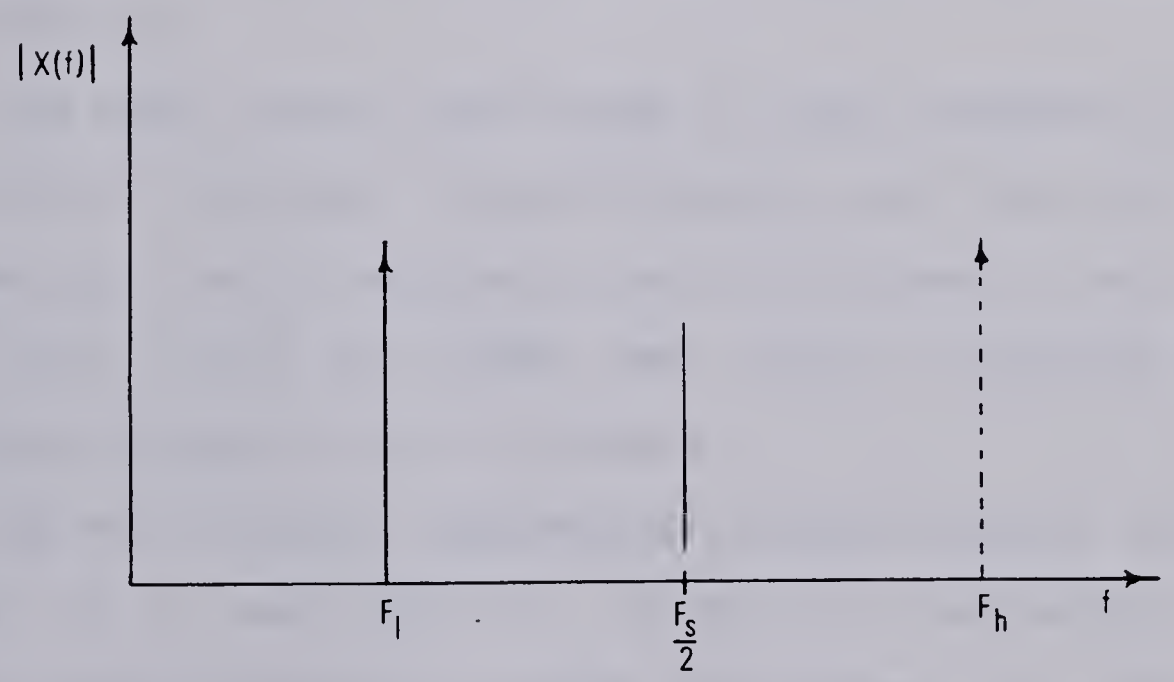

(b) As F_h is higher than the folding frequency ($F_s/2$), the power of the signal appears at F_l Hz , where $F_l = F_h - F_s$.

Figure 2.1 Aliasing

power lying above the folding frequency is sufficiently low, the error introduced by aliasing will be small. Alternatively, the continuous signal may be low pass filtered (in effect, artificially bandlimited) prior to sampling.

2.3.3 Picket fence effect

The DFT calculates the Fourier coefficients at discrete frequencies, each separated from the other by 1/NT Hz. At each discrete Fourier frequency there exists a spectral window, as is illustrated in figure 2.2(a). (Note that the sidelobes are omitted for clarity.) If the transformed data consists of components at only the integer multiples of 1/NT Hz, no error will occur. If, however, components exist at frequencies which are not confined to these discrete frequencies, the so-called picket fence effect requires consideration.

The worst error occurs when a signal component falls at the midpoint between two coefficients, and the signal power as seen by the two adjacent spectral windows is only .406 of its true value. The effect then is one of viewing the true spectrum through a set of pickets.

By artificially lengthening the data record with zero terms to a new length N', the DFT will calculate a set of Fourier coefficients at integer multiples of 1/N'T lying between the integer multiples of 1/NT Hz. This procedure, known as "padding" the data record, does not affect the width of the spectral window, which is dependent only on the

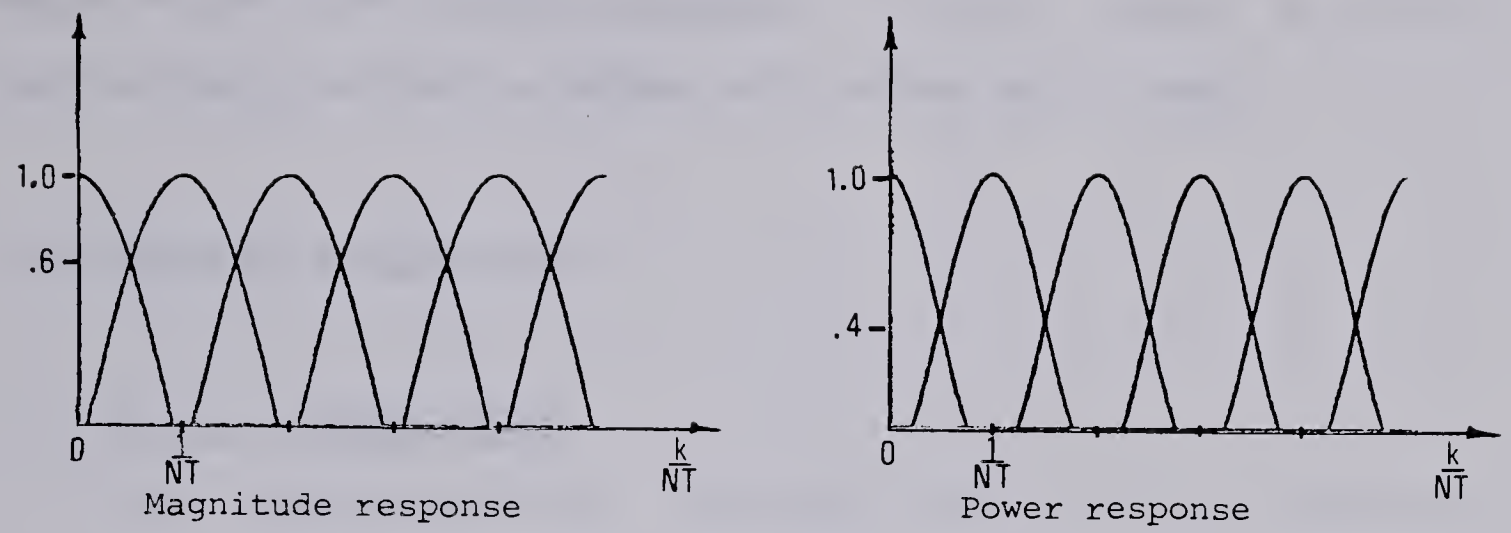

(a) Picket fence effect

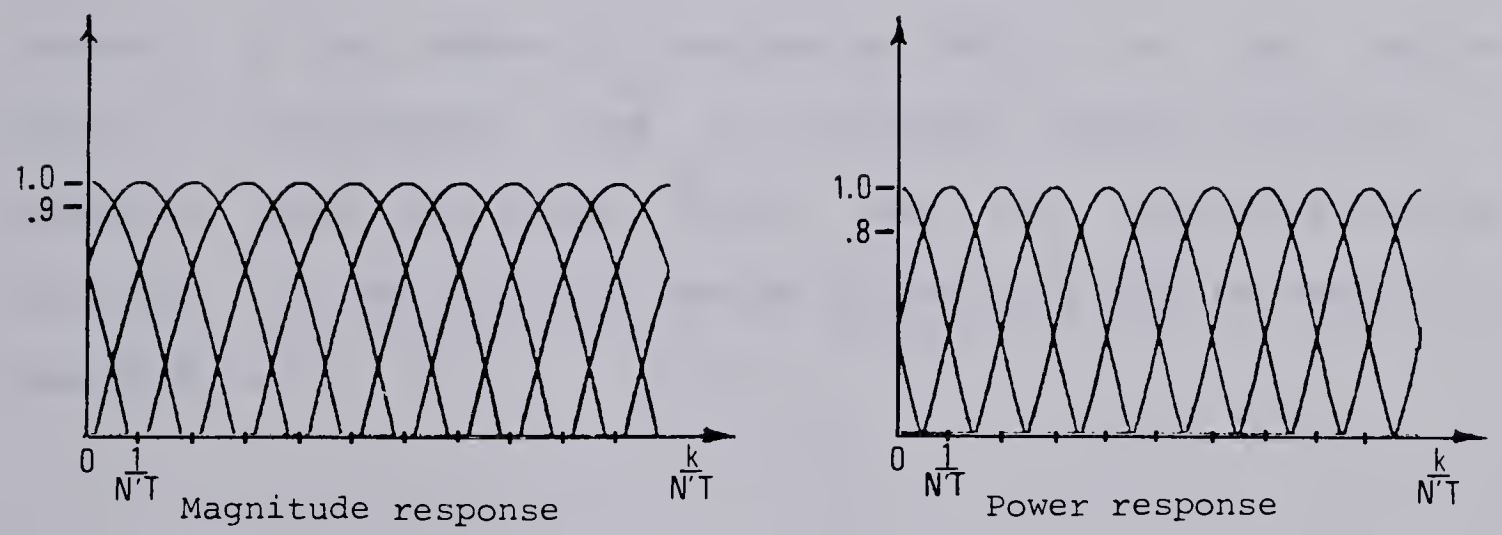

(b) Reduction of picket fence effect through computation of additional Fourier coefficients.

Figure 2.2 Picket fence effect

"true" length of the data. The result is considerably more overlap of adjacent windows. This is demonstrated in figure 2.2(b) for the case N'=2N. The consequences of the picket fence effect are further reduced in most cases by using non-rectangular data windows with wider main lobes.

2.4 Spectral estimation

2.4.1 Introduction

The autocorrelation function R(kT) of an infinite series x(nT) is defined as:

$$R(kT) = \lim_{L\to\infty} \frac{1}{2LT} \sum_{n=-L}^{+L} x(nT)x(nT+kT)$$

$$-L < k < +L \qquad (2.8)$$

where k is the number of samples by which the time series x(nT) is separated from its "lagged" version x(nT+kT). A commonly used estimator $\hat{R}(kT)$ for the autocorrelation function of an infinite series based on a finite sample of length N is:

$$\hat{R}(kT) = \frac{1}{N} \sum_{n=0}^{N-|k|-1} x(nT)x(nT+kT)$$

$$-N+1 \leq k \leq N-1 \qquad (2.9)$$

It is well known that the power spectral density S(mF) and autocorrelation function R(kT) are related by the DFT relation:

$$S(mF) = \sum_{k=-\infty}^{+\infty} R(kT)e^{-j2\pi mFkT}$$

$$-\infty < m < +\infty \qquad (2.10)$$

Logically a suitable estimator $\hat{S}(mF)$ for the power spectrum of an infinite process based on a finite sample of length N, is related to the autocorrelation function of the sample $\hat{R}(kT)$ by:

$$\hat{S}(mF) = \sum_{k=-N+1}^{N-1} \hat{R}(kT)e^{-j2\pi mFkT}$$

$$0 < m < N-1 \qquad (2.11)$$

If equation (2.9) is substituted into equation (2.11) the result may be written in terms of X(mF), the discrete Fourier coefficients of the time series x(kT) (ref. equation

(2.6)). The power spectrum estimate is then given by:

$$\hat{S}(mF) = (1/N)|X(mF)|^2 \qquad (2.12)$$

The advent of the FFT algorithm has brought this form of the estimator into widespread usage. $\hat{S}(mF)$, sometimes called the periodogram, indicates the distribution in frequency of the power present in the sample x(kT). Hence, the periodogram will elicit the presence of any strong periodic components. Care must be taken in the interpretation of the periodogram, however, as there are two problems associated with the use of $\hat{S}(mF)$ as a power spectrum estimator:

(1) The time series being analyzed is only a finite sample of a time series of theoretically infinite length. When the power spectrum of the infinite time series is estimated from this sample, the finite length of the sample leads to the problem known as leakage.

(2) $\hat{S}(mF)$ is an inconsistent estimator of the power spectrum of a random and infinite time series.

Suitable techniques may be employed to reduce the detrimental effects of each.

2.4.2 Leakage

For practical reasons, the power spectrum of a time

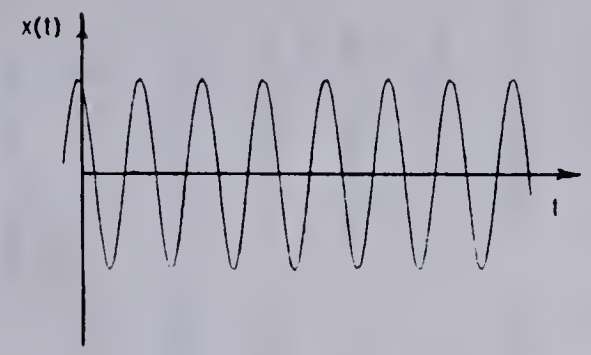

(a) Time series of infinite length

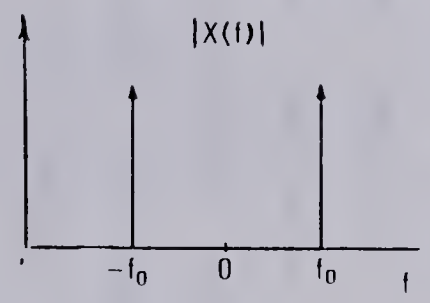

(b) Fourier transform of x(t)

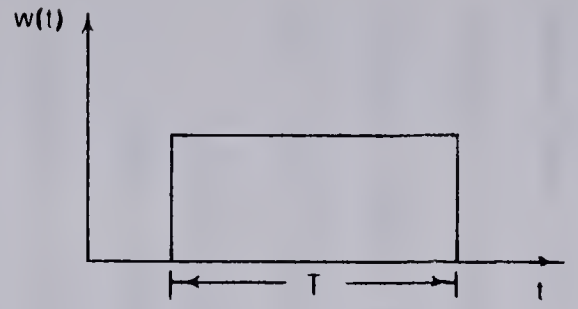

(c) Rectangular data window

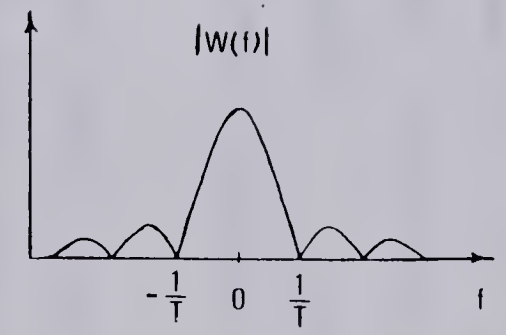

(d) Fourier transform of w(t)

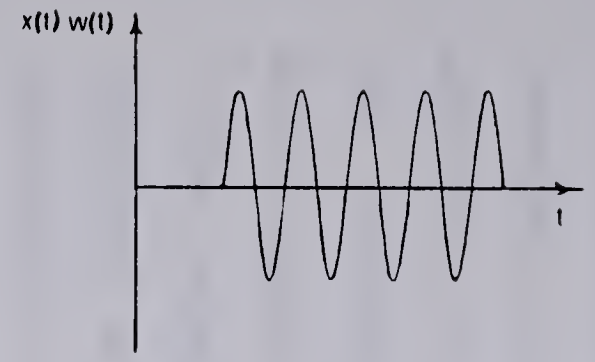

(e) Finite length sample of infinite length time series

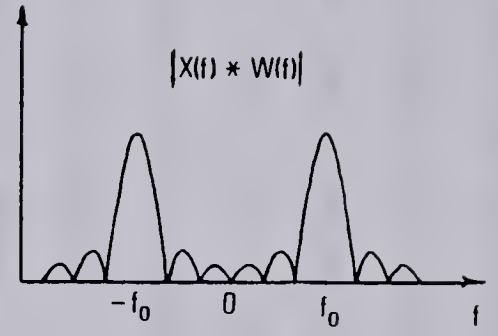

(f) Fourier transform of x(t)w(t)

Figure 2.3 Effect of finite length of data.

series of theoretically infinite length is estimated from a sample of finite length. In effect, the finite length sample is obtained by viewing the time series of infinite length through a rectangular data window of finite length and unit amplitude (fig. 2.3(e)). The continuous Fourier transform of the rectangular window has the form of $(\sin x)/x$. Multiplication in the time domain corresponds to convolution in the frequency domain (and vice versa); hence the Fourier transform of the finite length of data is equivalent to the transform of the infinite length of data convolved with the transform of the rectangular window (fig. 2.3(f)). Therefore, the calculated power at any frequency will be biased by leakage from adjacent frequencies. By using a data window other than the rectangular , it is possible to better localize the contribution of each frequency component.

2.4.3 Inconsistency

Two criteria are commonly used in the evaluation of an estimator: bias, and variance. Bias refers to the difference between the mean of a number of separate estimates of the value of a certain statistical parameter using the same estimator, and the expected value of the parameter. Variance refers to the mean squared deviation of the various estimates from the expected parameter value. An unbiased estimator is one whose bias approaches zero as the number of estimates increases; a consistent estimator is one whose variance approaches zero as the length of the data used by the estimator increases.

The bias and variance of spectral estimates obtained using equation (2.12) have been examined. It has been shown (Schwartz and Shaw,1975) that the mean of the distribution of estimates of the autocorrelation estimator $\hat{R}(kT)$ is related to R(kT) by:

$$E\{\hat{R}(kT)\} = (1-(|k|/N))R(kT) \tag{2.13}$$

where k is the lag number defined in equation (2.8).

By making the appropriate substitutions into equation 2.10, it can be shown that:

$$E\{\hat{S}(mF)\} = \sum_{k=-\infty}^{+\infty} R(kT)w(kT)e^{-j2\pi mFkT} \tag{2.14}$$

where w(kT) is defined as:

$$\begin{aligned} w(kT) &= 1-(|k|/N) \qquad |k| \leq N \\ w(kT) &= 0 \qquad\qquad\quad |k| > N \end{aligned} \tag{2.15}$$

It can be seen by comparing equations (2.9) and (2.14) that $E\{\hat{S}(mF)\}$ differs from S(mF) by the factor w(kT). Therefore, the periodogram is a biased estimator of the power spectrum. The term w(kT) is known as a window function and results from the use of data of less than infinite duration. However, as N is increased the bias is reduced.

Unfortunately, the same cannot be said for the variance of the estimator.

If the data comes from a Gaussian process, it can be shown (Jenkins and Watts,1968) that

$$\lim_{N \to \infty} \text{var } \hat{S}(mF) \approx S^2(mF) \tag{2.16}$$

i.e. the variance of S(mF) approaches the square of the true spectrum at each frequency mF. Equation (2.16), which applies approximately to non-Gaussian data as well, implies that calculations using different sets of N samples from the same signal could yield radically different estimates of the true power spectrum, even for large N.

It can be shown that the variance of an estimate of the power spectrum using equation (2.12) using N data samples can be reduced by segmenting the data into shorter pieces and then averaging the periodograms calculated from the pieces (Welch,1967). An alternate method involves a smoothing operation, performed on the periodogram obtained from a single complete record (Schwartz and Shaw,1975).

2.5 Convolution

Since the multiplication of the Fourier transforms of two signals is equivalent to the Fourier transform of the convolution of the two signals, the process of convolution can be achieved by three Fourier transformations and a

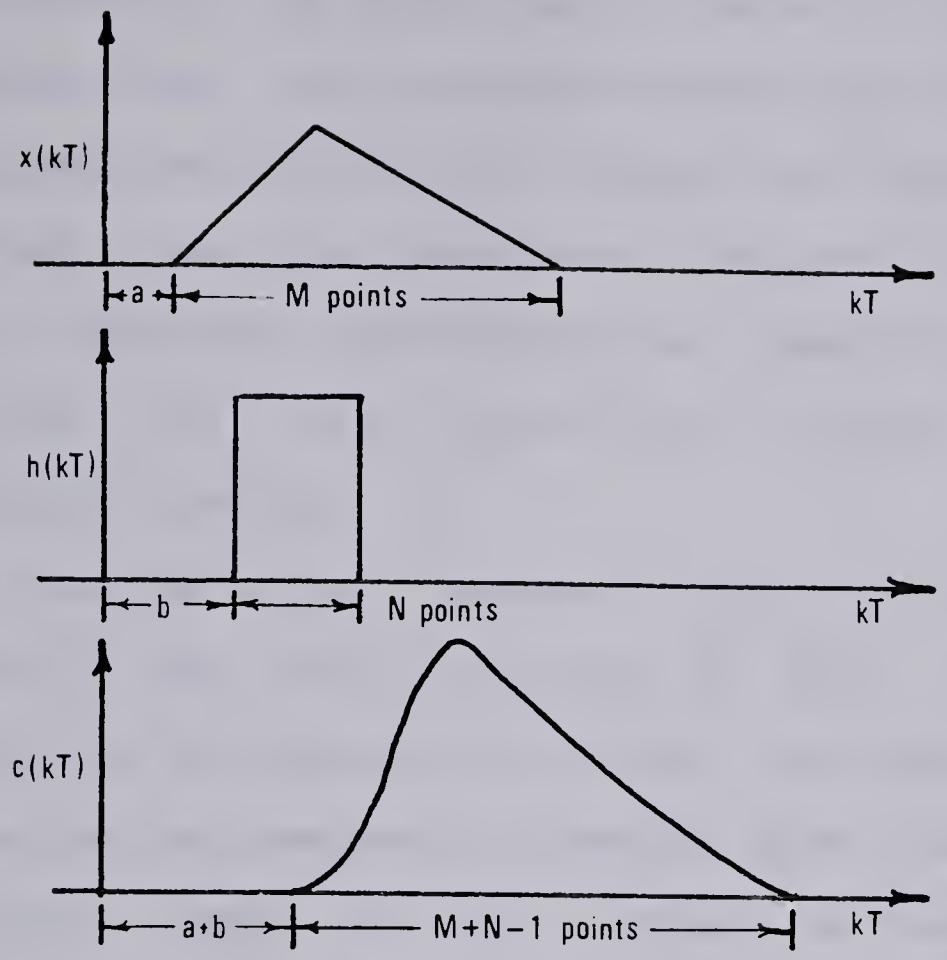

Figure 2.4(a) Aperiodic series x(kT) and h(kT), and their aperiodic convolution c(kT).

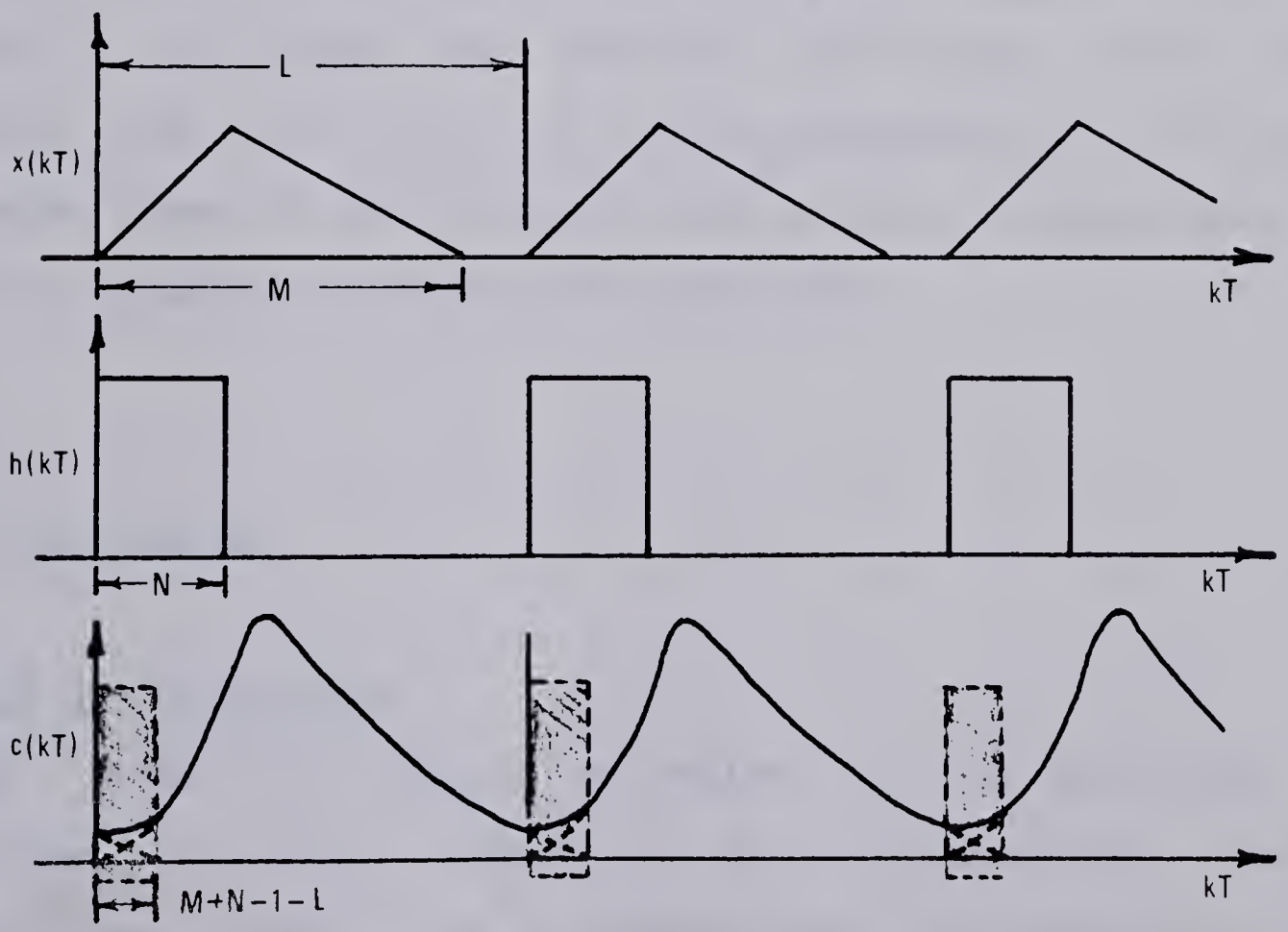

Figure 2.4(b) Periodic series x(kT) and h(kT), and their periodic convolution c(kT). Intervals of interference are shaded.

multiplication. For sufficiently large N it has been shown (Stockham,1966) that convolution achieved through frequency transformation with the FFT algorithm requires much less computing time than performing the convolution in the time domain. Therefore, evaluating the convolution integral by utilizing the FFT algorithm is known as the "fast convolution" method.

A problem arises, however, since the FFT applies to the DFT only, and multiplication of DFTs corresponds to convolution of periodic functions, not aperiodic ones. This problem may be overcome by padding both functions with a sufficient number of zero values to render the periodic convolution into an aperiodic one. If x(kT) is defined for $0 \leq k \leq M-1$ and h(kT) is defined for $0 \leq k \leq N-1$, then each of the functions must be padded out to a new length L, where $L \geq M+N-1$, to render the periodic convolution into an aperiodic one (fig. 2.4). It is also necessary for L to be an integer power of two to obtain the maximum computational expediency possible with the FFT algorithm.

2.6 Filter design

2.6.1 Introduction

In order to obtain estimates of the particles' velocities, it was necessary to differentiate the position-time data. As a conventional differentiation

process was expected to cause undue emphasis of the random high frequency components present in the time series representing particle trajectories, the need for low pass filtering was anticipated. The design of a bandlimited differentiator was therefore investigated.

As shown in equation (2.2), the inverse Fourier transform of X(f) is given by:

$$x(t) = \int_{-\infty}^{+\infty} X(f)\, e^{j2\pi ft}\, df$$

The derivative of x(t) is therefore given by:

$$\begin{aligned} \frac{d}{dt}\{ x(t) \} &= \frac{d}{dt} \int_{-\infty}^{+\infty} X(f)\, e^{j2\pi ft}\, df \,\} \\ &= \int_{-\infty}^{+\infty} X(f) \frac{d}{dt} \{ e^{j2\pi ft} \}\, df \\ &= \int_{-\infty}^{+\infty} (j2\pi f)\, X(f)\, e^{j2\pi ft}\, df \end{aligned} \qquad (2.17)$$

Thus it can be seen that differentiation with respect to time of a function of time x(t) may be performed in the frequency domain by multiplying its Fourier transform X(f) by the function H(f), where $H(f) = j2\pi f$, and then computing the inverse Fourier transform of the product. The expression for a bandlimited differentiator in the frequency domain is given by:

$$H(f) = j2\pi f \qquad |f| \leq Fcut$$
$$= 0 \qquad \text{otherwise} \qquad (2.18)$$

where Fcut is the filter cutoff frequency.

For a number of practical reasons ideal filters like the above can only be approximated. Methods such as frequency sampling, ripple equalization, and Fourier expansion and windowing have all been used (Childers and Durling,1975; Antoniou,1979). Each method uses a different criterion to define the "best" approximation to a given "ideal" filter. They all, however, lend themselves to application in either the time or the frequency domain, with identical results.

2.6.2 Filtering with fast convolution

Implicit in the principles of fast convolution is the periodicity of the functions being convolved, and hence the result of fast convolution is periodic, rather than aperiodic convolution. Unless both functions are of finite duration the condition $L \geq M+N-1$ discussed in Section 2.5 as being required to render the periodic convolution into an aperiodic equivalent, cannot be met for any L.

On initial examination it would appear that "ideal" filtering could be performed in the frequency domain. One need only specify the continuous frequency response of the desired filter, sample this response to obtain the Fourier

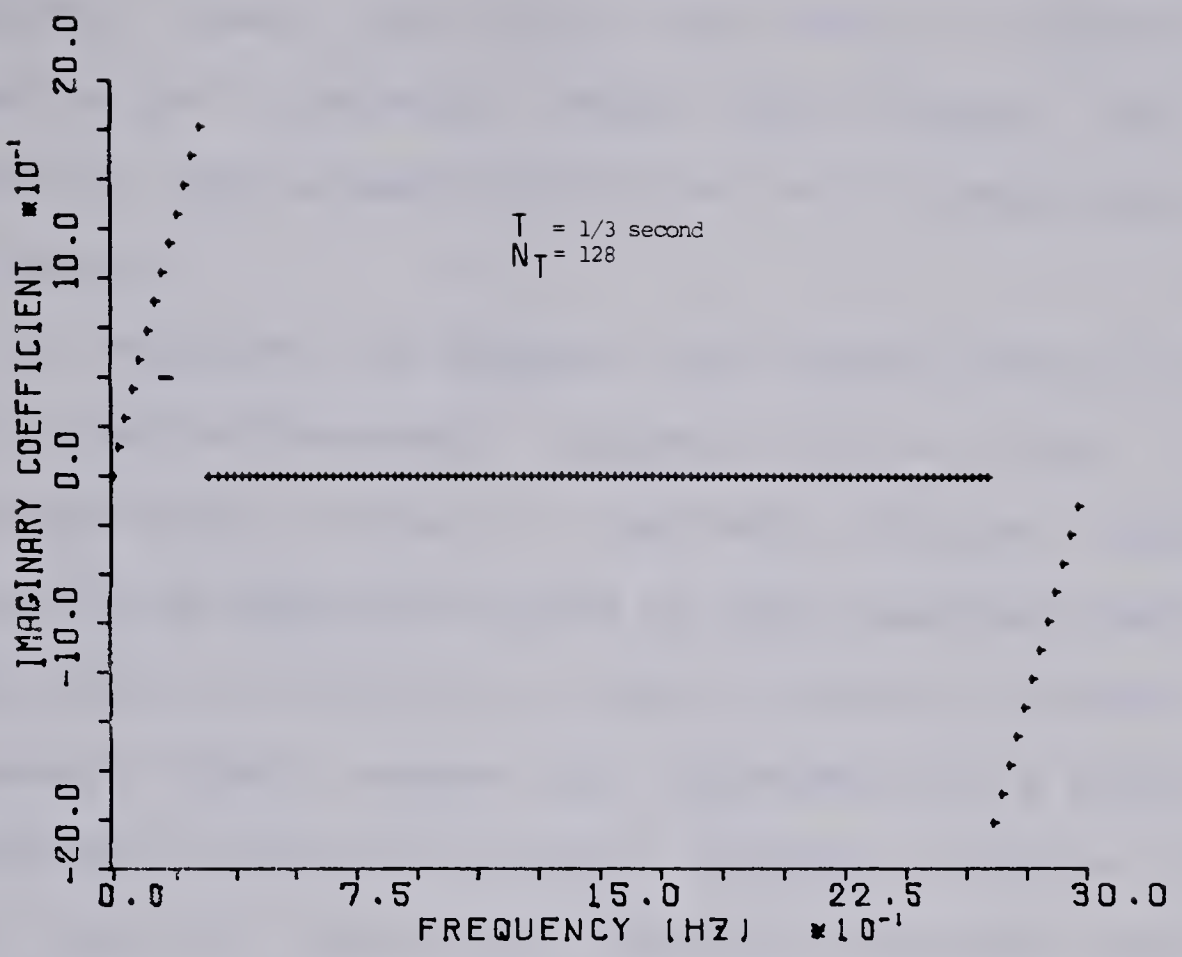

(a) Frequency domain coefficients of low pass differentiator

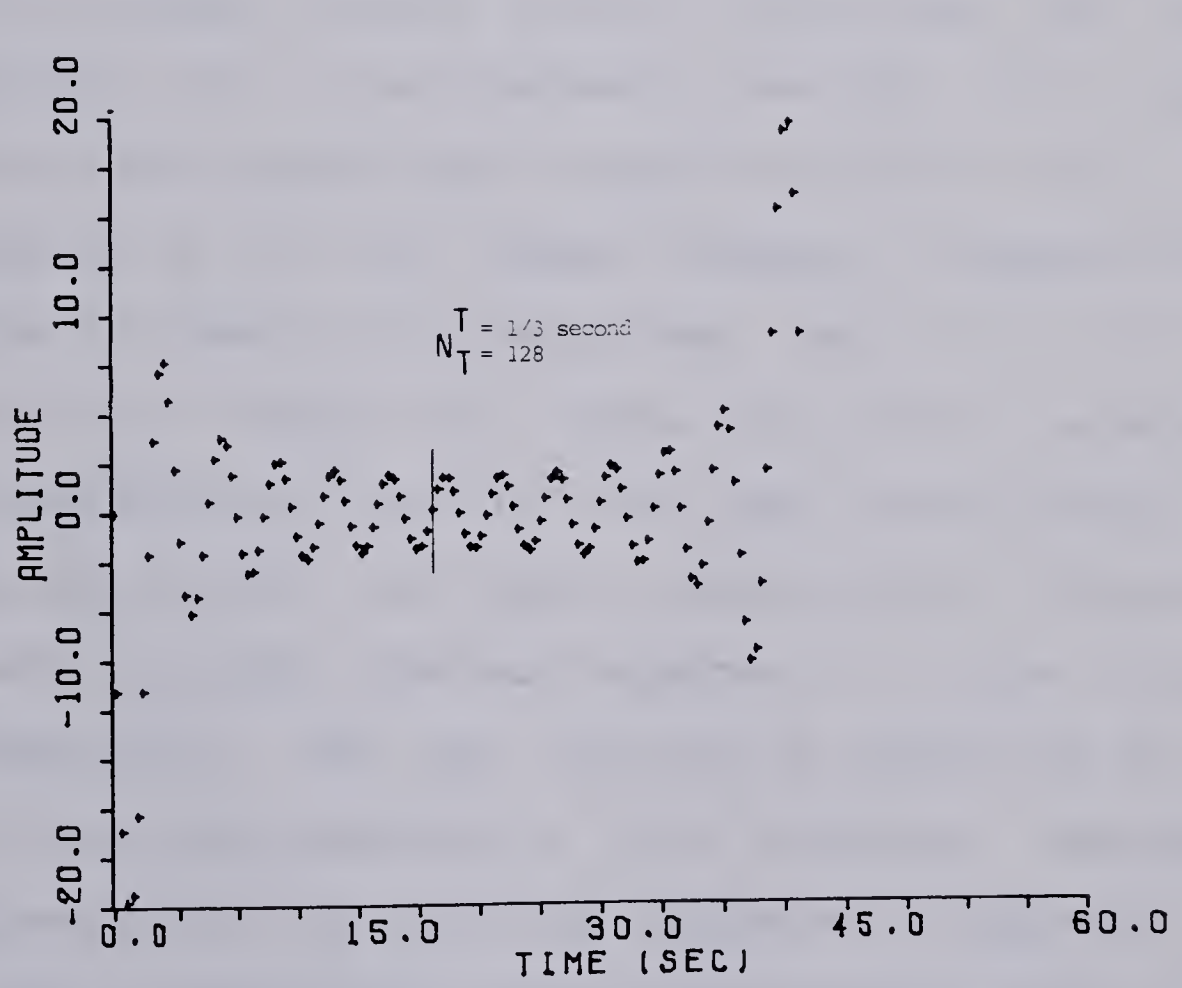

(b) Impulse response of filter specified in (a)

Figure 2.5

coefficients of the discrete version of the filter in the frequency domain, multiply the Fourier transform of the signal to be filtered by these coefficients, and inverse transform the product to obtain the filtered output in the time domain.

If, however, one computes the inverse Fourier transform of the sampled frequency response of an ideal low pass differentiating filter, a periodic impulse response is obtained. The periodic nature of this response results in an effect which is similar to the aliasing problem in the frequency domain caused by undersampling a signal in the time domain. The tails of each impulse response interfere with those of adjoining impulse responses due to their infinite length. Figure 2.5(a) illustrates the imaginary components of the frequency response of a low pass differentiator specified in equation (2.18) with a cutoff frequency of .3 Hz, whose frequency response has been sampled N_T times in the range from from 0 to 1/T Hz at intervals of $1/N_TT$ Hz. (Note that for the case of the differentiating filter all the real coefficients in the frequency domain are zero). Figure 2.5(b) illustrates the periodic sampled impulse response of this low pass differentiator, and was obtained by computing the inverse DFT of the N_T samples of the frequency response. The interference of the adjoining responses is apparent.

This interference can only be eliminated by truncating the impulse response of the filter (in effect, cutting off

the tails). Truncation, however, gives rise to Gibb's phenomenon, which manifests itself as a fixed percentage overshoot and ripple before and after any sudden transitions in the frequency response. In the case of the low pass differentiator, this occurs at the cutoff frequency, where the function H(f) abruptly goes from $H(f)=j2\pi f$ to $H(f)=0$.

Considerable efforts have been made by workers in the field to decrease the overshoot and ripple. It has been shown that "windowing" the truncated impulse response can significantly reduce the effect of Gibb's phenomenon (Kuo and Kaiser,1966; Helms,1968; Rabiner et al.,1970). The truncated and windowed impulse response can sometimes be made to yield an acceptable approximation to the "ideal" filter originally specified.

The shape of window used will obviously alter the filter characteristics. Selection of an appropriate window is usually based on consideration of the trade-offs inherent in minimizing the duration of the filter's impulse response, the ripple in the filter's frequency response, and the width of the region of filter response lying between passband and reject band known as the transition width. As windows are a major topic in Fourier analysis, their use was examined in some detail.

2.6.3 Window carpentry

The topic of window design has been widely explored in the literature (Childers and Durling,1975; Bloomfield,1976; Hamming,1977). The objective is usually to determine a time

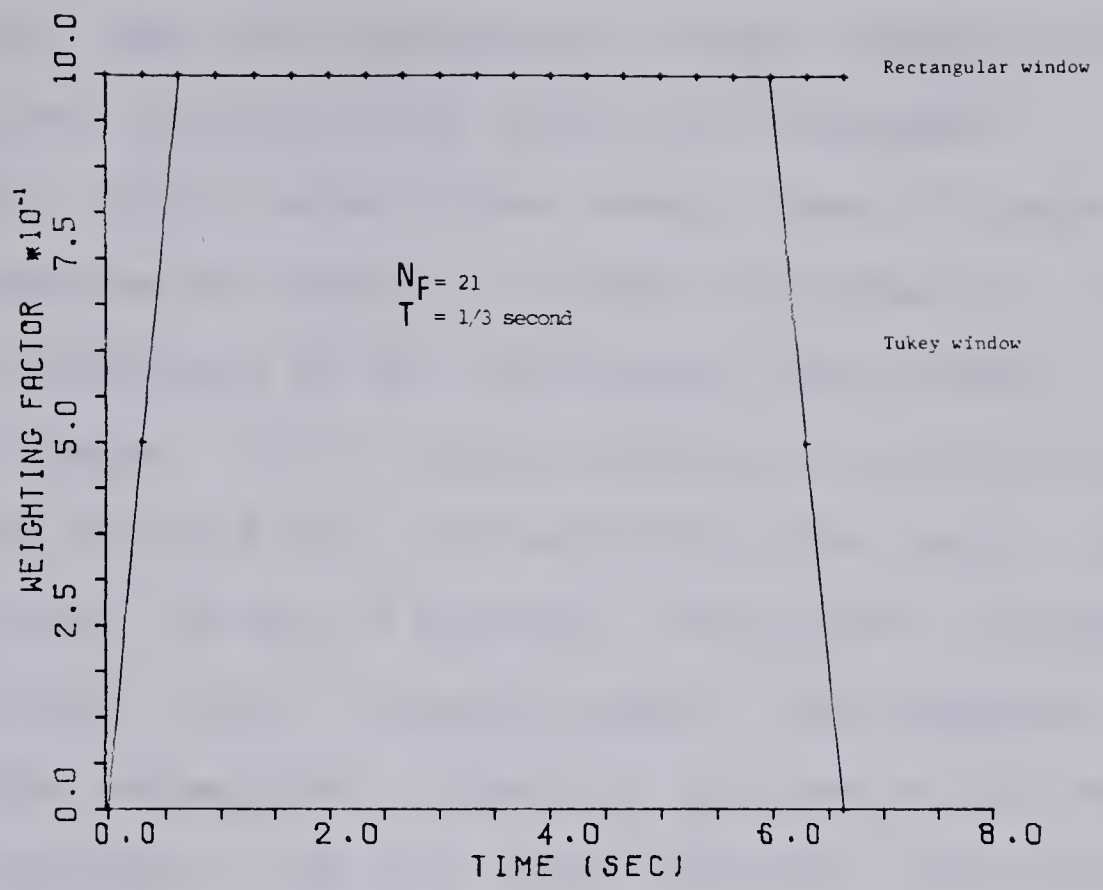

(a) Tukey and rectangular data windows

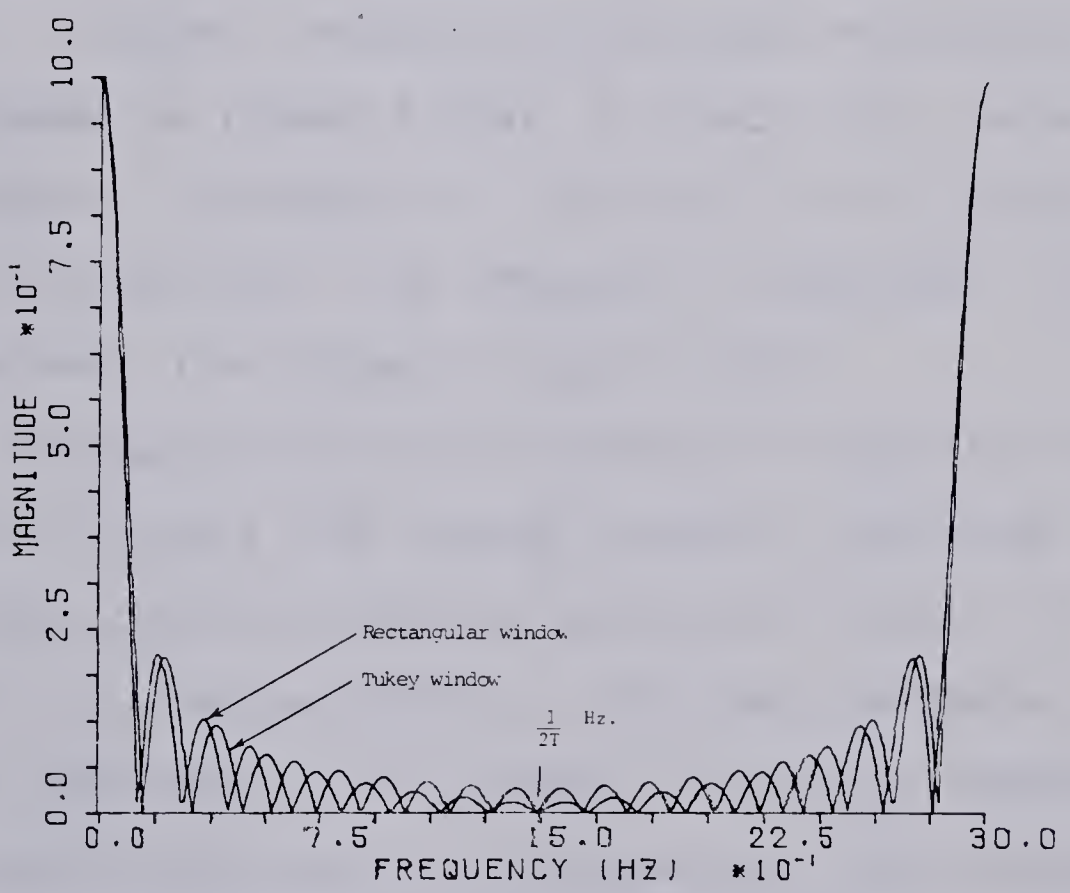

(b) Comparison of the frequency response of the Tukey and rectangular windows

Figure 2.6 The Tukey and rectangular data windows

domain window which has lower sidelobes in the frequency domain than does the rectangular window. Windows could be used at several points in the analytical procedure:

(1) The "Tukey" data window, among others, is often used in power spectrum estimation to reduce the effect of leakage through the sidelobes of the rectangular data window in the frequency domain. This window consists of a raised cosine shaped taper of the first and last 10% of the data, and a constant value of one in between. The smaller sidelobes of this data window in the frequency domain when compared with those of the rectangular window are obtained at the cost of a slight increase in the main lobe bandwidth. The continuous time functions of these two windows were each sampled N_F times at T second intervals to produce the discrete time functions shown in figure 2.6(a). It should be noted that the frequency responses of discrete time windows are continuous and periodic. The frequency responses of these two windows are illustrated in figure 2.6(b).

(2) A window can be used to modify the impulse response of a filter in the filter design process. The Kaiser window has been shown to have characteristics well suited to this application. By adjusting α, the shape parameter of the window, the sidelobes of the window's frequency response can be diminished at the cost of increased main lobe bandwidth.

2.6.4 Kaiser window

An ideal window would be one which, in the frequency domain, had a main lobe of negligible width, and sidelobes

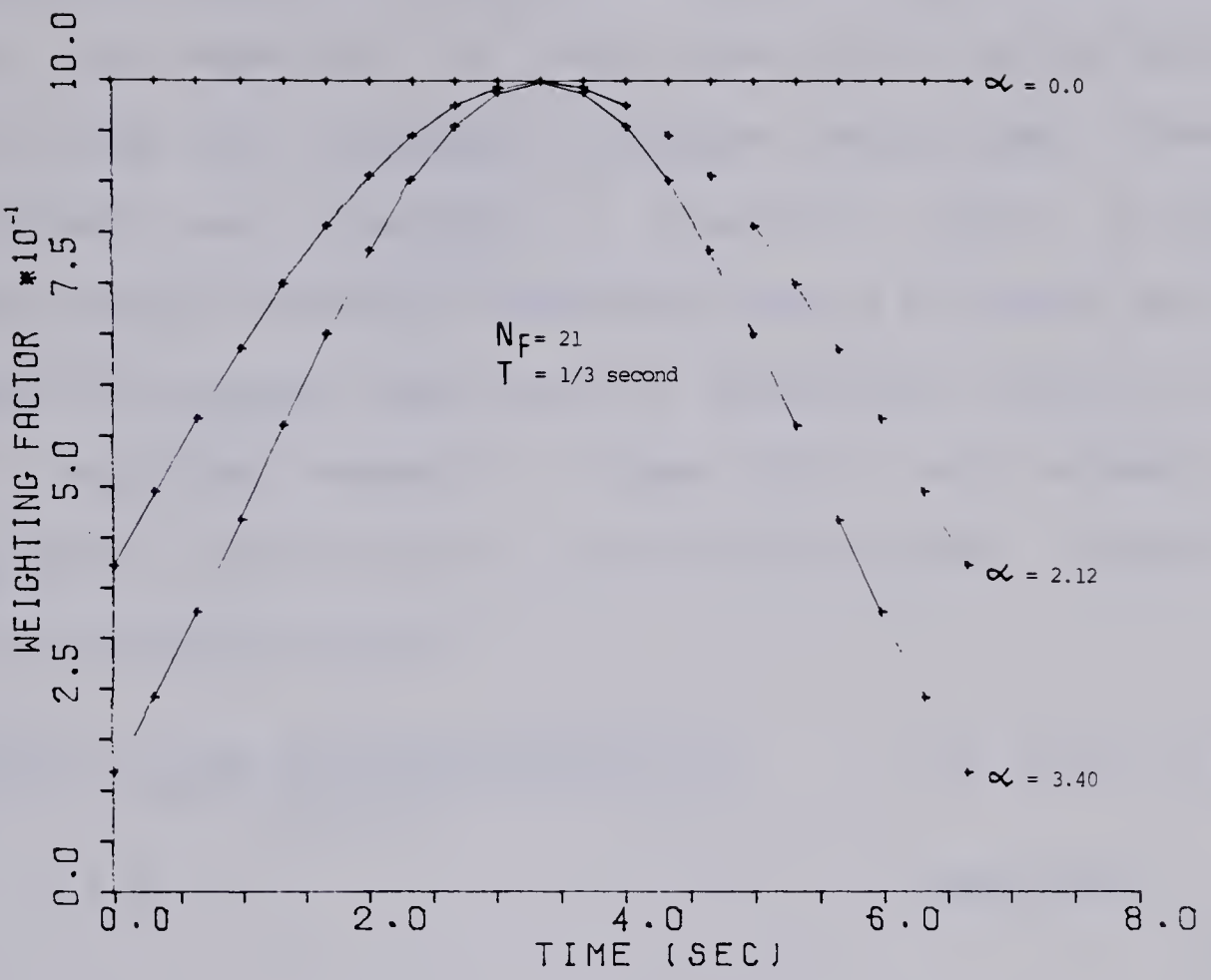

(a) The effect of the shape parameter on the Kaiser window

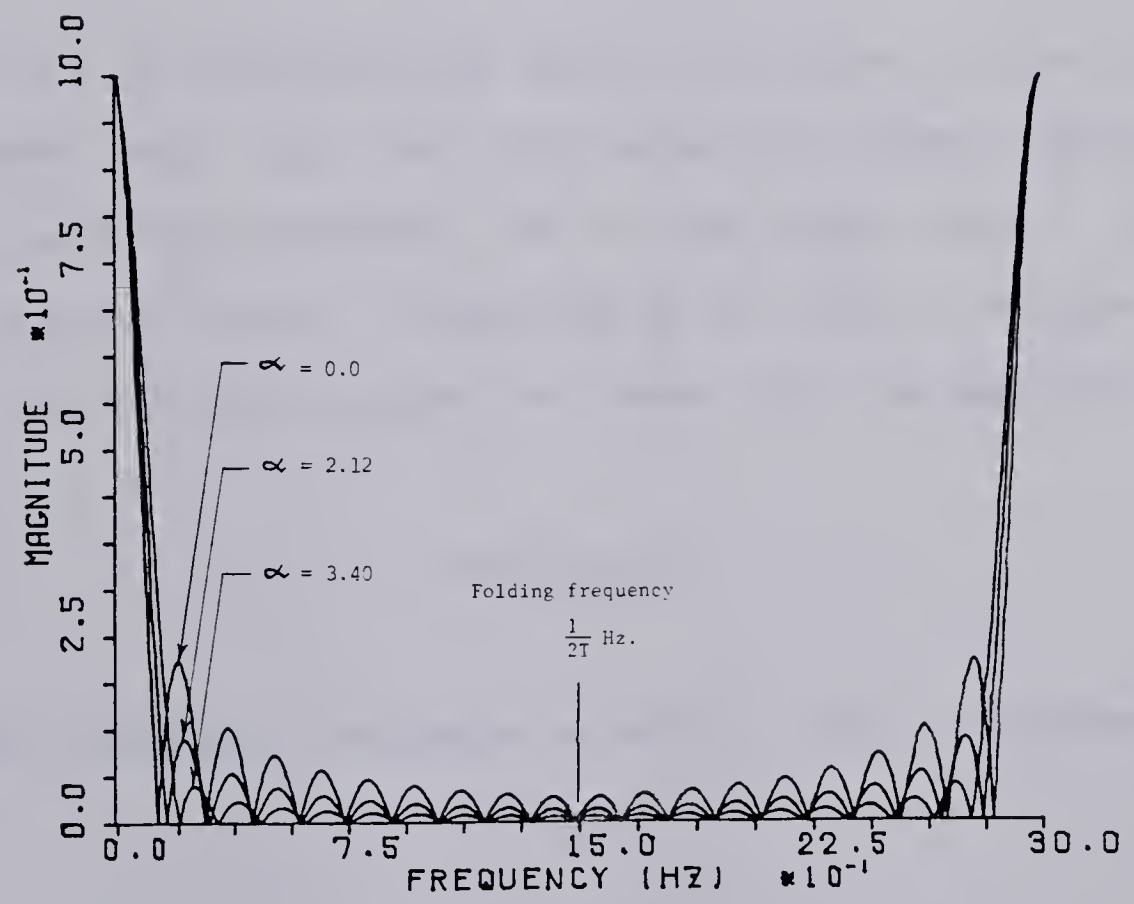

(b) The effect of the shape parameter on the frequency response of the Kaiser window

Figure 2.7 The Kaiser window

of negligible magnitude. In practice, this is impossible to achieve, as reduction of main lobe width can be obtained only at a cost of increased sidelobe magnitude. However, J.F. Kaiser has developed a flexible family of window functions whose frequency responses have a narrower mainlobe bandwidth for a given magnitude of sidelobes than any other window function presently known (Kuo and Kaiser,1966; Hamming,1977). This function, called the Kaiser window, is given in discrete form by:

$$w(kT) = \frac{I_o\{\alpha \sqrt{1-(2k/(N_F-1))^2}\}}{I_o\{\alpha\}} \qquad |k| \leq (N_F-1)/2$$

$$= 0 \qquad \text{otherwise} \qquad (2.19)$$

where I_o is the modified Bessel function of the first kind of order zero, N_F is the number of terms comprising the window, and the parameter α is the shape factor. The width of the Kaiser window is denoted by D, and is related to N_F and T, the period between the terms, by the equation:

$$D = (N_F-1)T \qquad (2.20)$$

The frequency response of w(kT), W(f), is given by:

$$W(f) = \frac{D \sinh\{\alpha\sqrt{1-(f/f_a)^2}\}}{I_o\{\alpha\}\sqrt{1-(f/f_a)^2}} \qquad f < f_a$$

$$= \frac{D \sin\{\alpha\sqrt{(f/f_a)^2-1}\}}{I_o\{\alpha\}\sqrt{(f/f_a)^2-1}} \qquad f > f_a$$

$$= \frac{D}{I_o\{\alpha\}} \qquad f = f_a$$

(2.21)

where

$$f_a = \alpha/\pi D.$$

(2.22)

The effect of varying the shape parameter on a Kaiser window of width D seconds sampled N_F times at intervals of T seconds, and on its frequency response may be seen in figure 2.7.

2.7 Digital filter design

Several parameters are usually important in the design of digital filters using the Kaiser window: D, the duration of the filter's impulse response; Δf, the transition width between the reject and pass band in the filter's frequency response; and δ, the magnitude of the maximum ripple in the filter's frequency response normalized to the maximum magnitude of the response. The three parameters are not

independent, making it necessary to specify only two of the three. The parameters are related by the following equation:

$$D = \frac{2(A-7.95)T}{28.72\Delta f} \qquad (2.23)$$

where A is known as the attenuation factor, and gives the magnitude of the maximum response in the filter's frequency response relative to that of the maximum ripple, in units of dB. A is related to δ by:

$$A = -20 \log (\delta) \qquad (2.24)$$

A formula has been empirically determined by Kaiser (Kaiser,1974;Hamming,1977) relating the window shape parameter α to the attenuation factor A.

$$\begin{aligned} \alpha &= .1102(A-8.7) && A>50 \\ &= .5842(A-21)^{.4} + .07886(A-21) && 21<A\leq 50 \\ &= 0 && A\leq 21 \end{aligned} \qquad (2.25)$$

These equations may be used in conjunction with the Fourier Transform and the Kaiser window to perform filter design. The method may be easily implemented on a digital computer, and despite its computational simplicity, the resultant nonrecursive filter compares very favourably with filters designed with much more involved calculations, such as the least squares, Chebyshev, and other methods (Kuo and Kaiser,1966; Rabiner et al.,1970; Rabiner,1971).

Assume it is necessary to filter a time series consisting of M equally spaced data points sampled at T second intervals, utilizing fast convolution. Using the Kaiser window and the Discrete Fourier Transform as tools, a suitable filter would be designed as follows (refer to figure 2.8):

(a) two of the three filter characteristics- transition width Δf, maximum normalized ripple δ in the frequency response, and duration D of the impulse response- are specified. The third parameter is calculated from the other two, using equations 2.22 and 2.23. The window shape parameter α is calculated from the maximum ripple specification, using Eq. 2.24. D is constrained by the condition necessary to render the periodic convolution into an aperiodic equivalent that $D < (L-M)T$, where L is the number of points in the Fourier transform to be used in performing the filtering via fast convolution.

(b), the frequency response of the desired filter is specified over the range 0 Hz to 1/T Hz, and is sampled N_T times at intervals of $1/N_T T$ Hz, where N_T is the number of points in the Fourier transform to be used in the filter design process. If the impulse response of the resultant filter is to be limited to D seconds, it is suggested that $N_T \geq 16(D/T + 1)$ (Rabiner et al.,1970). This will reduce the error in estimating the filter impulse response h(kT) caused by the interference of adjacent tails of the periodic impulse response.

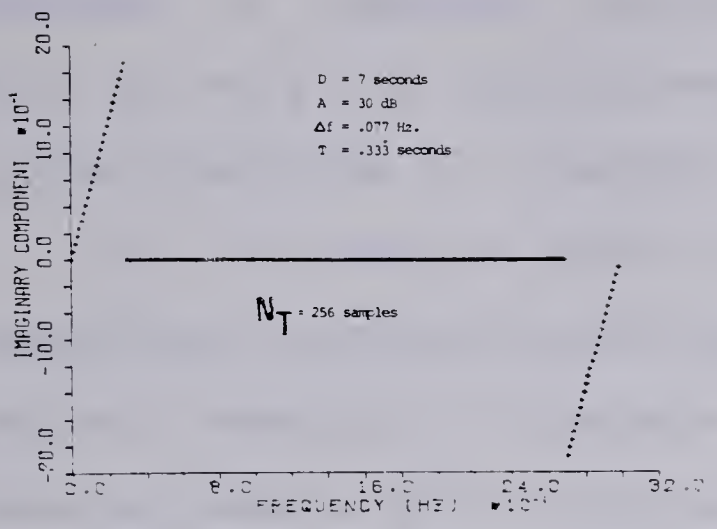

a Imaginary components of sampled frequency response.

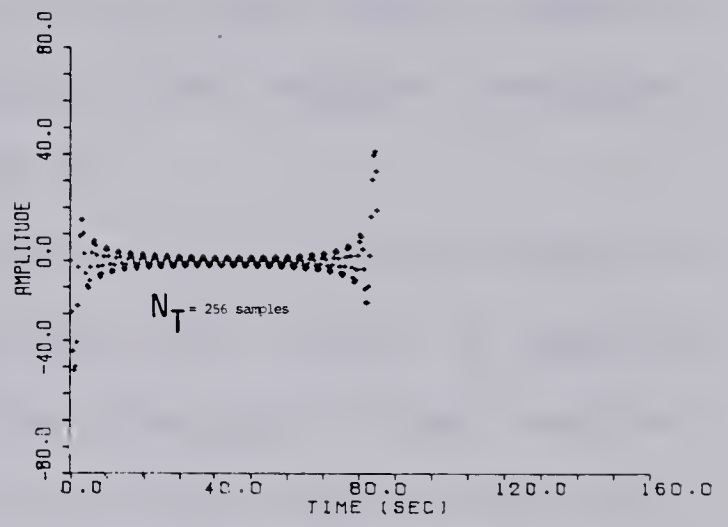

(b) Sampled impulse response after inverse DFT of sampled frequency response.

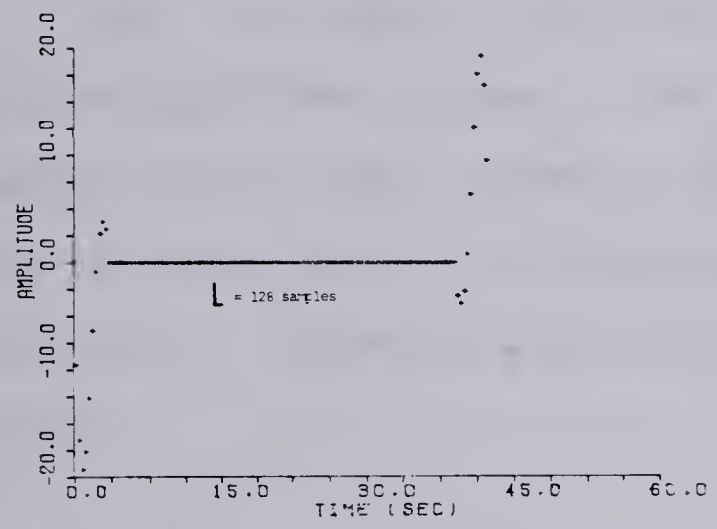

(c Sampled impulse response after truncation, Kaiser windowing, and padding to L samples.

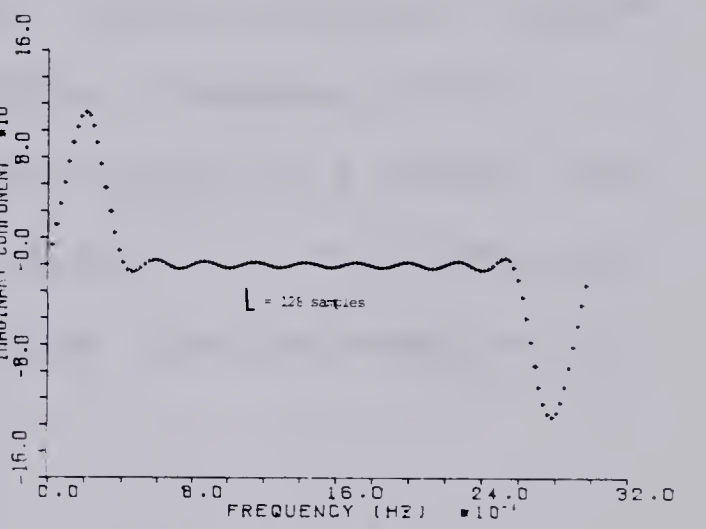

(d) Imaginary components of sampled frequency response.

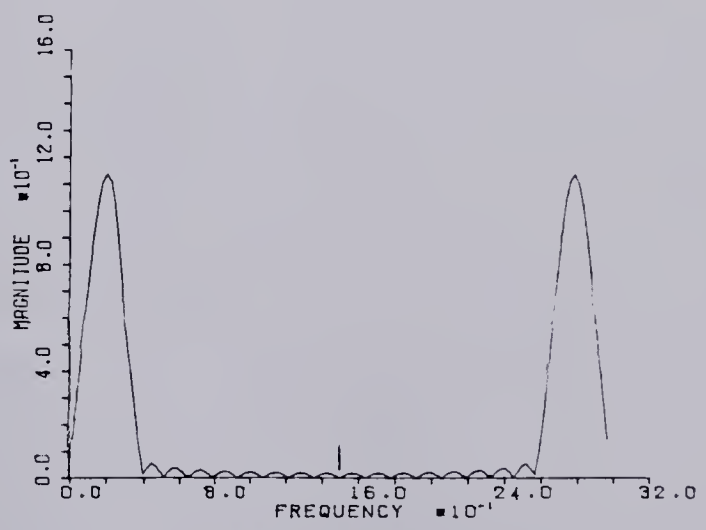

(e) Frequency response of designed filter.

Figure 2.8 Filter design

(c), the inverse DFT of the N_T samples of the frequency response is computed, resulting in the time domain samples h(kT) of the filter impulse response. The impulse response is then truncated to a duration of D.

(d), the samples w(kT) of the Kaiser window of width D seconds are calculated using equation 2.18, with a period between terms of T seconds. The truncated filter impulse response samples h(kT) computed in (c) are tapered with this window.

(e), the result is h'(kT), the sampled impulse response of the specified filter. The impulse response h'(kT) is padded with zero terms to a total length of L points, and the filtered output is then obtained by fast convolving the data of L points with the filter impulse response of L points.

CHAPTER III

FILTER DESIGN AND EVALUATION

3.1 Introduction

A band limited differentiating filter was designed using the windowed Fourier expansion method. Simulated particle trajectories were analyzed with this filter, and the results thus obtained compared with those obtained using a two term approximation to an ideal differentiator.

3.2 Design

D, the duration of the impulse response of the filter, was limited by the formula $D \leq (L-M)T$, the condition necessary to render the periodic convolution into an aperiodic equivalent. The longest trajectory data set consisted of 350 samples (T= 1/3 second); therefore M, the number of samples in the longest data set to be filtered, was conservatively chosen to be 400. L, the number of Fourier coefficients to be used in the fast convolution procedure, was limited by available memory space to 1024 terms, allowing a frequency resolution of about .003 Hz. As a result, D was limited to a maximum of 208 seconds (N_F=625). Therefore, an impulse response of up to 625 samples could be convolved with a data set of up to 400 samples, with no error introduced by cyclic convolution.

In the majority of applications, a filter with a relatively short impulse response is used to process a

signal of comparatively long duration. In this way the errors due to the so-called "end effects" appear in only a small percentage of the output. However, a reduction in the number of terms comprising the filter's impulse response results in a less accurate frequency response when compared with that of an ideal filter. Errors due to end effects were reduced by shortening the filter impulse response, at the expense of increasing the error of the filter frequency response. A filter with a impulse response of N_F terms will introduce end effect errors into N_F-1 terms of the output. Since the data being filtered in this application was of short length (34-350 readings), the filter used had an impulse response of much less than 625 terms. Since eighty-eight of the one hundred seventy-two trajectory data sets contained more than 100 data points, it was decided to design the filter such that end effects appeared in a maximum of 20 terms of the output. (Thus, end effects appeared in no more than 20% of the results obtained from each of eighty-eight trajectories). A filter with an impulse response of $\leq$ 21 terms was required.

The filter design procedures utilizing the Kaiser windowed Fourier expansion method were implemented in HP FORTRAN IV on a Hewlett Packard Model 2100A minicomputer. Available memory space limited the length of the Fourier transform used in the filter design procedures to a maximum of 2048 terms thus determining N_T. Rabiner's suggestion that N_T be chosen $\geq 16N_F$ to keep aliasing error in the design

procedure to an insignificant level (Rabiner et al., 1970), was therefore easily met in all cases. Filters composed of 21, 31, and 41 terms were designed. The remaining window parameters were calculated from equations (2.23), (2.24), and (2.25). Some possible combinations are shown below:

A(db)	N_F	Δf(Hz)	α
20	21	.042	0.0
20	31	.028	0.0
20	41	.021	0.0
30	21	.077	2.12
30	31	.051	2.12
30	41	.038	2.12
40	21	.112	3.4
40	31	.074	3.4
40	41	.056	3.4

Table 3.1

The nine filters specified in the preceding table were designed to perform band limited differentiation on data sampled at 3 Hz. The cutoff frequency was chosen to be .3 Hz, based on consideration of the signals' power spectra (ref. Section 5.3). The frequency responses of the filters specified in table 3.1 are plotted in figure 3.1. Note that although the frequency responses are periodic only the region of interest (i.e. from 0 to 1.5 Hz) has been plotted. The trade-offs among reduction of the transition width and ripple in the frequency response, and of the duration of the impulse reponse in the time domain, are apparent.

The "best" filter to use in the analysis of particle

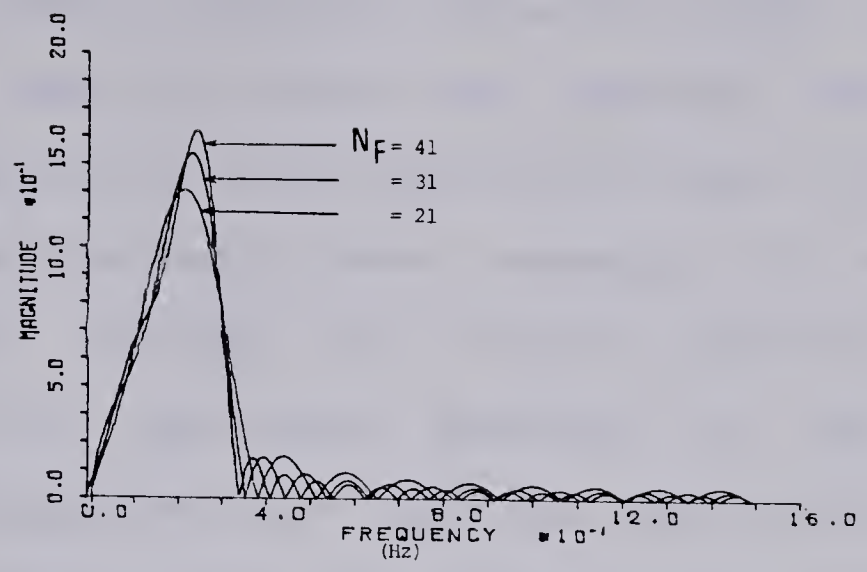

(a) A= 20 dB.

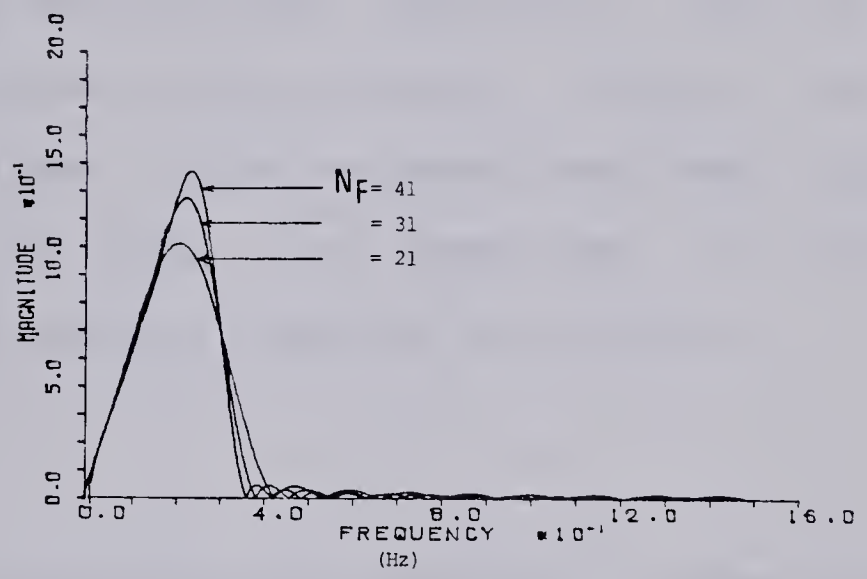

(b) A= 30 dB.

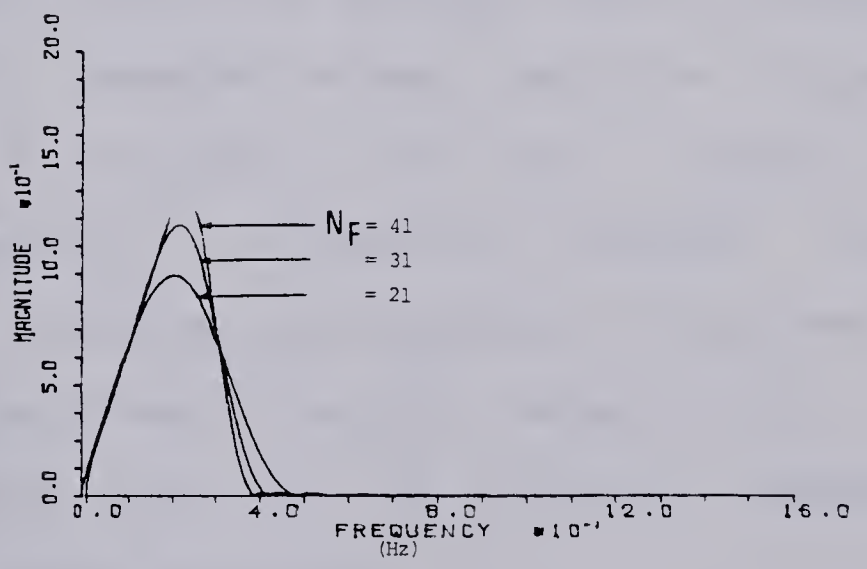

(c) A= 40 dB.

Figure 3.1 Comparison of filter frequency responses

motion was not clearly indicated. Since the cutoff frequency used in the low pass filtering was somewhat arbitrarily chosen, the transition width was not critical. This would not have been the case had it been necessary to eliminate strong components falling only slightly above the cutoff frequency. In all of the cases examined, at the cutoff frequency the trajectory power spectrum had dropped several orders of magnitude from its peak power, hence the transition width was of minor importance. Three of the nine designs were selected to be evaluated through the use of simulations. Filters whose maximum normalized ripples were approximately 30 dB below the magnitude of the maximum response in the frequency response were chosen.

3.3 Simulations

Simulated trajectories generated by a summation of sine and cosine terms to which an average velocity component had been added closely resembled actual particle trajectories, and were used to estimate the error inherent in the instantaneous velocity estimation methods. Simulation parameters were based on observations of real particles' x and y average velocities ($\overline{Vx}$ and $\overline{Vy}$ respectively), and on the frequency and magnitude of periodic components (as evidenced by the power spectrum).

For example, the position coordinates at any time t could be given by:

$$x(t) = 2.0\cos(.05t) + .5\sin(.02t) + \overline{Vx}\,t$$

$$y(t) = .1\cos(.03t) + .08\sin(.025t) + \overline{Vy}\,t$$

$$d(t) = \sqrt{\{x(t)-x(0)\}^2+\{y(t)-y(0)\}^2}$$

and the velocities, through differentiation, were given by

$$Vx(t) = -.1\sin(.05t) + .01\cos(.02t) + \overline{Vx}$$

$$Vy(t) = -.03\sin(.03t) + .002\cos(.025t) + \overline{Vy}$$

$$Vd(t) = \frac{Vx(t)x(t) + Vy(t)y(t)}{\sqrt{\{x(t)-x(0)\}^2 + \{y(t)-y(0)\}^2}}$$

A finite number of samples N were taken at T second intervals from each of the functions x(t), y(t), and d(t). In some cases the effect of noise was simulated by adding to each sample a random number from a Gaussian distribution of numbers with a specified mean and standard deviation. With a distribution mean of zero, this population contains equal power at all frequencies. The standard deviation of the population was made sufficiently large to ensure that the power present above .3 Hz in the new "noisy" trajectory was at least as great as that seen in a real trajectory. The new noisy displacement samples were computed from the noisy x and y position samples. The instantaneous velocity components were estimated from these samples using a variety of methods. The estimates thus obtained were compared with the true velocities as given by the expressions derived for Vx, Vy, and Vd. The error in the estimates was calculated from the difference between the estimated and the true

velocity at each of the N sample points. The mean and standard deviation of the N differences were calculated in each case. As the standard deviation of the differences was consistently at least one order of magnitude larger than the mean, it was chosen as the measure of error in the method. The error of a method shall henceforth refer to the standard deviation of the error in the estimates it produces. The objective was to select the method with the smallest error.

Figure 3.2 illustrates the position-time data for an actual particle. Figure 3.3 illustrates this data for a simulated trajectory, and figure 3.4 illustrates this data for the simulated trajectory with added noise. In figure 3.5 the estimated power spectra of the sampled sets x(kT) from the three trajectories after trend removal and Tukey windowing may be compared. Note that for increased resolution the portions of the spectra above .3 Hz have been plotted on a separate scale.

3.4 Filter and procedure selection

The velocities of a number of simulated particles were estimated with a variety of methods in order to select the best of these for application to real particles. The results for a typical series of analyses are presented in tables 3.2 and 3.3. Using minimization of the method error as the criterion, filter 'A' and procedure (b) were selected as the best method.

I Filters

FILTER A	FILTER B	FILTER C
N_F=21	N_F=31	N_F=41
A=30 dB.	A=30 dB.	A=30 dB.
Δf=.077 Hz	Δf=.051 Hz	Δf=.038 Hz
α =2.12	α =2.12	α =2.12

II Filtering procedures

(a) remove trend from data, convolve modified data with filter.
(b) remove trend from data, convolve modified data with filter, discard first and last 10 terms of the results.
(c) remove trend from data, cosine taper first and last 10 terms of the data, convolve modified data with filter.
(d) remove trend from data, cosine taper first and last 10 terms of the data, convolve modified data with filter, discard first and last 10 terms of the results.

III Simulations

Case 3.4(a)

$$x(t)= \overline{Vx}\ t + Bx + \sum_{m=1}^{5} \{A_m\cos(2\pi f1_m t) + B_m\sin(2\pi f1_m t)\}$$

$$y(t)= \overline{Vy}\ t + By + \sum_{n=1}^{3} \{C_n\cos(2\pi f2_n t) + D_n\sin(2\pi f2_n t)\}$$

$$d(t)= \sqrt{\{x(t)-x(0)\}^2 + \{y(t)-y(0)\}^2}$$

$\overline{Vx}$=1.0 $\overline{Vy}$=.04
Bx=0.0 By=5.0

A_1=1.0	B_1=.1	$f1_1$=.03	C_1=.2	D_1=.3	$f2_1$=.02
A_2=.8	B_2=1.2	$f1_2$=.05	C_2=.3	D_2=.5	$f2_2$=.08
A_3=.4	B_3=.3	$f1_3$=.08	C_3=.4	D_3=.3	$f2_3$=.125
A_4=.6	B_4=.5	$f1_4$=.1			
A_5=.2	B_5=.1	$f1_5$=.13			

Positions sampled N=100 times at interval T=1/3 second

case 3.4(b)

$$x'(kT)=x(kT)+N(0.0,0.13)$$
$$y'(kT)=y(kT)+N(0.0,0.13)$$

$$d'(kT)=\sqrt{(x'(kT)-x'(0))^2+(y'(kT)-y'(0))^2}$$

N(a,b)- function that generates pseudo-random Gaussian noise of mean 'a' and standard deviation 'b'.

Case 3.4(a) results

Filter	Estimate method	Vx error (um/sec)		Vy error (um/sec)		Vd error (um/sec)	
		Mean	S.D.	Mean	S.D.	Mean	S.D.
A	(a)	-2.9E-2	1.3E-1	+6.3E-4	2.8E-2	-3.0E-2	1.4E-1
A	(b)	+7.7E-4	1.3E-2	+9.5E-4	1.3E-2	+1.1E-3	1.4E-2
A	(c)	-6.1E-2	2.2E-1	-4.7E-3	6.2E-2	-6.1E-2	2.2E-1
A	(d)	+2.7E-3	2.4E-2	+8.8E-4	1.3E-2	+3.0E-3	2.5E-2
B	(a)	-3.0E-2	1.4E-1	-6.9E-5	2.7E-2	-3.0E-2	1.4E-1
B	(b)	-3.6E-3	1.6E-2	-3.7E-4	6.4E-3	-3.4E-3	1.5E-2
B	(c)	-6.2E-2	2.3E-1	-5.4E-3	6.4E-2	-6.2E-2	2.2E-1
B	(d)	+2.4E-4	2.1E-2	-8.2E-6	8.8E-3	+4.4E-4	2.3E-2
C	(a)	-3.0E-2	1.4E-1	+5.6E-4	2.7E-2	-3.0E-2	1.5E-1
C	(b)	-2.4E-3	2.4E-2	-1.4E-5	7.2E-3	-2.2E-3	2.2E-2
C	(c)	-6.2E-2	2.3E-1	-4.7E-3	6.4E-2	-6.2E-2	2.3E-1
C	(d)	+2.5E-3	2.0E-2	+5.7E-4	8.7E-3	+2.6E-3	2.2E-2

Table 3.2

Case 3.4(b) results

Filter	Estimate method	Vx error (um/sec)		Vy error (um/sec)		Vd error (um/sec)	
		Mean	S.D.	Mean	S.D.	Mean	S.D.
A	(b)	-1.4E-3	5.0E-2	-1.1E-3	5.6E-2	-1.1E-3	4.7E-2
A	(d)	+8.6E-4	5.9E-2	-6.5E-4	5.7E-2	+1.1E-3	5.6E-2
B	(b)	-6.0E-3	5.3E-2	-2.2E-3	5.3E-2	-5.8E-3	5.2E-2
B	(d)	-1.6E-3	6.0E-2	-1.3E-3	5.4E-2	-1.5E-3	5.8E-2
C	(b)	-4.7E-3	5.7E-2	-1.9E-3	5.6E-2	-4.6E-3	5.6E-2
C	(d)	+7.6E-4	5.9E-2	-6.7E-4	5.6E-2	+8.4E-4	5.8E-2

Table 3.3

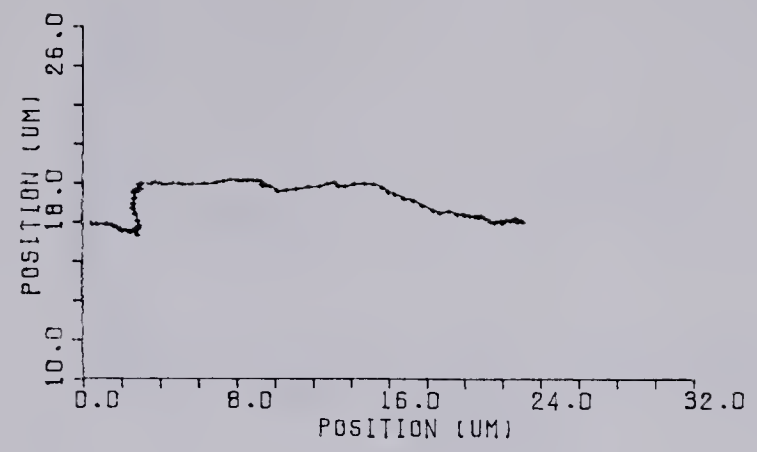

(a) Trajectory S4

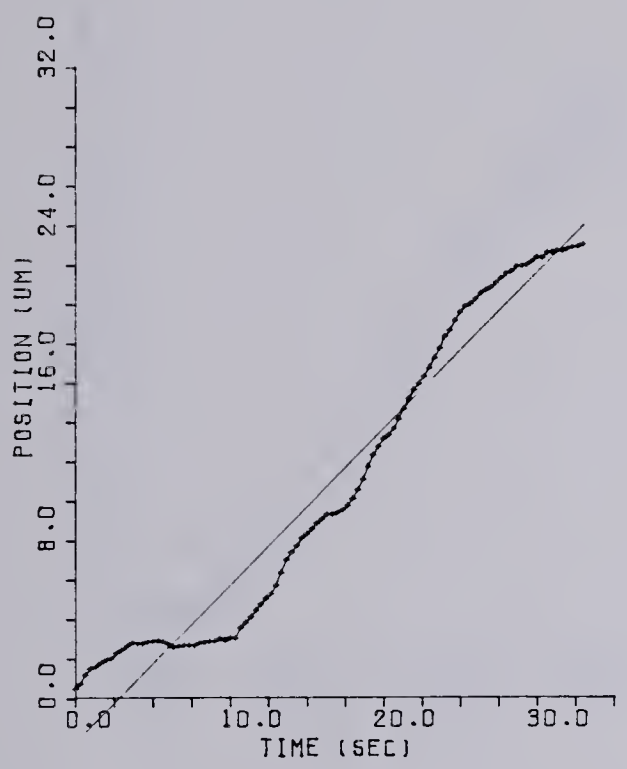

(b) X position versus time

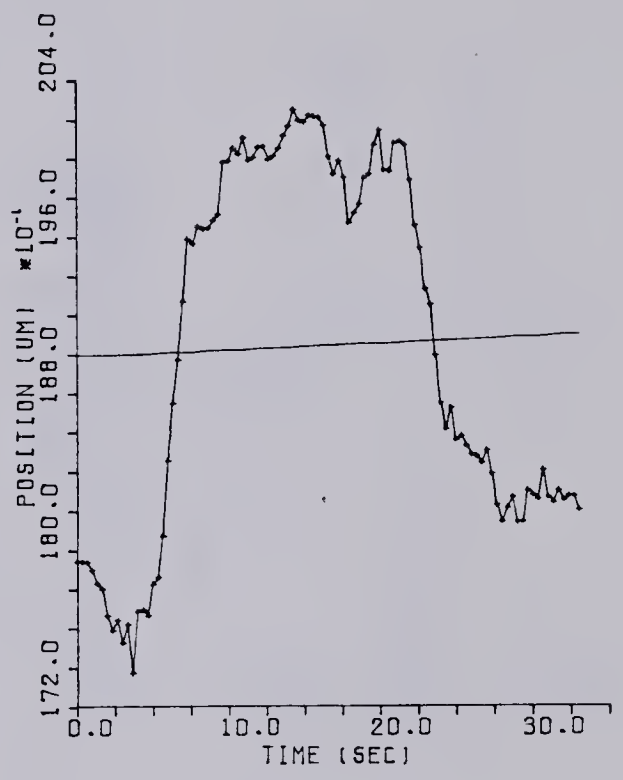

(c) Y position versus time

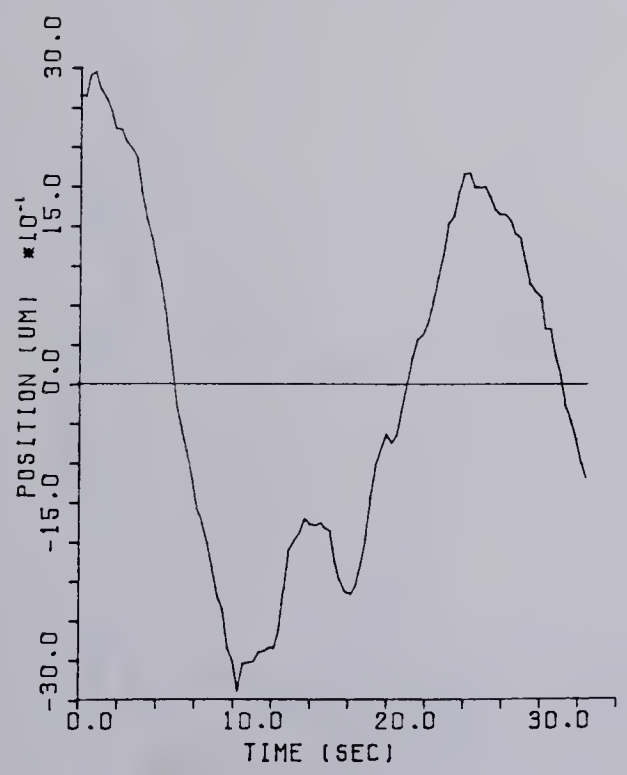

(d) X deviations from straight line fit

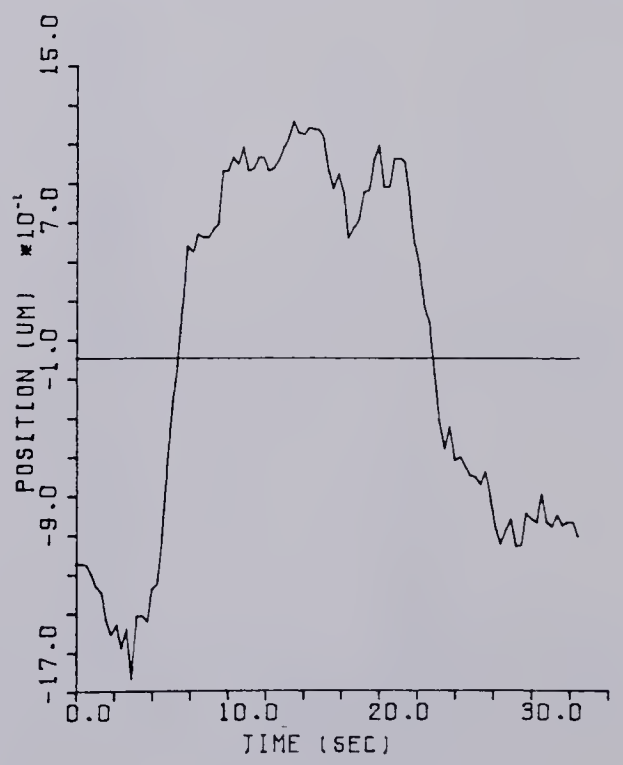

(e) Y deviations from straight line fit

Figure 3.2 Position-time data for a real trajectory.

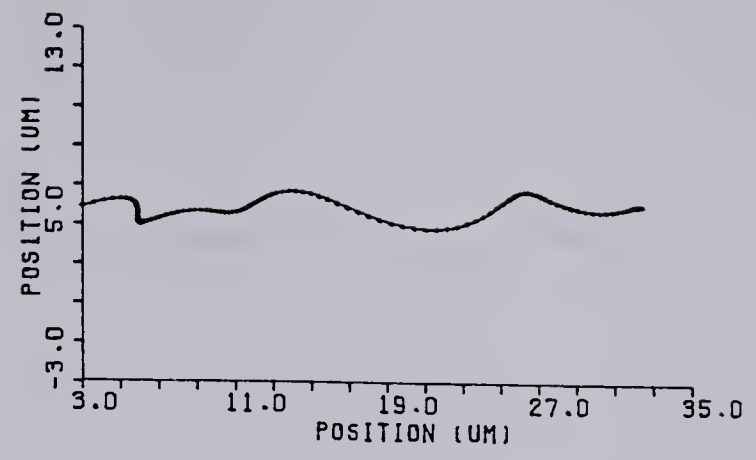

(a) Simulated trajectory

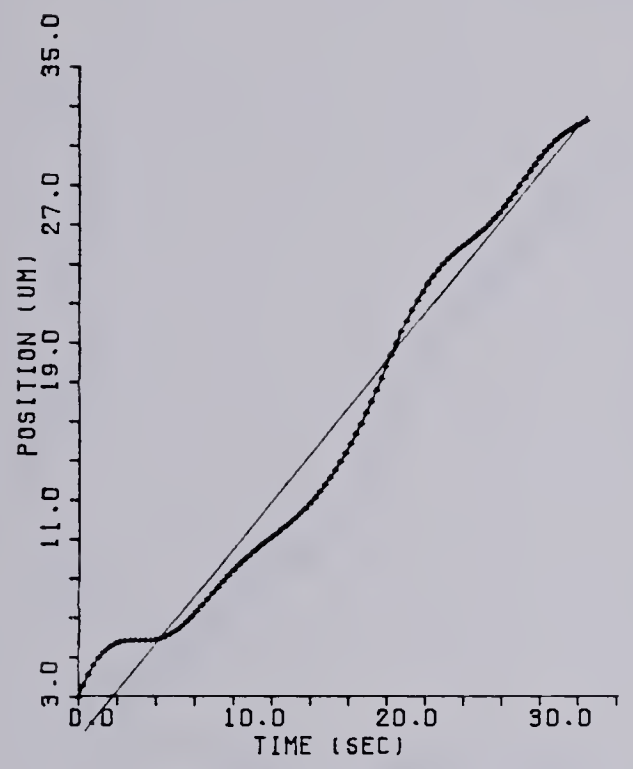

(b) X position versus time

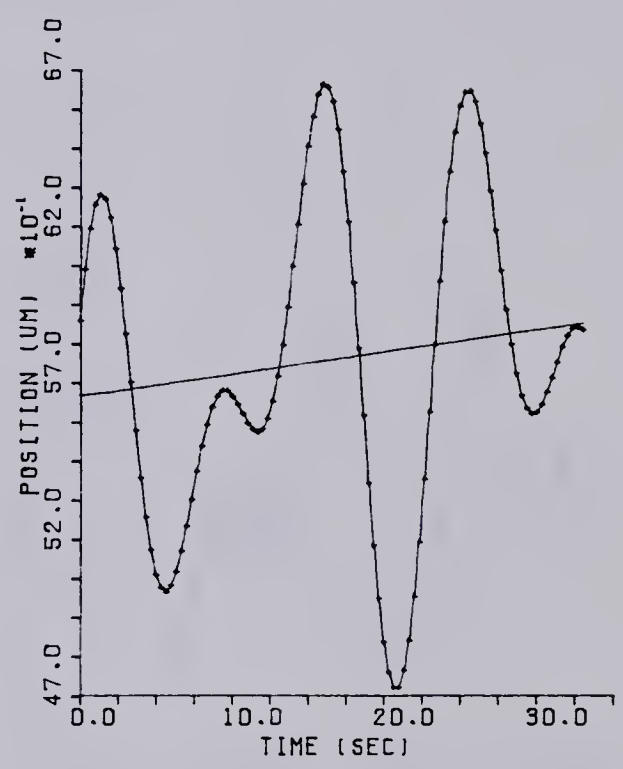

(c) Y position versus time

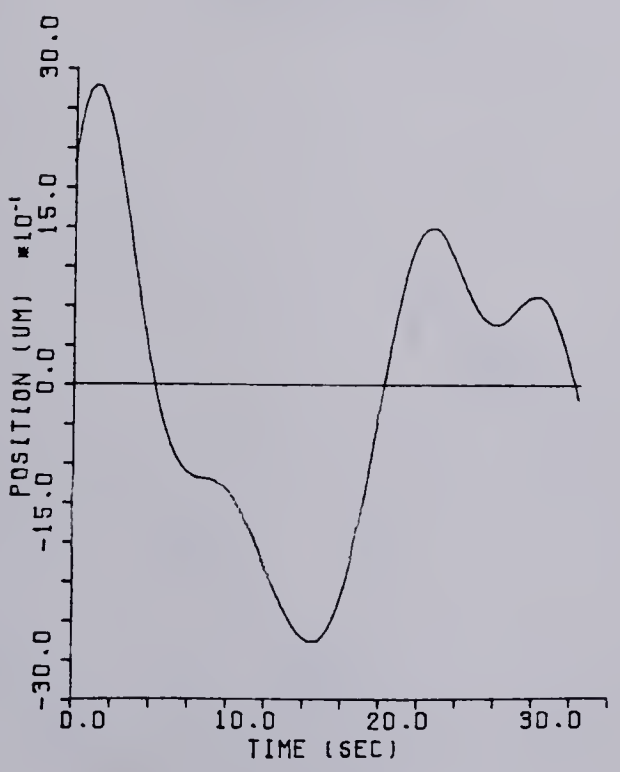

(d) X deviations from straight line fit

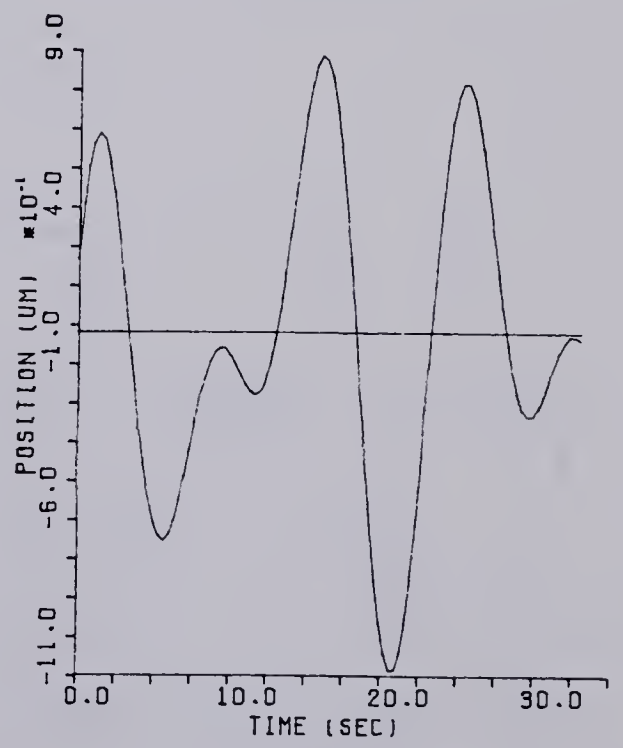

(e) Y deviations from straight line fit

Figure 3.3 Position-time data for a simulated trajectory

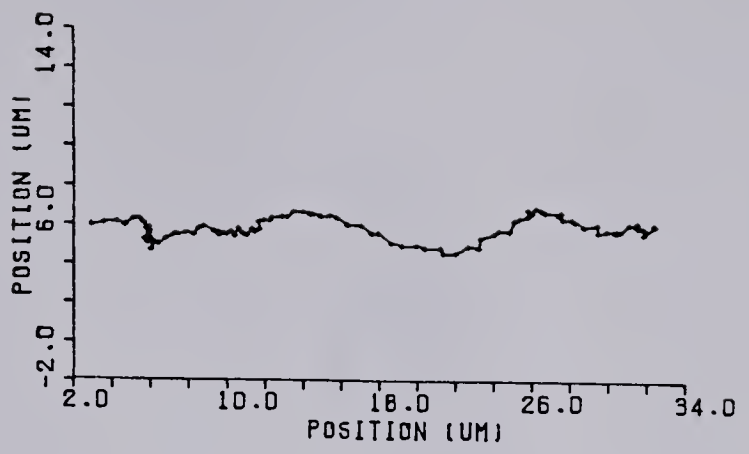

(a) Simulated trajectory with noise added

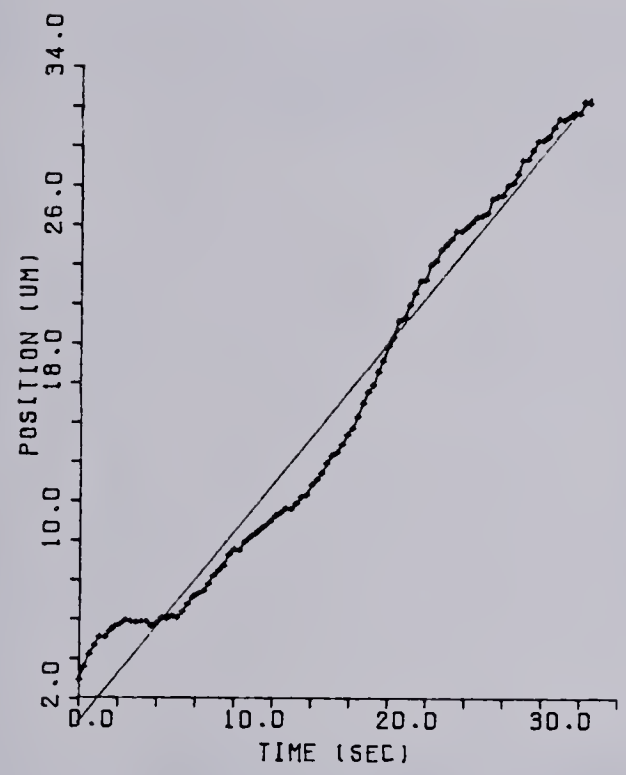

(b) X position versus time

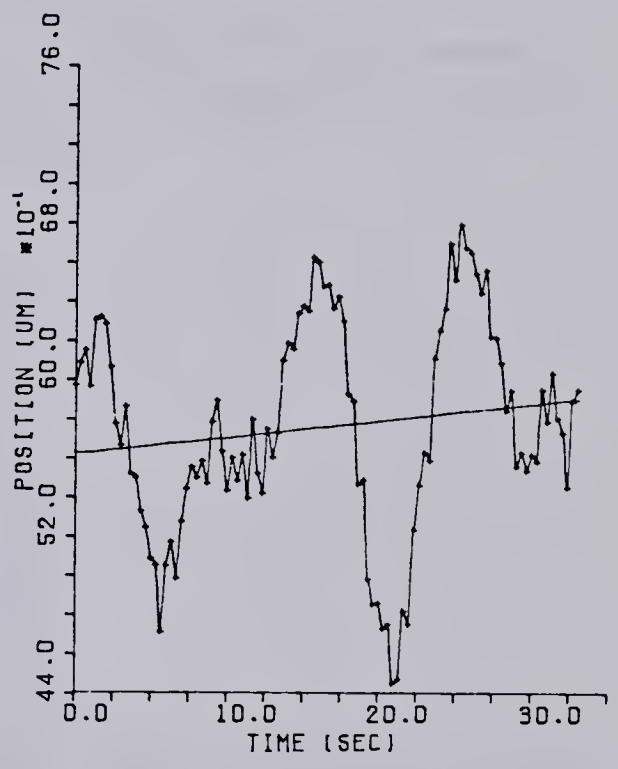

(c) Y position versus time

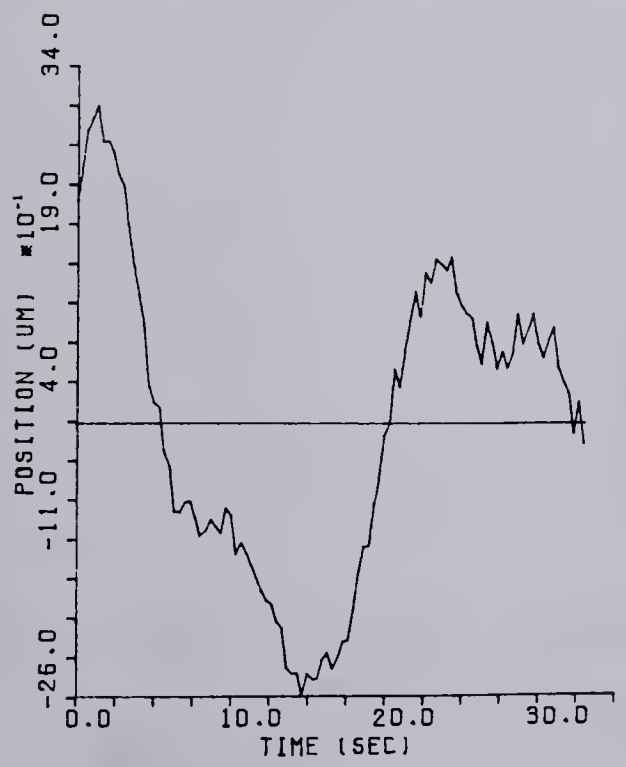

(d) X deviations from straight line fit

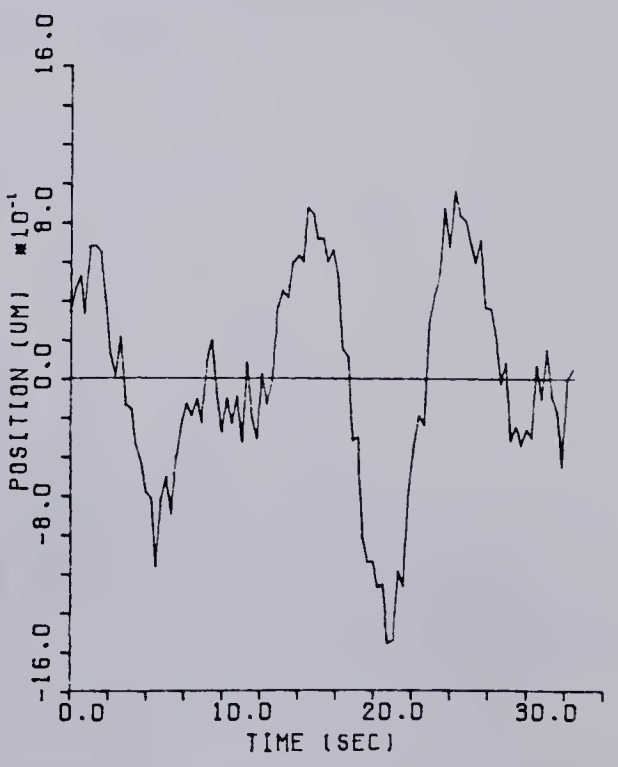

(e) Y deviations from straight line fit

Figure 3.4 Position-time data for simulated trajectory with noise

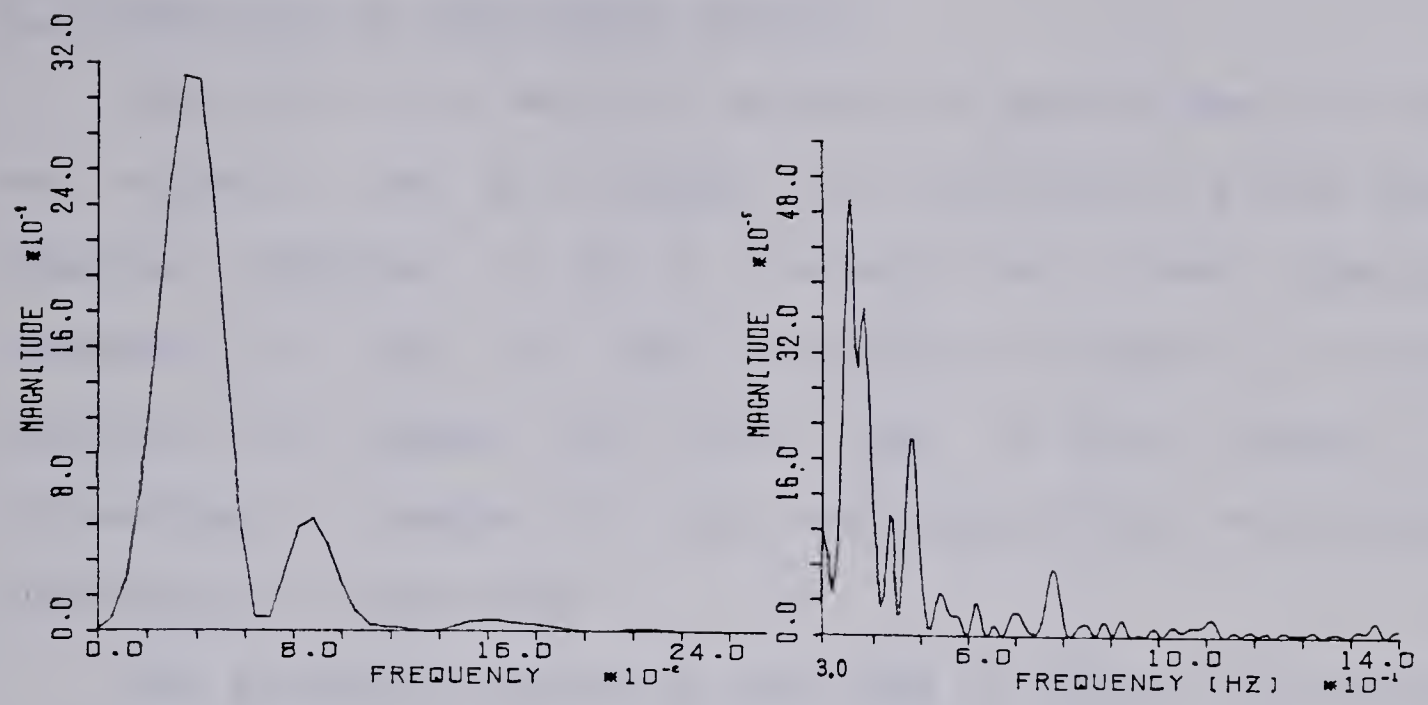

(a) Power spectrum of actual trajectory

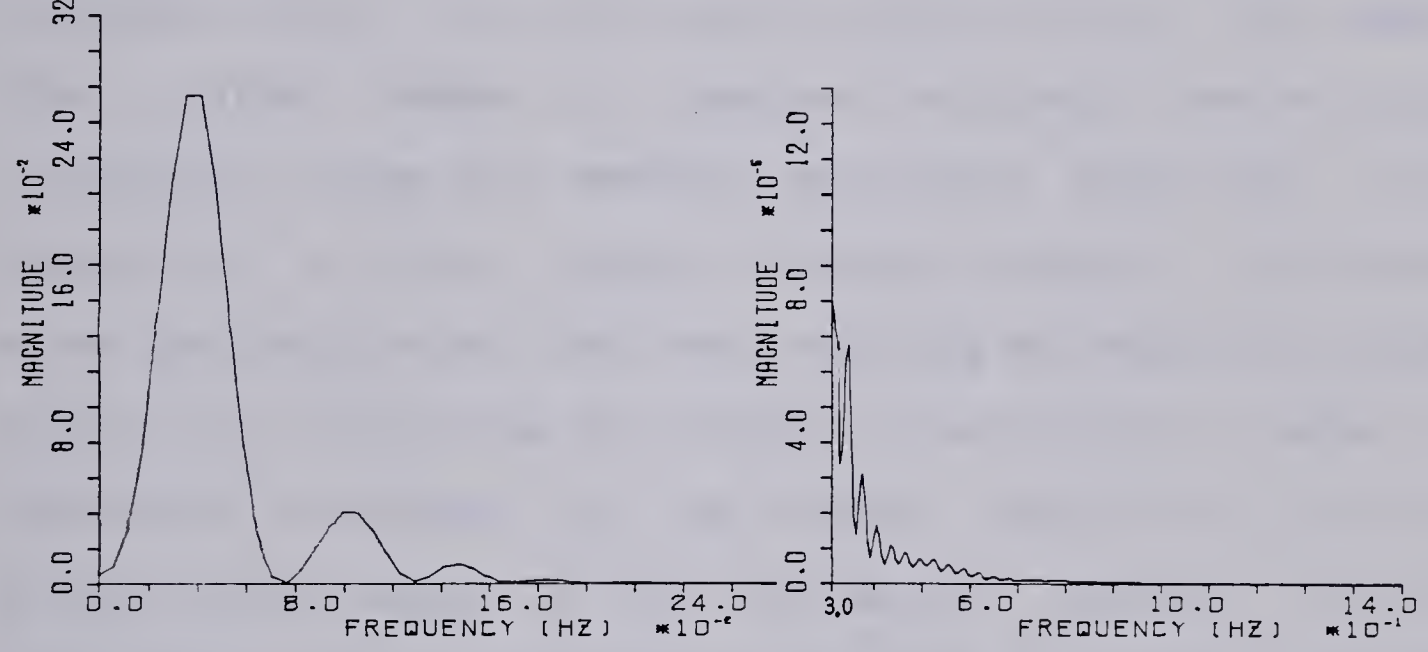

(b) Power spectrum of simulated trajectory with no noise.

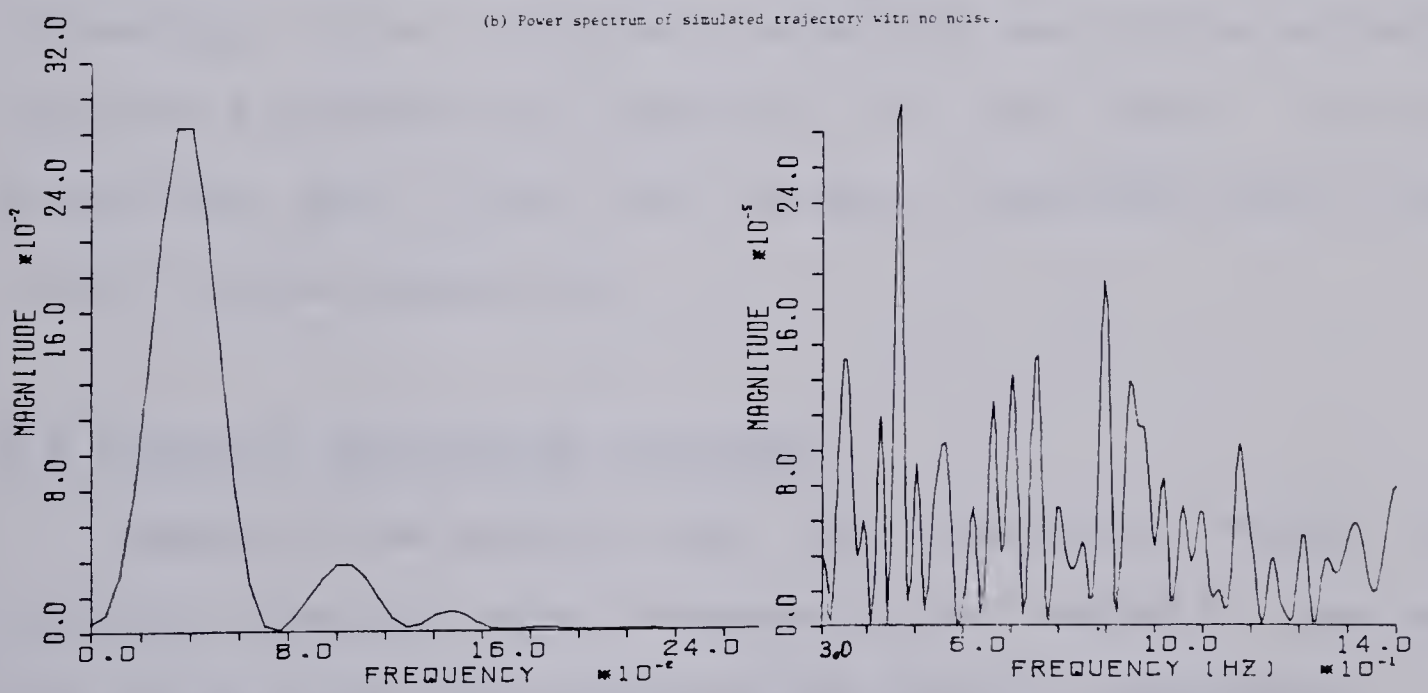

(c) Power spectrum of simulated trajectory with noise added.

Figure 3.5 Power spectra of the x component.

3.5 Reduction of end effect errors

The error in a velocity estimation method due to filter end effects can be reduced by employing a filter whose impulse response is of a comparatively short duration compared to that of the data being filtered. It is also possible to reduce the error due to end effects by discarding a number of the end points from the velocity estimates of a particle.

The following procedure was used to assess end effects. Estimates of Vx, Vy, and Vd were obtained from 100 samples (the typical number of samples obtained from an actual trajectory) using the method previously described. After discarding a given number of result endpoints, the method error was calculated from the remaining estimates as before. Figure 3.6 illustrates the effect of varying the number of endpoints discarded on the method error in Vx, with and without noise added to the trajectory samples. Clearly, discarding up to five points from each end of the estimates produced a substantial reduction of the error. However, discarding more than five points from each end achieved little further reduction.

3.6 Velocity estimation procedure

Based on the results from the preceding trials, the following method (later referred to as 'method 2') was used to estimate particle instantaneous velocity components:

(a) the trend as estimated by the linear regression

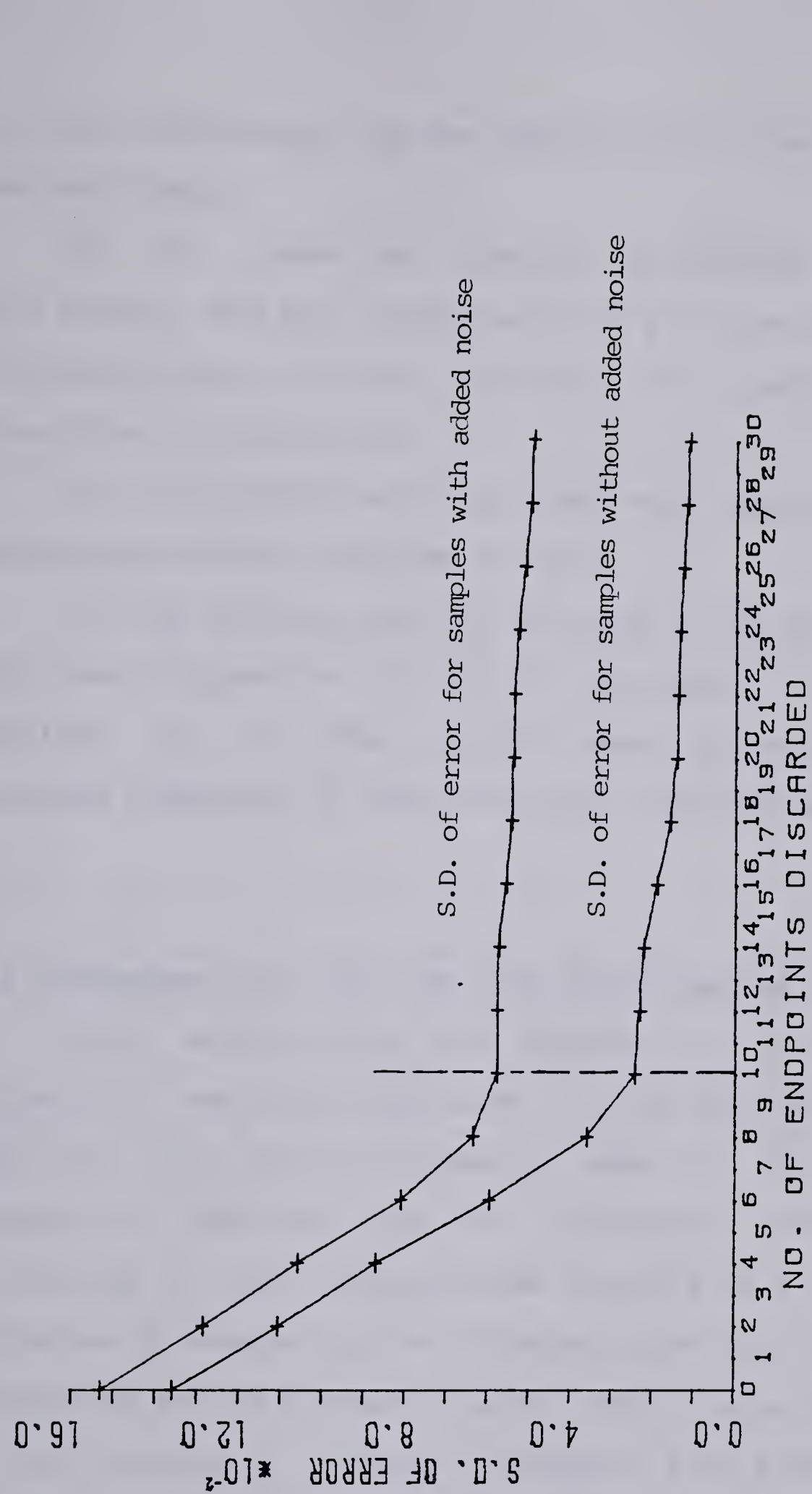

Figure 3.6 Effect of discarding result endpoints on the error in the estimates of Vx.

line was subtracted from the samples of the desired position component data.

(b) the trend-free samples were padded with zeros to 1024 points, and fast convolved with a 21 term band limited differentiating filter (filter 'A'), using a Fourier transform of 1024 points.

(c) five points were discarded from each end of the velocity estimates obtained in (b).

(d) the average velocity estimate given by the slope of the linear regression line in (a) was added to the estimates obtained in (c). The results were the estimates of the selected component of the particle's instantaneous velocity.

3.7 Comparison with the two term approximation

After establishing the method by which velocity estimation would be undertaken, it was desirable to compare this with the method commonly used in the literature. Henceforth referred to as the "incremental distance" method or 'method 1', the instantaneous velocity of a particle is estimated by measuring the distance a particle moves between successive motion picture frames, and dividing this distance by the period T between successive film frames (refer to equation (1.4)). When movement in the y coordinate is much smaller than that in the x coordinate, as it is in the case of axonal particle movement, equation (1.4) reduces with little error to:

$$V((k+1)T) = \frac{x((k+1)T) - x(kT)}{T} \tag{3.1}$$

This is equivalent to convolving the x position-time samples of the trajectory with a two term approximation to an ideal differentiating filter. The magnitude and phase responses can be shown to be given respectively by:

$$|H(f)| = (2/T) \sin \pi fT \qquad |f| \leq 1/2T \tag{3.2}$$

$$\angle H(f) = \pi(1-2fT)/2 \qquad |f| \leq 1/2T \tag{3.3}$$

This frequency response is compared with that of the twenty one term filter and that of an ideal low pass differentiating filter in figure 3.7.

Simulated trajectories were used to assess the error of methods 1 and 2, and examine the effect of noise in the data on the error of each.

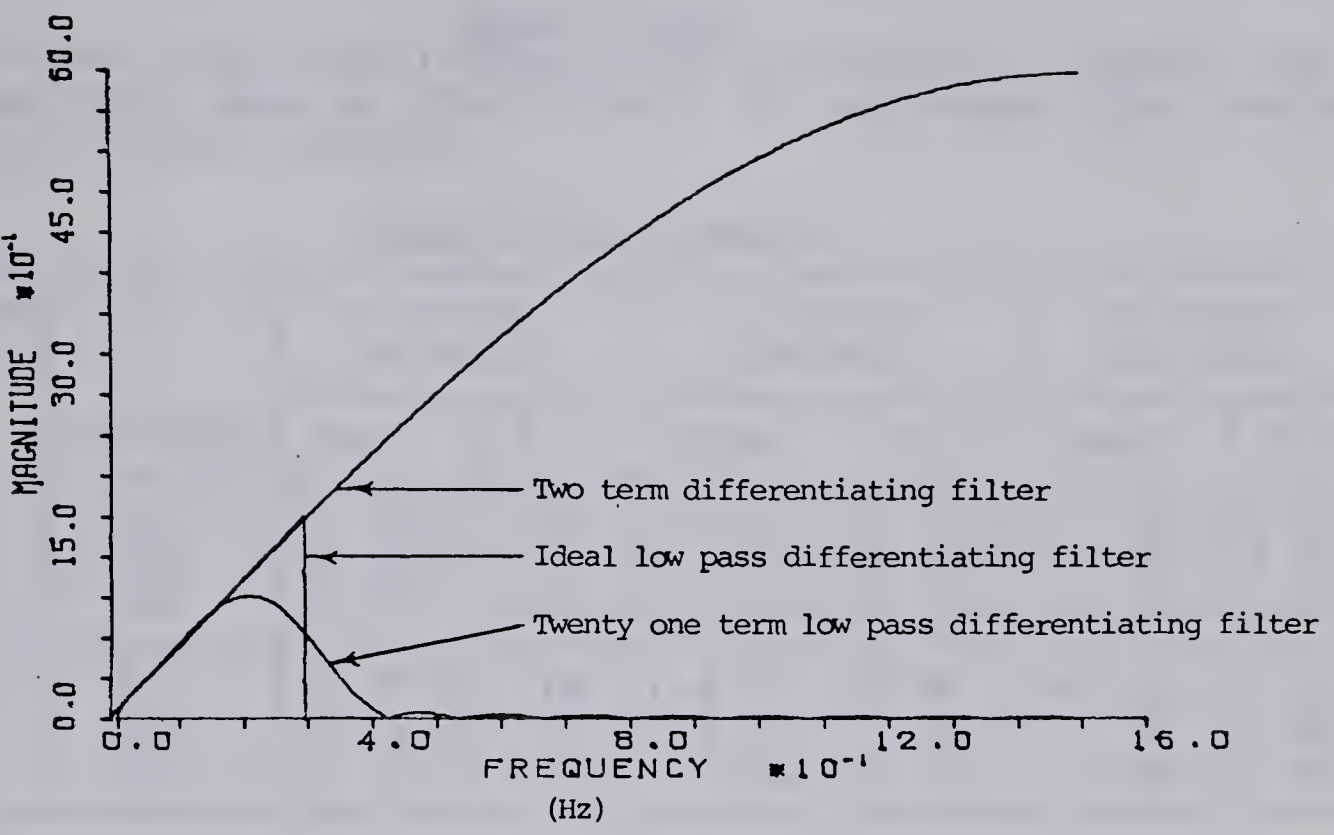

(a) Magnitude response of the filters

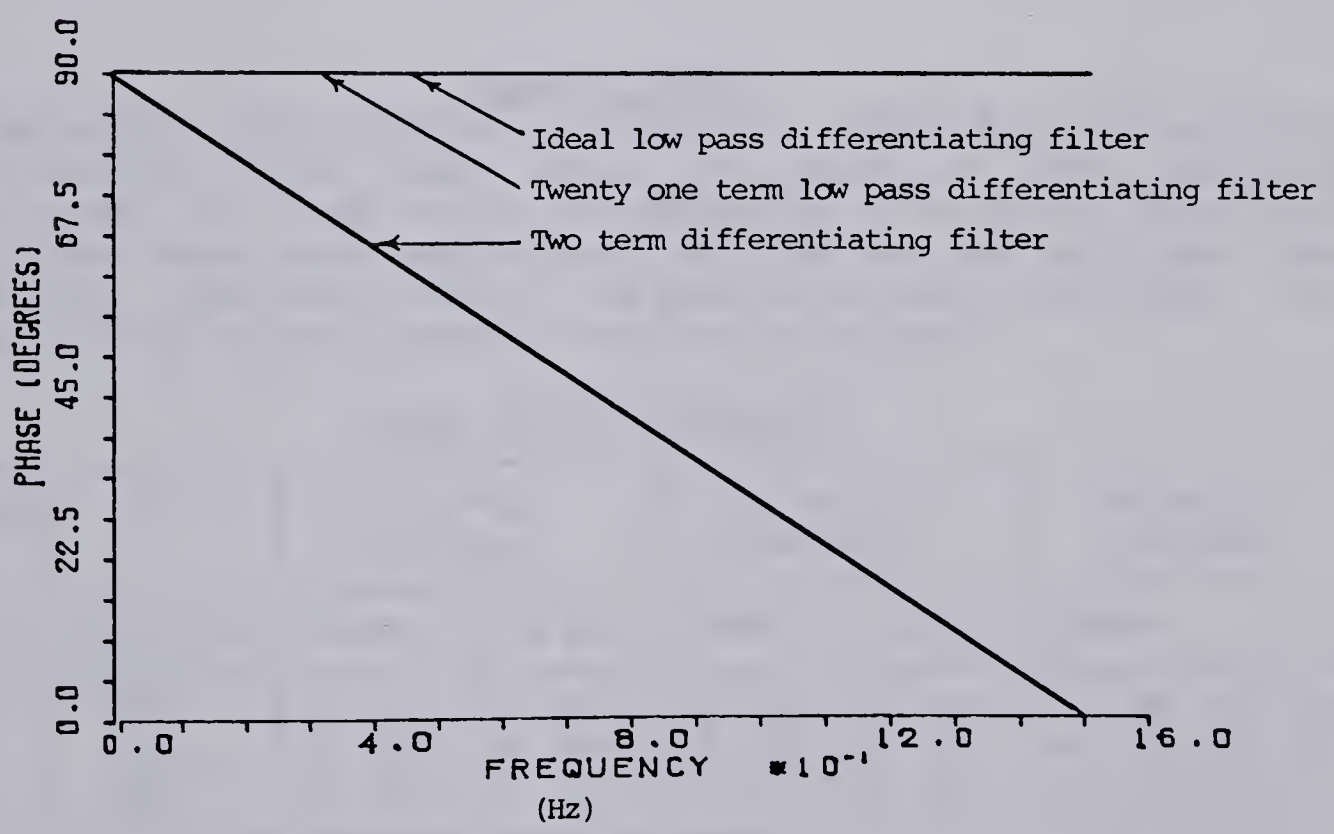

(b) Phase response of the filters

Figure 3.7 Comparison of the filter frequency responses

Case 3.7(a)

Three simulated trajectories of different lengths were analyzed with each of the filters to estimate the errors inherent in each method.

Case 3.7(a) results

Method	N	Vx error (um/sec)		Vy error (um/sec)		Vd error (um/sec)	
	(points)	Mean	S.D.	Mean	S.D.	Mean	S.D.
1	50	-5.3E-3	5.3E-2	-4.8E-3	3.9E-2	-1.1E-2	5.3E-2
1	100	-6.2E-3	4.5E-2	-2.3E-3	4.1E-2	-8.7E-3	4.5E-2
1	200	-2.8E-3	5.0E-2	-2.5E-3	4.1E-2	-4.2E-2	5.0E-2
2	50	+5.7E-3	1.6E-2	+1.6E-3	8.4E-3	+6.5E-3	1.8E-2
2	100	+7.7E-4	1.3E-2	+9.5E-4	1.3E-2	+1.1E-3	1.4E-2
2	200	-2.4E-4	1.6E-2	-1.6E-4	1.3E-2	-1.2E-4	1.6E-2

Table 3.4

Case 3.7(b)

Gaussian distributed noise of mean=0.0 and standard deviation of .13 um was added to each of the position coordinates of the three trajectories previously analysed. This noise level was equivalent to that of the noisiest real trajectory. The new 'noisy' trajectories were analysed, and the errors in the estimates were calculated.

Case 3.7(b) results

Method	N	Vx error (um/sec)		Vy error (um/sec)		Vd error (um/sec)	
	(points)	Mean	S.D.	Mean	S.D.	Mean	S.D.
1	50	-8.3E-3	5.4E-1	-3.3E-3	5.2E-1	-1.3E-2	5.3E-1
1	100	-3.6E-3	5.9E-1	-5.3E-3	5.1E-1	-6.9E-3	5.9E-1
1	200	-2.6E-3	5.7E-1	-2.3E-3	5.0E-1	-3.7E-3	5.7E-1
2	50	+8.4E-3	5.1E-2	-2.3E-3	5.3E-2	+1.0E-2	5.8E-2
2	100	+2.2E-3	5.3E-2	+8.7E-3	5.9E-2	+2.6E-3	5.4E-2
2	200	+6.9E-4	4.5E-2	+1.3E-3	5.2E-2	+8.2E-4	4.5E-2

Table 3.5

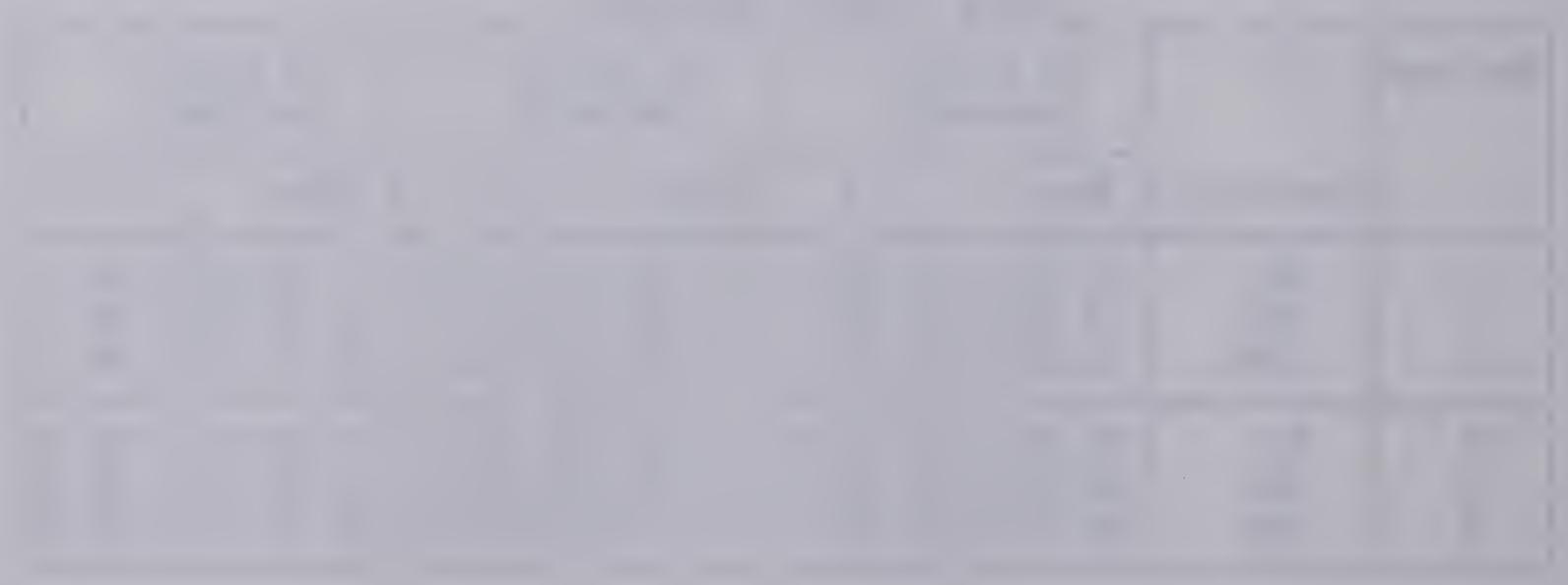

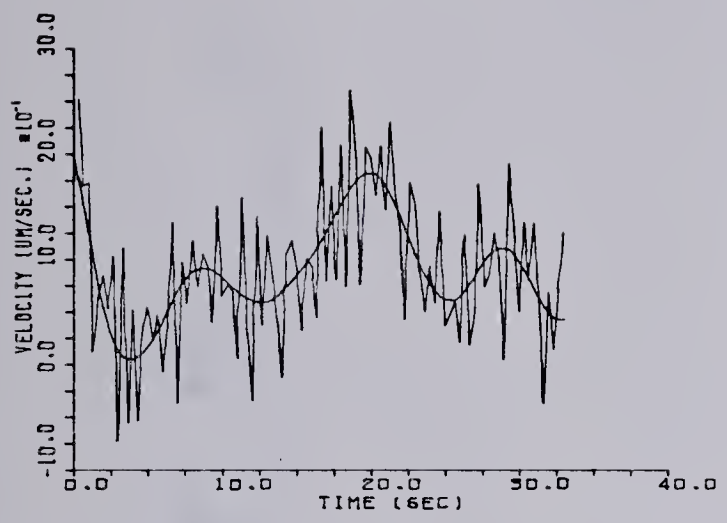

Actual and estimated instantaneous velocity

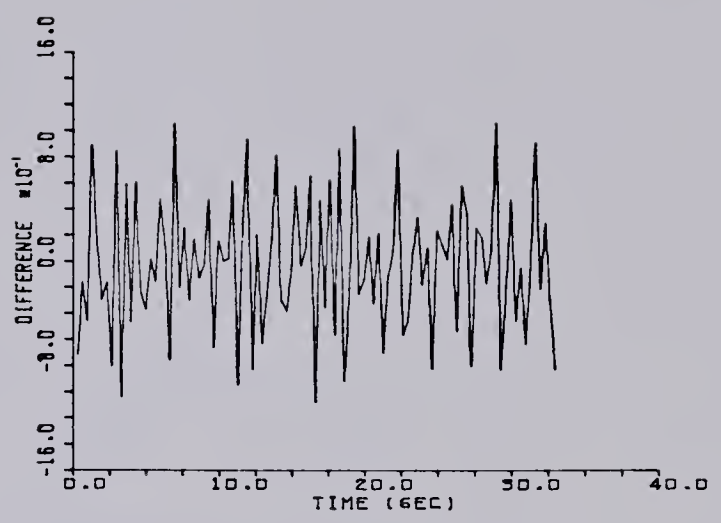

Difference between actual and estimated instantaneous velocity

Figure 3.8 Estimation of Vx with method 1.

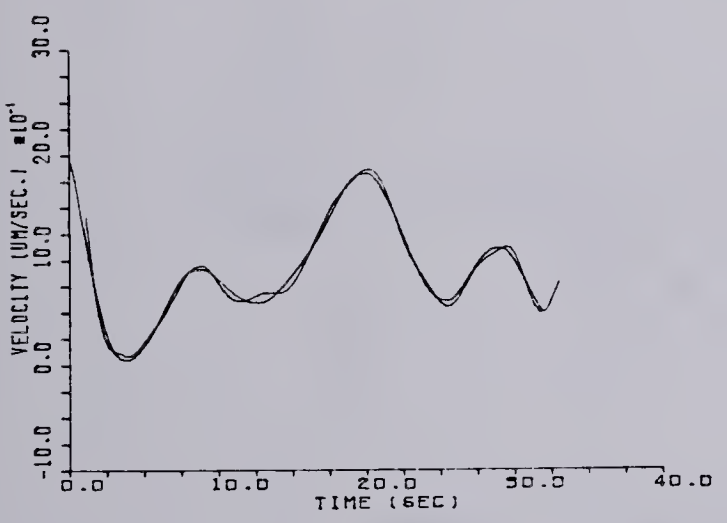

Actual and estimated instantaneous velocity

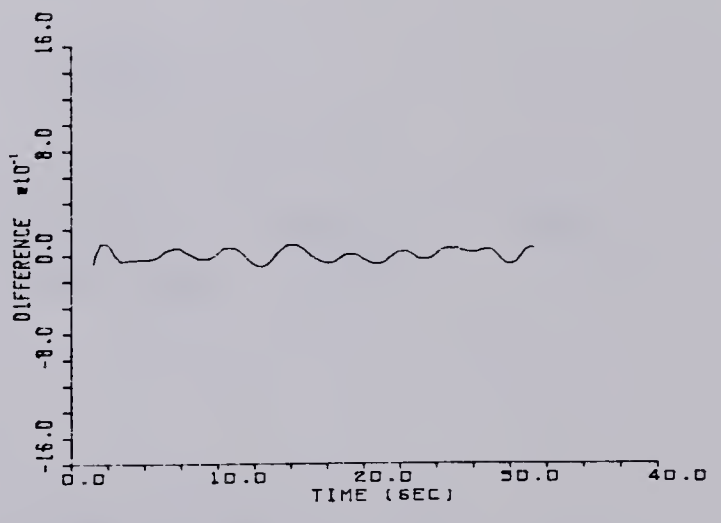

Difference between actual and estimated instantaneous velocity

Figure 3.9 Estimation of Vx with method 2.

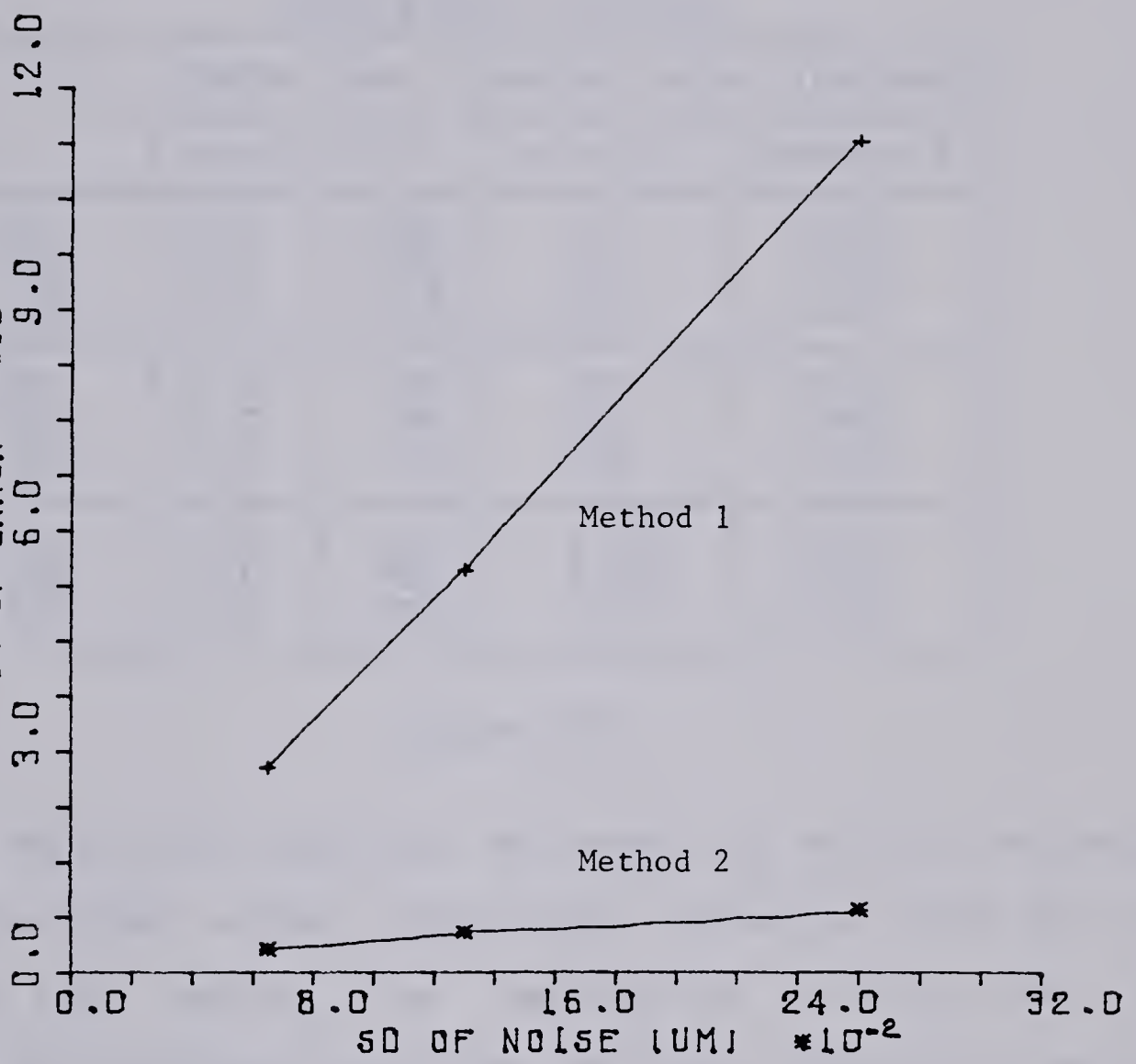

Figure 3.10 Error in the estimates of Vx as a function of noise level.

Case 3.7(c)

The standard deviation of the Gaussian noise added to the three trajectories was varied to determine the relationship between noise and estimation error for each of the methods. The method error for estimates of Vx is given in table 3.6 for a variety of cases.

Case 3.7(c) results

N	Noise (um)		method error (um/sec)	
	mean	S.D.	method 1	method 2
50	0.0	.065	.31	.036
100	0.0	.065	.28	.033
200	0.0	.065	.26	.032
50	0.0	.130	.53	.052
100	0.0	.130	.55	.056
200	0.0	.130	.54	.049
50	0.0	.260	1.05	.091
100	0.0	.260	1.14	.087
200	0.0	.260	1.07	.120

Table 3.6

It should be noted that although the velocity estimates and associated errors discussed throughout this work are discrete time series, for reasons of clarity they are plotted as continuous functions of time. Figures 3.8 and 3.9 illustrate the estimates of Vx and their associated errors obtained with the two methods for the simulated trajectory shown in figure 3.4. The effect of the level of added noise on the estimation error of Vx for a variety of cases is tabulated in table 3.6. Figure 3.10 illustrates the error with different noise levels for N=100. Method 2 was found to be approximately one order of magnitude less sensitive to noise than method 1.

3.8 Conclusions

The error in the estimates of instantaneous velocity obtained with the method developed in this thesis was approximately one order of magnitude less than that obtained with the incremental distance method of velocity estimation. This increase in accuracy was obtained at the cost of the loss of ten points of the estimates for each trajectory, and an increase in the computing time required.

CHAPTER IV

PROCEDURE

As reported previously, (Cooper and Smith, 1974), 16 mm motion picture films at framing rates of 3 and 4 frames/sec were made of single nerve axons of Xenopus laevis at room temperature, utilizing darkfield microscopy. Two populations of moving particles were observed within each axon, one consisting of particles moving somatopetally, and one of particles moving somatofugally.

The films were mounted on an L-W Photo Optical Data Analyzer and projected onto the ground glass screen of a Photographic Analysis Ltd. Digitizer. Prior to filming in all cases the longitudinal axis of the axon had been oriented such that on the film records it was parallel to the x coordinate axis of the digitizer. Segments of film were repeatedly viewed to locate particle trajectories satisfying two basic requirements: (1) the particle's position could be clearly discerned for a large number of successive frames (preferably > 100) and (2) the nerve preparation did not move appreciably during the course of the trajectory. Suitable trajectories were recorded on punched paper tape by making frame by frame readings of the selected particle's x and y coordinates, and the movie frame number.

The trajectories recorded from ten normal, healthy axons (see table 4.1) were selected from those recorded from

a number of axons, to be analyzed in detail. The optical quality of the recorded images was good, and there was little apparent movement in each case of the axon relative to the filming apparatus. One hundred thirty-three of the selected trajectories were somatopetal, thirty-nine were somatofugal. The difference in population sizes reflected the fact that a greater number of detectable particles move towards the cell body (somatopetally) than away from it (somatofugally) (Cooper and Smith,1974).

Trajectories recorded

Nerve	Record Designation	Number of Trajectories	
		Somatopetal	Somatofugal
A	F,FF Film R1(a)	10	2
B	G,GG Film R1(b)	10	4
C	J,JJ Film R48	11	2
D	M,MM Film R50	10	3
E	N,NN Film R51	10	7
F	O,OO Film R52	10	1
G	P,PP Film R53	10	3
H	R,RR Film R35	10	3
I	S,SS Film R55	42	9
J	T,TT Film R54	10	5
Total Population=		133	39

Table 4.1

A typical trajectory is shown in figure 4.1.

The spatial characteristics of particle movement were also of interest. Axon 'I' was arbitrarily selected to be analysed in particular detail; therefore, more trajectories (the S and SS series) were recorded from this axon than from

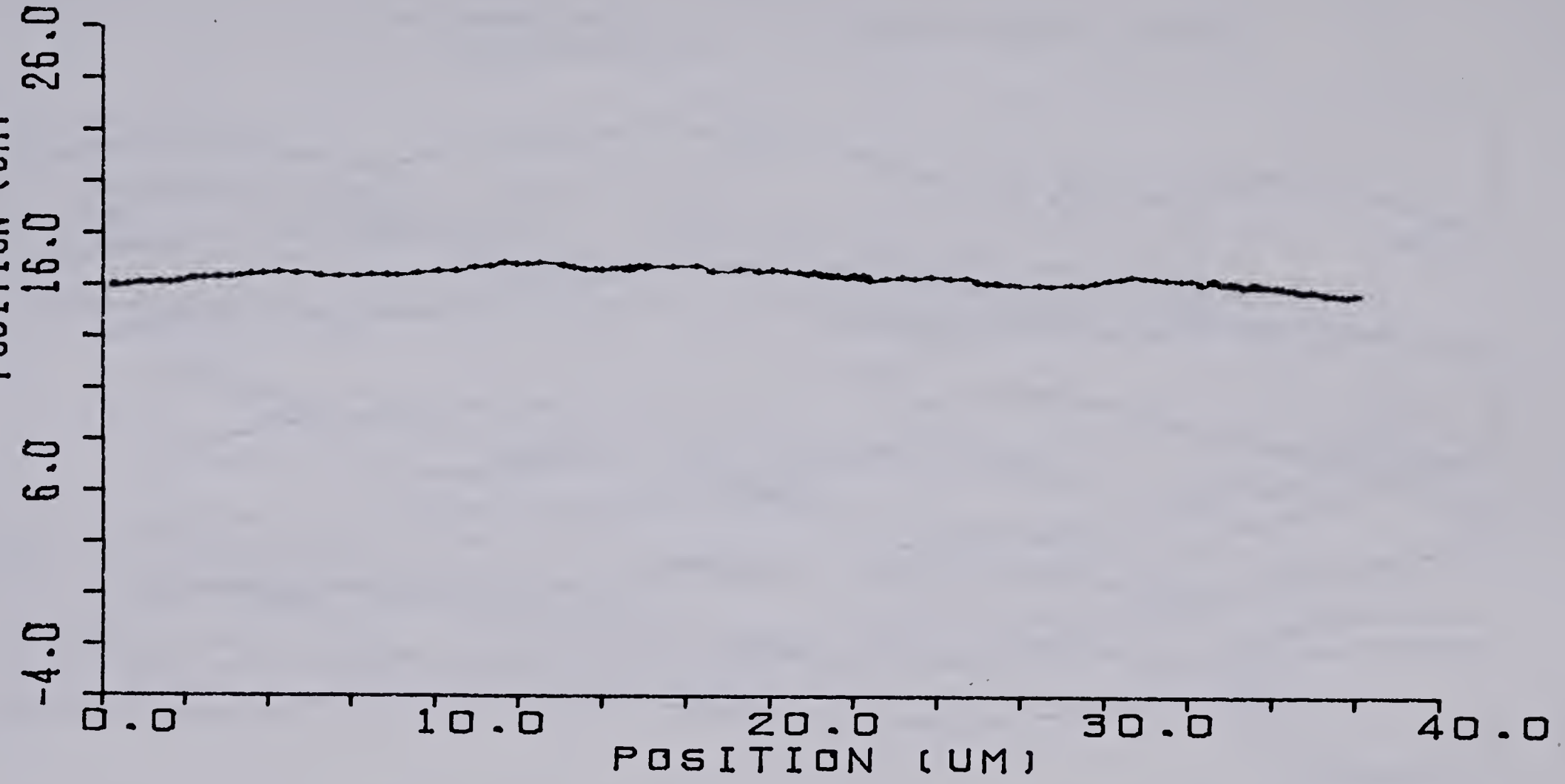

Figure 4.1 Typical particle trajectory

LEGEND

AW Axonal wall
M Rod mitochondria

\+ Particle position reading

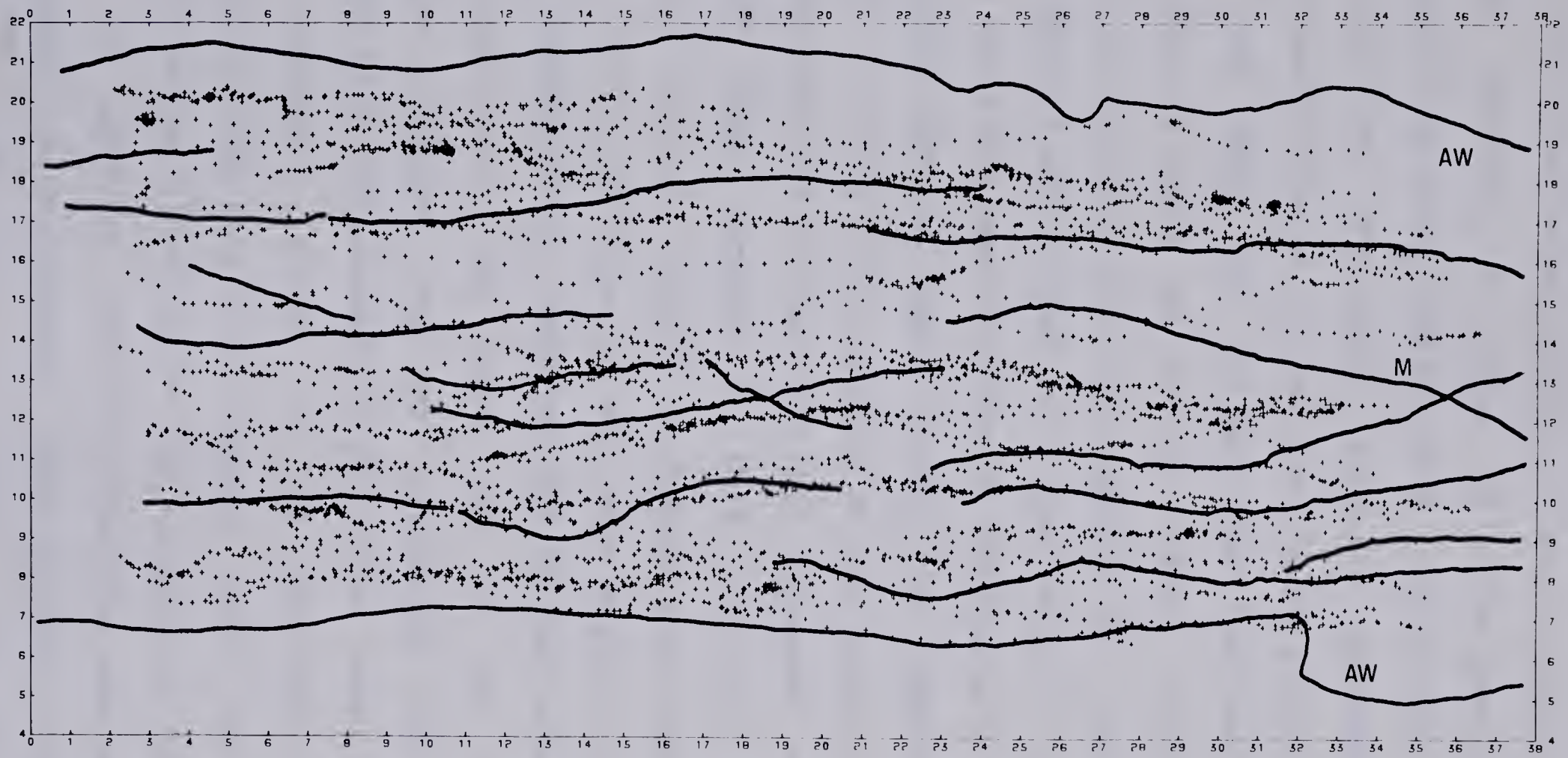

Figure 4.2 Axonal structures and particle trajectories.

the others. Also, in order to overlay positional data (i.e. the trajectories and the related velocity components) it was necessary to show that the positional frame of reference (the axon) did not move appreciably relative to the digitizer. Three small, separate, apparently stationary objects were located in this axon lying within the field of view from which the trajectories had been recorded. All three objects could be fairly clearly resolved for the entire duration of the film segment. As it was assumed that these objects were indeed stationary relative to the axon, their positions were recorded at intervals of approximately 300 frames over the length of the film (approximately 2000 frames) to obtain an estimate of the amount of movement of the axon relative to the digitizer. Apparent movement over an 1100 frame segment of this film was found to be particularly small. Over this segment the largest ranges in the x and y positions of the three objects were .52 um and .33 um respectively. Therefore the maximum apparent movement of the axon over 1100 frames was of the order of one particle diameter, and was considered very small when compared with the movement of particles over much shorter film segments. Hence it was concluded that spatial information from this film segment could be "overlapped" with little positional error due to apparent movement of the nerve. In addition, position readings were made from this film segment of the apparent inner surface of the axon, and of long stationary rod-shaped organelles (probably

rod-shaped mitochondria) which were visible. Figure 4.2 is a plot of the position readings of the inner surfaces of the axonal wall, the outlines of the rod-shaped organelles, and the particle trajectories.

CHAPTER V

ANALYTICAL METHODS

5.1 Initial processing

Despite all precautions, the position samples occasionally contained gross errors. These could have arisen from dirt on the digitizer contact wires, or errors in the digitizer and teletype. Since it was impossible to eliminate totally this type of error at the source , the first procedure in the analysis of the data attempted to identify and correct such points. It was essential to remove these so-called outliers as they were of large amplitude and could contain a substantial portion of the power in the data.

Chauvenet's criterion for rejection of outliers was used to identify erroneous readings (Neville and Kennedy,1970). It was necessary to replace such points with interpolated values, rather than merely discarding them, since the type of Fourier analysis used assumed the data consisted of evenly spaced samples.

The x(kT) and y(kT) sampled position sets describing the trajectories were stored in the computer. The sets were examined, and points identified as outliers were discarded and replaced with interpolated values. The only exceptions were from film frames in which the particles being tracked had been observed to make very large, sudden movements. Such movements occurred rarely, but were due to "real" movements of the particle, not instrument or observer error, and

therefore were not replaced.

A third sample set; the radial displacement of a particle at time kT from its initial position at kT=0, d(kT); was formed from the corrected x(kT) and y(kT) data:

$$d(kT) = \sqrt{\{x(kT)-x(0)\}^2+\{y(kT)-y(0)\}^2}$$

$$k=0,1,2...N-1$$
$$N=\text{number of samples}$$
$$T=\text{sampling period}$$

(5.1)

The time series x(kT), y(kT), and d(kT) were subsequently analyzed.

5.2 Spectral estimation

Trend removal is recommended in Fourier analysis to prevent the misinterpretation of spectrum peaks caused by leakage, and to prevent leakage from masking more subtle phenomena. Therefore, linear regression lines were calculated for the sample sets x(kT), y(kT), and d(kT); and the trends, as given by the slopes of the regression lines ($\overline{Vx}$, $\overline{Vy}$, and $\overline{Vd}$ respectively) and their axis intercepts (Bx, By, and Bd respectively), were subtracted from each of them. The results were trend-free series given by:

$$X'(kT)=x(kT)-\overline{Vx}\ kT-Bx \tag{5.2}$$

$$y'(kT)=y(kT)-\overline{Vy}\ kT-By \tag{5.3}$$

$$d'(kT)=d(kT)-\overline{Vd}\ kT-Bd \tag{5.4}$$

k=0,1,... N-1
N=number of samples
T= sampling period

Bx =x axis intercept of linear regression line
By =y axis intercept of linear regression line
Bd =d axis intercept of linear regression line

The sets x'(kT), y'(kT), and d'(kT) were tapered with the Tukey window to further reduce leakage, producing tapered trend-free data sets x''(kT), y''(kT), and d''(kT) respectively. Computer memory space available with the power spectrum estimation program limited the data record to a maximum of 512 points. This was more than adequate, allowing a maximum resolution of the power spectrum of about .006 Hz (1/512T). As well, none of the data sets were longer than 350 points, well below this limit. Sufficient zeroes were added to the end of the data sets x''(kT), y''(kT), and d''(kT) to pad each out to a length of 512 points. This procedure increased the resolution of the resulting spectrum, and reduced the detrimental effect of the picket fence phenomenon.

The windowed trend-free data was then transformed from

the time to the frequency domain, utilizing the FFT algorithm as implemented by Munro (Munro,1971). The transform of 512 data points resulted in 512 unique Fourier coefficients, which sampled the frequency space from zero Hz up to one half the sampling frequency, in increments of 1/512T Hz. The periodogram, used as the estimate of the power spectrum, was calculated from the Fourier coefficients and plotted.

Using these procedures, power spectrum estimations were obtained from the x''(kT), y''(kT), and d''(kT) data sets obtained from one hundred and seventy-two trajectories tracked in a total of ten axons. A typical power spectrum consisted of several peaks below .3 Hz. The power above .3 Hz was very small compared to that at lower frequencies. It was concluded from the examination of a number of power spectra that the film framing rate (3 Hz) had been sufficiently high to reduce aliasing error to a very small value.

The power at low frequency in y''(kT) was typically one or more orders orders of magnitude smaller than that in x''(kT), and the d''(kT) power spectrum was almost identical to that of x''(kT). As the x component of particle motion was the one contributing to the net movement of the particles along the axon, it was the power spectra of the x''(kT) series, henceforth simply referred to as the 'power spectra', which were examined in detail.

To examine the differences, if any, between the power

spectra of somatopetal and somatofugal trajectories the average power spectra of each of the two trajectory populations was calculated from the power spectra of the individual trajectories. It was necessary when averaging the power spectra to introduce a scaling factor to compensate for the varying lengths of data from which the various spectra had been obtained. The average power spectra were calculated with the following equation:

$$\overline{\hat{S}}(mF) = 1/N_S \sum_{j=1}^{N_S} Kj\, \hat{S}j(mF) \qquad (5.4)$$

$m=0,1,2...N_T$

N_S- the number of spectra averaged

Kj- the scale factor N_T/Nj

N_T- the number of points in each spectrum

Nj- the number of samples of trajectory j

5.3 Determination of filter cutoff frequency

Instantaneous velocity estimates could have been obtained by wide band differentiation of the sampled trajectory data. However, with this method the effect of the very weak components in the trajectory at higher frequencies on the velocity estimates could have been at least as significant as that of the much stronger components at lower frequencies. Before proceeding with the estimation of particle velocities it was therefore necessary to make some assumptions concerning the relative significance of the

various frequency components of particle motion.

All power spectra indicated that the majority of power fell in the frequency band from 0 to .3 Hz. At frequencies above .3 Hz the power was typically three orders of magnitude less than that at lower frequencies. These components were due to a number of factors including observer error, digitizer error, random movements of the particle, film, microscope, and projector movement. Any component in the data due to measurement error was indistinguishable from that due to "real" random movement of the particle.

At frequencies below about .2 Hz the power due to measurement error was insignificant compared to the power due to particle motion, and hence had a relatively insignificant effect on the estimates of instantaneous velocity. However, at higher frequencies the power due to measurement error was estimated to be at least as great as that due to actual particle motion, and hence could introduce considerable error into the velocity estimates. Consequently it was necessary to remove or reduce the effects of the higher frequency components on the estimates of the instantaneous velocity. A low pass differentiating filter was used in the estimation procedure to accomplish this. It was recognized that the use of such a filter resulted in the components of particle motion above the cutoff frequency being discarded along with the components due to measurement error. The loss of these components of

particle motion was unavoidable. However, their loss was considered to be of minor consequence, as power due to them was so much less than the power at frequencies below the filter cutoff frequency.

If the average power level of the higher frequency components had been consistent from trajectory to trajectory, the filter cutoff frequency for each trajectory analysis could have been specified as that frequency below which the power in the spectrum rose above a level based on this average value. Unfortunately, the high frequency power varied with each trajectory, as one could track a small, sharply defined particle which remained clearly in focus with less error than a large, fuzzy, oval particle which dipped in and out of focus. Therefore, the filter cutoff frequency was established by other means.

Ten trajectories were digitized and their power spectra estimated. The percentages of total power falling below a number of cutoff frequencies were calculated for a group of trajectories, the results of which are plotted in figure 5.1. As the cutoff frequency was decreased, the percentage of total power remaining decreased in a nonlinear fashion. Decreasing the cutoff frequency from .5 Hz to .2 Hz did not substantially reduce the power for the majority of particles. However, as the cutoff frequency was reduced below .2 Hz the percentage of remaining power began to drop off more rapidly. The cutoff frequency was conservatively chosen to be .3 Hz, and for the sake of consistency the same

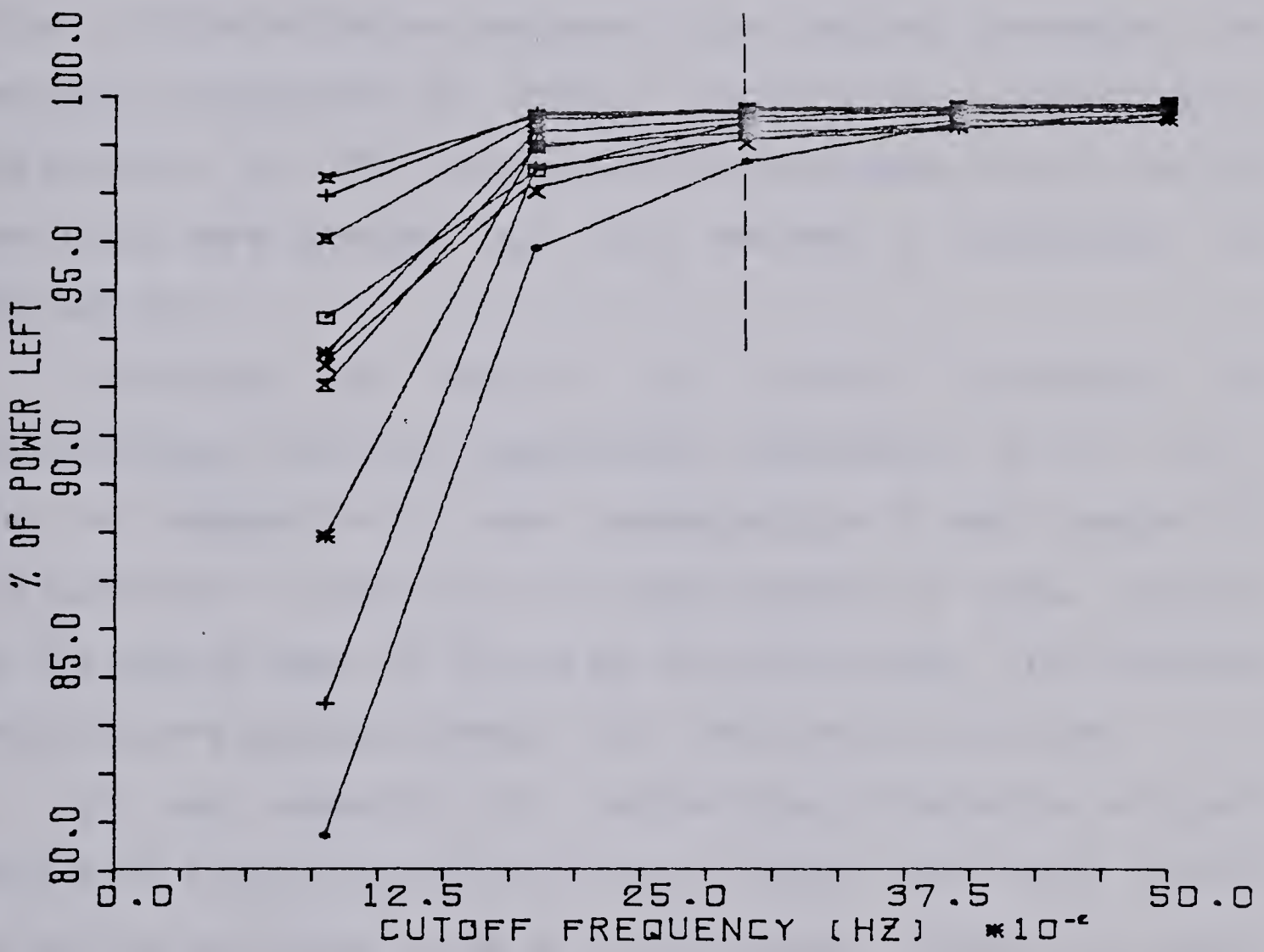

Figure 5.1 Effect of filter cutoff frequency on remaining signal power.

cutoff frequency was used for all particles. More than 99% of the power of the averaged spectral estimates lay below this frequency.

5.4 Velocity estimation by low pass differentiation

The optimum procedure for instantaneous velocity estimation of noisy simulations which closely resembled actual trajectories was assumed to be the best procedure for velocity estimation of actual trajectories. Accordingly, estimations of the average and instantaneous velocities of particles were carried out with method 2, developed in Chapter III.

Estimates of the x, y, and d components of instantaneous velocity (henceforth referred to as Vx, Vy, and Vd respectively) were computed for a small number of trajectories. In addition, the magnitudes and phase angles of the vector sums of Vx and Vy were calculated. The various results were plotted versus time, and versus position.

It was essential to extract the information of most relevance from this vast quantity of data. The vector sum of Vx and Vy was found to be of little value, since it posed serious problems in interpretation. A serious problem associated with Vd was its dependence on the initial coordinates of each set of trajectory samples. When examining the results from the small number of trajectories initially analyzed, it was seen that Vy was very small when compared with Vx, and in most cases had an insignificant

contribution to the net movement of the particle (and therefore presumably an insignificant contribution to fast axoplasmic transport). As Vx lay along the axis along which the axonal material transport occurs, it would seem to be the component of particle motion most closely related to this transport process. Therefore, it was decided that Vx best described the movement of particles in the context of the physiological process of interest (axonal transport), in an easily interpretable form. It was Vx, henceforth referred to as the "instantaneous velocity", which was therefore analyzed in detail.

Each particle moved predominantly in one direction (i.e. either somatopetally or somatofugally); movement and corresponding velocity in the predominating direction shall henceforth be referred to as in the particle's "major" direction. Movement and corresponding velocity in the direction opposite to the major direction shall be referred to as in the particle's "minor" direction. The instantaneous velocity of a particle (as given by Vx) moving in its major direction was defined to be positive; and in its minor direction, negative.

Instantaneous velocity estimations were computed for one hundred and seventy-two trajectories recorded from ten axons.

5.5 Error analysis

5.5.1 Position recording error

The digitizer error was found to correspond to ± .015 um (± 2SD, n=59) at the magnification used. The total error in estimating the position of a moving particle was conservatively estimated to be ± .08 um (± 2SD, n=226).

5.5.2 Velocity estimation error

The error in the velocity estimation method was estimated in two ways: (a) by analyzing simulations whose characteristics closely resembled actual trajectories, and (b) by redigitizing the film records of previously tracked trajectories and re-estimating the velocity. To determine the consistency of the estimation method the estimates thus obtained were compared with those obtained for the same particle in previous trials.

Analysis of simulated particle motion (Chapter III) indicated that the x and y components of particle instantaneous velocity could be estimated with a maximum error of ± .12 um/sec (± 2SD).

The difference in results obtained by redigitizing two trajectories and re-estimating their velocities are tabulated in table 5.1.

Method	N	Vx difference (um/sec)		Vy difference (um/sec)		Vd difference (um/sec)	
	(points)	Mean	S.D.	Mean	S.D.	Mean	S.D.
1	149	-2.8E-3	2.1E-1	-4.2E-3	1.8E-1	-2.9E-3	2.2E-1
2	149	+2.5E-3	3.1E-2	+1.3E-3	2.9E-2	+2.5E-3	3.1E-2
1	88	+7.8E-3	2.1E-1	-7.0E-3	2.4E-1	+7.2E-3	2.1E-1
2	88	+1.4E-3	1.9E-2	+5.3E-4	2.2E-2	+1.3E-3	2.1E-2

Table 5.1

As expected, the error of method 2 was approximately one order of magnitude less than that of 'method 1', and was well within the limits predicted by simulation analysis. Estimates of the instantaneous velocity (given by Vx, as previously discussed) obtained by digitizing a trajectory twice and repeating the velocity estimation using the two different methods may be seen in figure 5.2. Also shown is the difference between the estimates for each of the methods.

5.5.3 Effect of ignoring y and z components of position

Throughout this work the movement of particles in the axon was treated as being two-dimensional. Movement in the z direction; that is, in the direction perpendicular to the microscope's plane of focus, was entirely ignored, since it was impossible to measure.

It was, however, possible to estimate the magnitude of this movement through two approaches: (a) consideration of the optical characteristics of the cinemicrophotographic

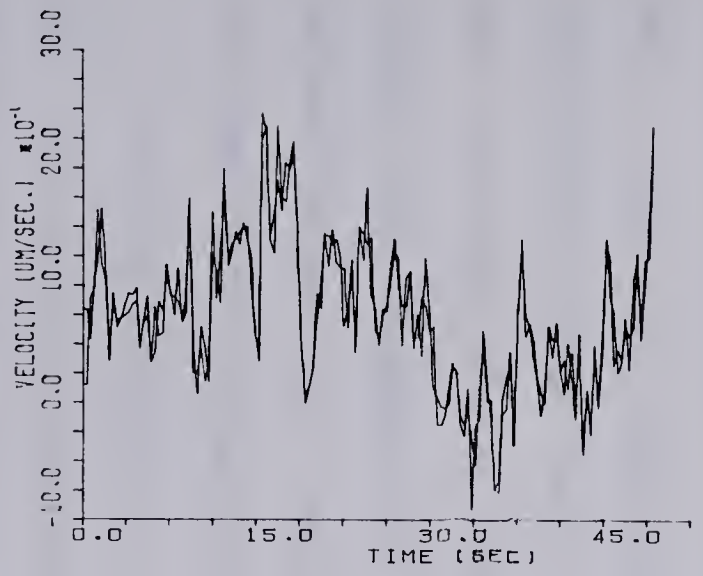

(a) Estimates of velocity with Method 1

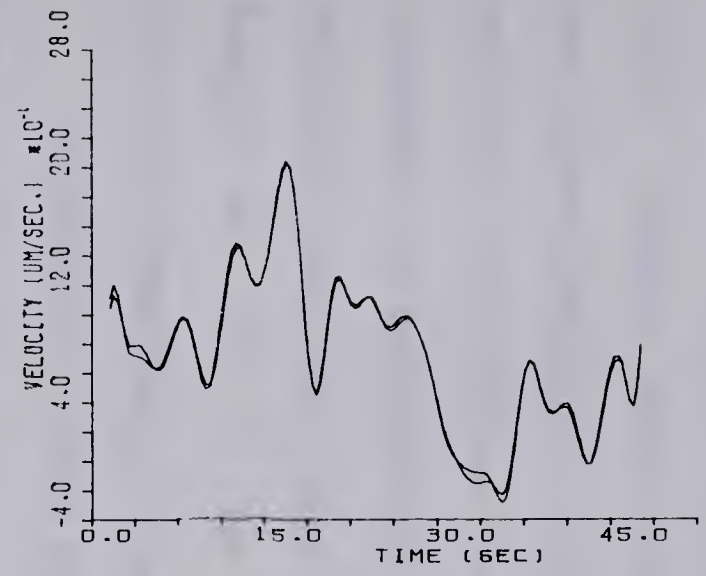

(b) Estimates of velocity with Method 2

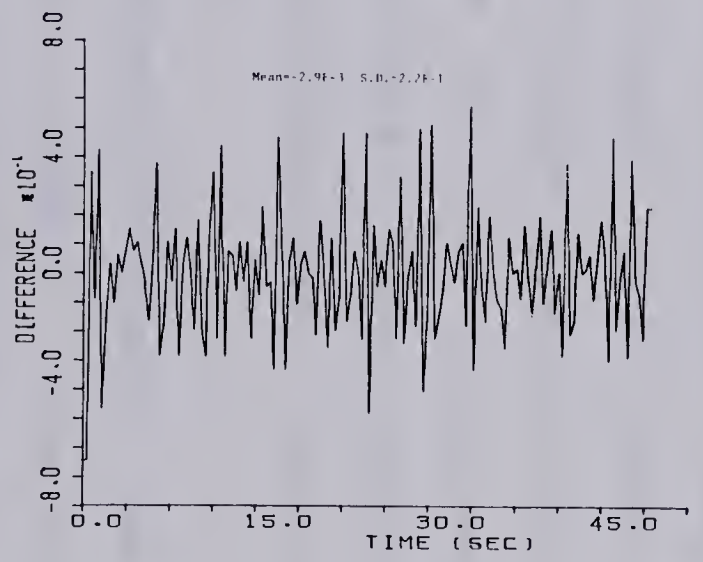

(c) Difference between estimates with Method 1

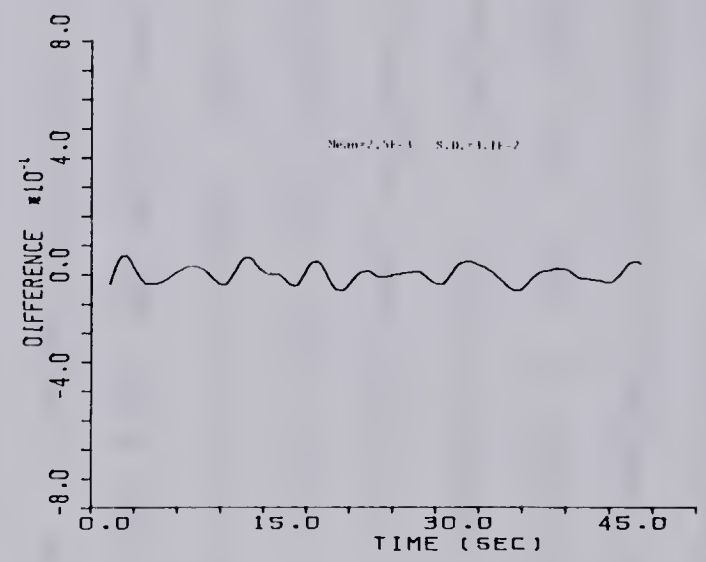

(d) Difference between estimates with Method 2

Figure 5.2

apparatus, and (b) consideration of the magnitude of the movement in the y coordinate.

It has been estimated (Smith, personal communication) that the depth of focus of the optical system used in this work through which these axonal particles can be discerned was approximately 1.5 um. That is, for a particle to be resolved for the entire length of its trajectory, its total movement in the z direction must be less than 1.5 um. This movement was small when compared with the typical trajectory length of 15 to 30 um and implied that the average z velocity component of such particles was very small.

To obtain a more quantitative estimate of movement in the z direction, movements of particles in the y coordinate were considered. It has been seen in this work that the displacements (and corresponding instantaneous velocity components) in the y coordinate were almost always at least one order of magnitude smaller than those in the x coordinate. Since the y coordinate arbitrarily determined the viewing plane through the axon it was reasonable to assume that movement of particles in the z direction, also perpendicular to the longitudinal axis of the axon, was of the same order of magnitude.

In this work the x component of velocity was used as the "particle instantaneous velocity". The error due to ignoring the y and z components of velocity was considered very small, and was conservatively estimated to be approximately ± .05 um/sec (± 2SD).

5.5.4 Conclusions of error analysis

The error in instantaneous velocity estimates as determined by retracking and reanalyzing several trajectories was approximately one half that of the error as predicted by the analysis of simulated trajectories. If the worst case is taken, and the error due to ignoring the y and z components of velocity is included, the error in the particle instantaneous velocity estimates used in this work is ± .17 um/sec (± 2SD).

5.6 Spatial Analysis

Many particle trajectories could be recorded from observation of an axon at a single location. In addition, the use of improved techniques in nerve preparation, cinemicrophotography, and analytical techniques enabled accurate estimation of the instantaneous velocities of a large number of particles in a single axon. These improvements in the quality and quantity of data available facilitated the examination of the spatial relationships between particle velocities. The scope of such spatial analysis is vast indeed, and the topic was therefore given only preliminary examination. It is hoped, however, that this work will suggest approaches for future trajectory analysis.

The topics of mapping and spatial analysis have been widely examined in the geographical and geophysical literature. However, many of the principles and techniques

thus developed have a wider scope and are suitable for use in other disciplines.

Associated with each instantaneous velocity estimate were corresponding x and y position readings. The data could be considered to be three dimensional, and was similar in concept to the data used in producing topographical contour maps. The x and y position readings corresponded to the geographical coordinates of the survey points; and the instantaneous velocity estimates to the elevation estimates. SURFACE II , a computer software system initially developed for use in topographical mapping, was found to be suitable for use in examining the velocity-position data.

SURFACE II was developed by the Kansas Geological Survey in the early 1970's. The system is quite general, and will display the form of any variable characterised by values at coordinates defined by two other variables. The only inherent restrictions are that the coordinate variables must be orthogonal, and the mapped variable must be single valued. A basic form of graphic display produced by SURFACE II is a contour map, a plot of the two coordinates on which values of the third variable are defined by lines of equal value.

The basis for all operations in SURFACE II is a rectangular grid of values, which is a numerical representation of the surface to be displayed. The grid is a numerical matrix whose elements are measurements of the z variable made at points identified by the two 'geographic'

coordinates, x and y. The contour plot representation of this matrix is obtained by linearly interpolating between grid nodes to locate the points where a contour line of specified value will cross the edge of a grid cell. The string of successive x and y coordinates of these intersections defines the contour line that will be drawn.

The velocity-position data consisted of points scattered irregularly over the 'map' area. Since the graphics display required a regular grid, the first procedure was to estimate such a grid from the irregularly spaced data.

There are two basic classes of methods for such grid estimation: global fit methods, and local fit methods. With global fit methods all data points are used in the estimation of each grid node value, whereas local fit methods assume that only the points in the "neighbourhood" of each node should be used in the estimation of its value. Global fit methods approximate the data values with three dimensional functions and use interpolation to estimate the values at the grid nodes; local fit methods estimate the node values with distance-weighted averages of the "nearest-neighbour" data points of each node. Local fit methods are generally considered to be the most appropriate for estimating points on complex surfaces (Sampson,1975), and were judged the most appropriate for use in the examination of spatial characteristics of particle velocities.

The "nearest-neighbours" of a grid node may be defined by a number of search techniques, some of which may provide "better" results than others in certain situations (primarily reflecting the nature of the data point distribution). For example, some methods may not be suitable when data points are collected along lines or traverses, as in the case of trajectory analysis. In such a case, a simple nearest neighbour search may find the specified number of points for an estimation entirely from a single trajectory. Such an estimate would be constrained in only one direction. The quadrant search technique, among others, is recommended in such cases to ensure some radial control in the estimation procedure (Sampson, 1975).

A quadrant search procedure divides the area around a grid node into four equal segments. The nearest n data points, where n is one of the search procedure parameters, are found in each segment, within a maximum search radius specified by another of the search parameters. If the distance to the nearest data point exceeds a specified distance, the search fails and the grid node is not estimated. Should less than a specified number of quadrants contain at least one data point within the maximum search radius, the search will fail and the grid node will not be estimated. Assuming the search has been successful, the value at the grid node is estimated by calculating a distance-weighted average of the data points found.

The x-y coordinate positions and corresponding

instantaneous velocities of forty two somatopetally moving particles, recorded in axon I, were stored on paper tape. This data was input to the University of Alberta Computing Services Amdahl 470 computer, and with the use of the SURFACE II software package, a number of contour maps were produced, using different algorithms and nearest-neighbours search techniques to estimate grids from the velocity-position data.

Rectangular grid matrices were estimated from the 4375 irregularly spaced x-y coordinate positions and corresponding instantaneous velocities. The matrices encompassed an area of 18 um by 38 um, and were evenly divided into 684 cells, each 1 um by 1 um. Selection of the cell size involved a tradeoff between minimizing computing time (i.e. using a small number of large cells), and maximizing spatial resolution (i.e. using a large number of small cells).

The quadrant search technique was used to estimate the values at the grid nodes from the velocity-position data. Determining suitable values for the search parameters required considerable planning, and a certain amount of trial and error. The estimation procedure in effect low pass filtered the data. Therefore, the area over which the data points were averaged had to be large enough to include samples from several trajectories, and yet small enough to be able to resolve localized variations in velocity.

The values used in the final analysis specified a

maximum search radius of 1.5 um. At least one point had to lie within 1.0 um of the grid node. A minimum of 3, and a maximum of 12, points were used to estimate the value at each node. The points selected by the search algorithm were weighted by the function 1/D (where D was the distance from the point to the grid node), and the value at the node obtained by averaging the weighted values.

CHAPTER VI

RESULTS OF THE ANALYSIS OF THE MOTION OF A GROUP OF INTRA-AXONAL PARTICLES

6.1 Spectral estimation

Examination of a number of power spectra indicated appreciable power at low frequencies. Above approximately .1 Hz the power in all cases rapidly decreased by more than two orders of magnitude to an insignificant level. At higher frequencies the power presumably arose from random components in the data, including all measurement error, and any "real" random movements of the particles which were indistinguishable from random error.

Two averaged power spectra were calculated from the power spectra obtained from the two trajectory populations (i.e. 133 somatopetal trajectories, and 39 somatofugal trajectories), and are plotted in figure 6.1. The shapes of the averaged power spectra for the two populations were similar. At low frequencies the average power of the somatopetal trajectories was somewhat more than twice that of the somatofugal trajectories, although at higher frequencies the average power of the two populations was the same.

6.2 Average velocities

The x, y, and d component average velocity estimates ($\overline{Vx}$, $\overline{Vy}$, and $\overline{Vd}$ respectively) were given by the slopes of

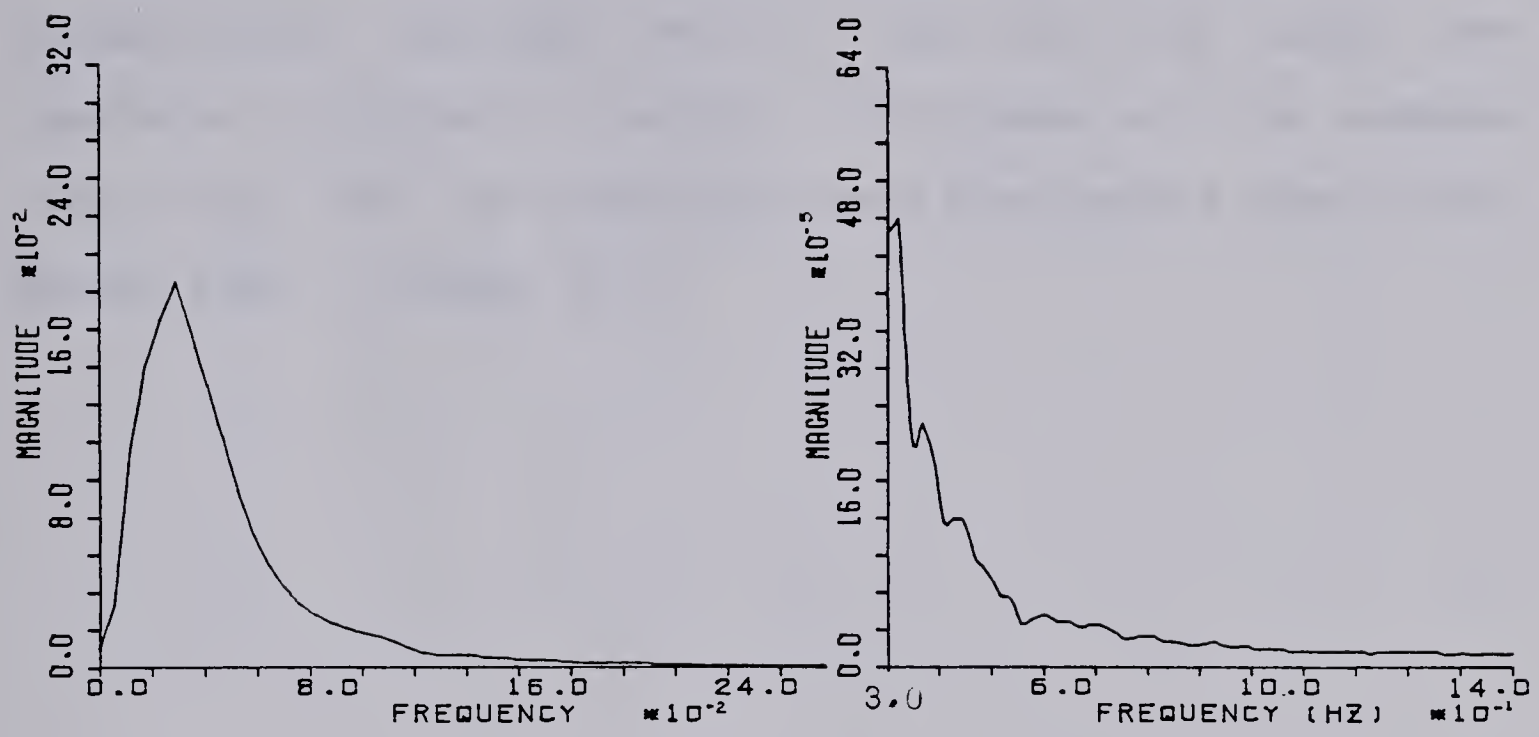

(a) Averaged power spectrum obtained from 133 somatopetal trajectories.

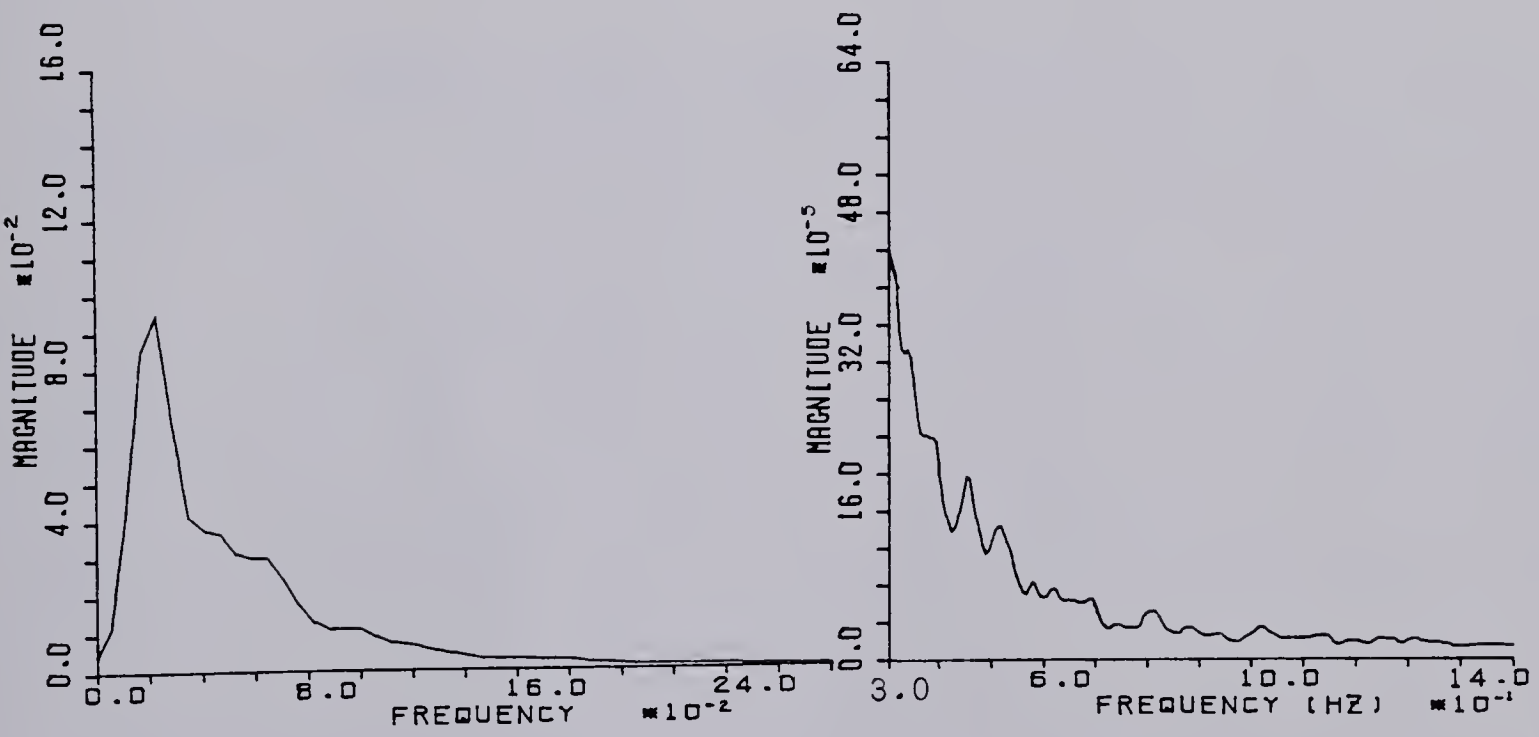

(b) Averaged power spectrum obtained from 39 somatofugal trajectories.

Figure 6.1 Averaged power spectra.

the linear regression lines of sampled sets x(kT), y(kT), and d(kT) respectively on time. The results for 172 particle trajectories recorded from a total of ten axons are tabulated in tables 6.1 and 6.2. Histograms of the average velocities for the somatofugal and somatopetal populations may be seen in figure 6.2.

Average velocity statistics by axon

Axon	Somatopetal Trajectories				Somatofugal Trajectories			
	n	Vx Mean (um/sec)	S.D.	Range min max	n	Vx Mean (um/sec)	S.D.	Range min max
A	10	.49	.38	.06 1.37	2	.98	.33	.75 1.21
B	10	.93	.41	.28 1.42	4	1.10	.62	.58 1.89
C	11	.83	.41	.30 1.44	2	.67	.06	.63 .71
D	10	1.07	.40	.57 1.91	3	.56	.14	.41 .68
E	10	.86	.34	.35 1.43	7	.67	.06	.59 .75
F	10	1.12	.35	.71 1.66	1	1.14	---	--- ----
G	10	1.16	.43	.39 1.68	3	.89	.42	.56 1.36
H	10	.91	.32	.45 1.41	3	1.01	.60	.63 1.71
I	42	.81	.32	.23 1.59	9	1.04	.60	.27 1.93
J	10	.98	.42	.32 1.81	5	1.07	.72	.25 1.95

Table 6.1

Pooled average velocity statistics

Component	Somatopetal			Somatofugal		
	Mean (um/sec)	S.D.	Range min max	Mean (um/sec)	S.D.	Range min max
Vx	.91	.38	.06 1.91	.93	.47	.25 1.95
Vy	.00	.11	-.29 .47	.02	.10	-.27 .32
Vd	.91	.38	.06 1.96	.93	.47	.25 1.94
	n=133			n=39		

Table 6.2

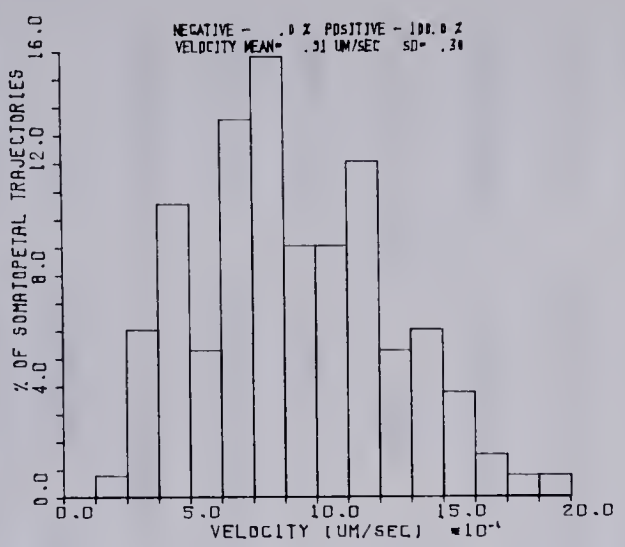

(a) Distribution of $\overline{Vx}$

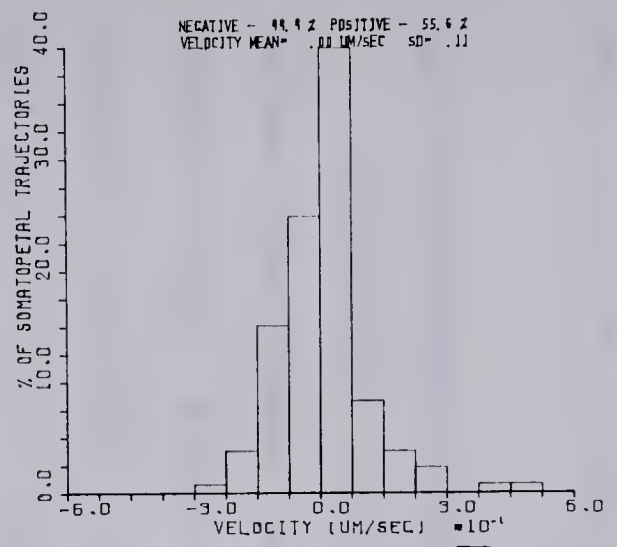

(b) Distribution of $\overline{Vy}$

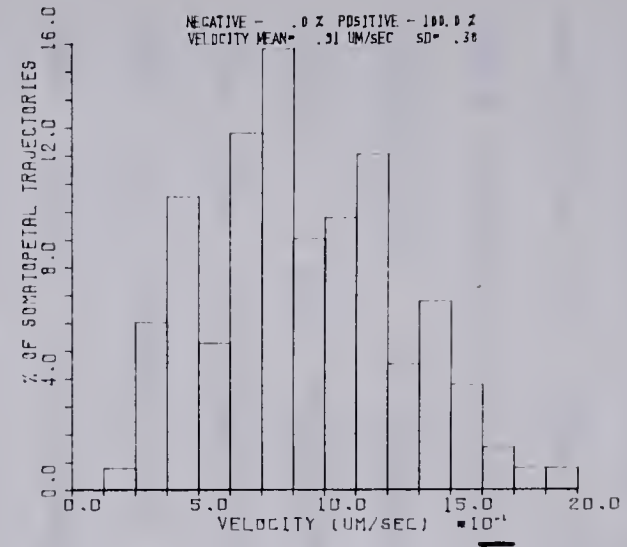

(c) Distribution of $\overline{Vd}$

SOMATOPETAL TRAJECTORIES

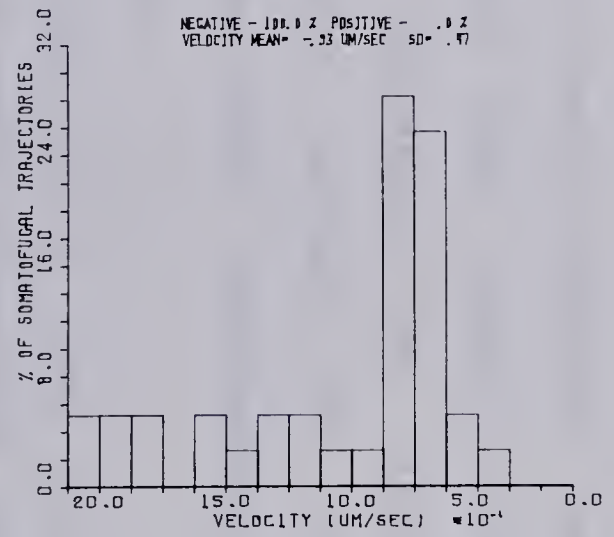

(d) Distribution of $\overline{Vx}$

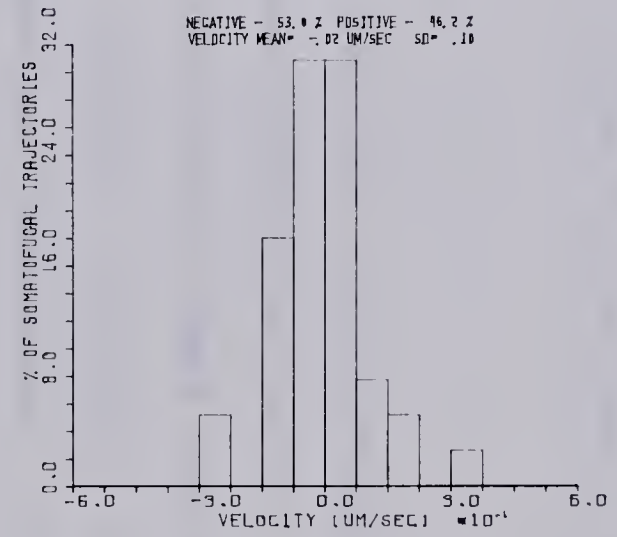

(e) Distribution of $\overline{Vy}$

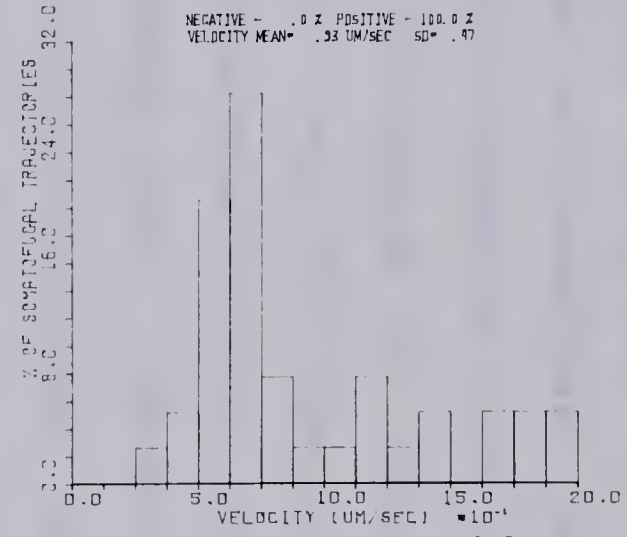

(f) Distribution of $\overline{Vd}$

SOMATOFUGAL TRAJECTORIES

Figure 6.2 Distributions of trajectory average velocities.

The somatofugal and somatopetal populations of trajectory average velocity were examined to determine the differences, if any, between them. Using the F test, the variances of the somatofugal and somatopetal populations were found to be significantly different at the 5% level. Therefore, to examine the difference in the population means, it was necessary to use a test which does not assume that the two population variances are the same. Using such a test (p.142,Neville and Kennedy,1970), the difference in mean velocities between the two populations was found not to be statistically significant at the 5% confidence level.

6.3 Instantaneous velocities

Examination of plots of particle instantaneous velocity versus time showed instantaneous velocities which smoothly varied (fig. 6.3(a),(b)). Intuitively these results seemed suspect, since the jerky or saltatory movement of axonal particles is a widely described phenomenon. If, however, plots of instantaneous velocity versus distance moved were examined, saltatory movements were clearly evident (fig. 6.3(c),(d)). Thus it was concluded that although the particles move in a saltatory manner with respect to position, their velocities are smooth, continuously varying functions with respect to time.

To examine the distribution of the instantaneous velocity estimates for each of the two particle populations the composite frequency distribution of instantaneous

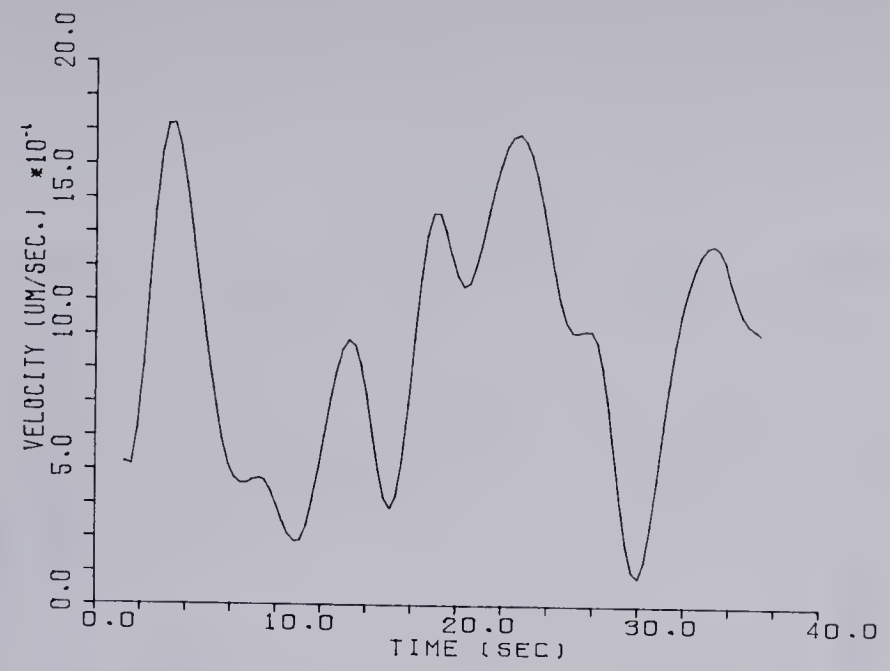

(a) Trajectory 1 - Plot of velocity vs time

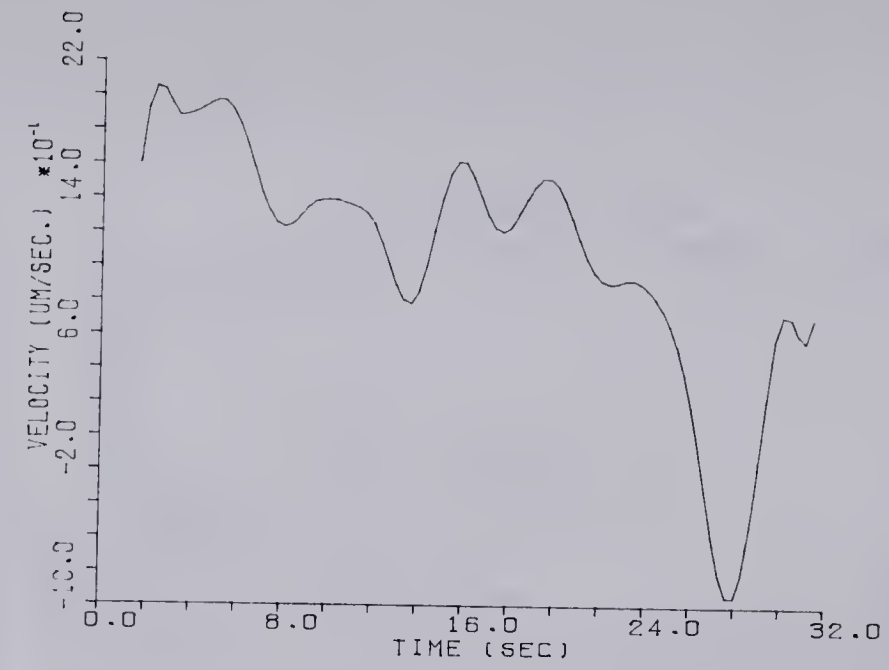

(b) Trajectory 2 - Plot of velocity vs time

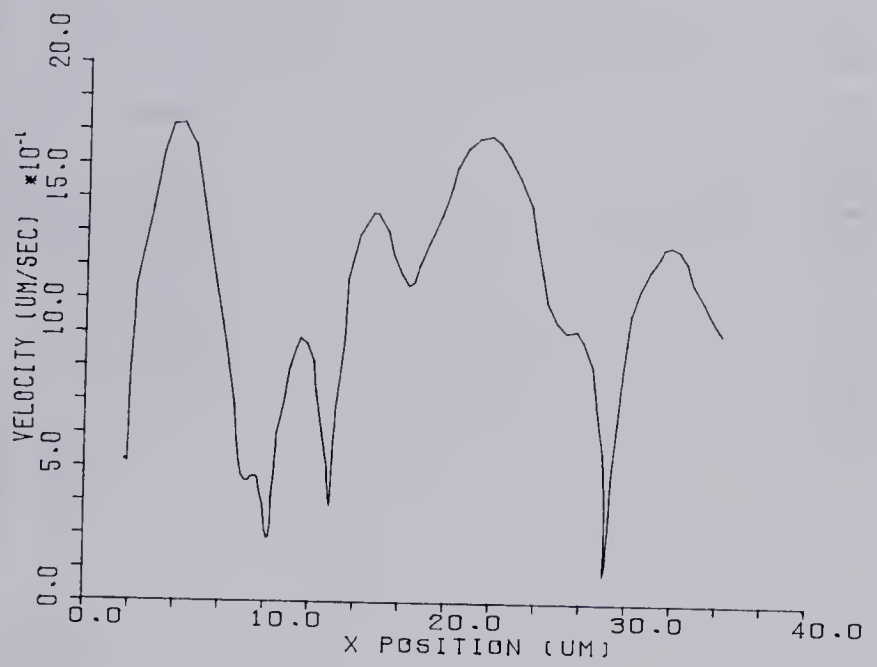

(c) Trajectory 1 - Plot of velocity vs position

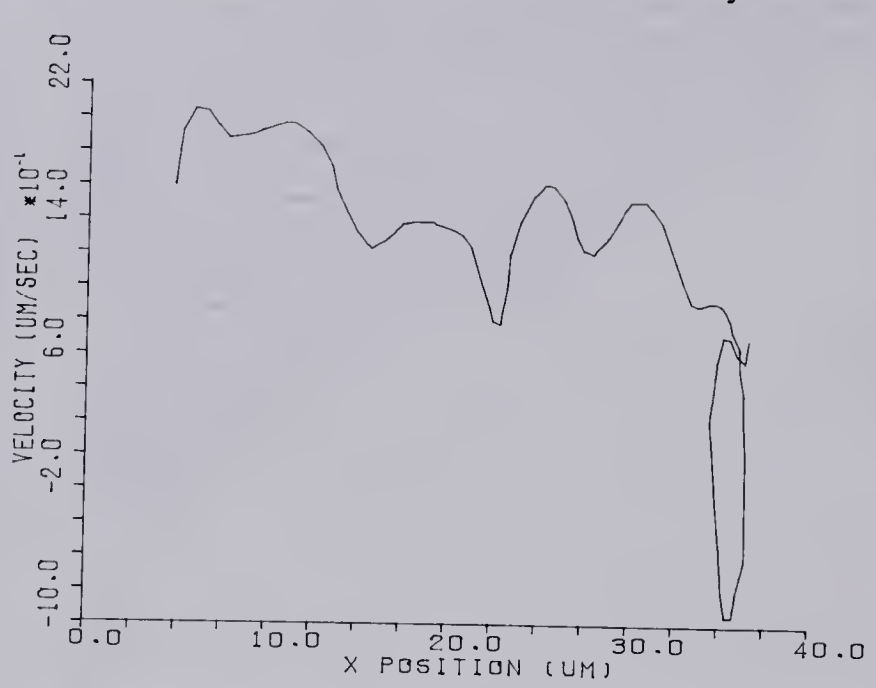

(d) Trajectory 2 - Plot of velocity vs position

Figure 6.3

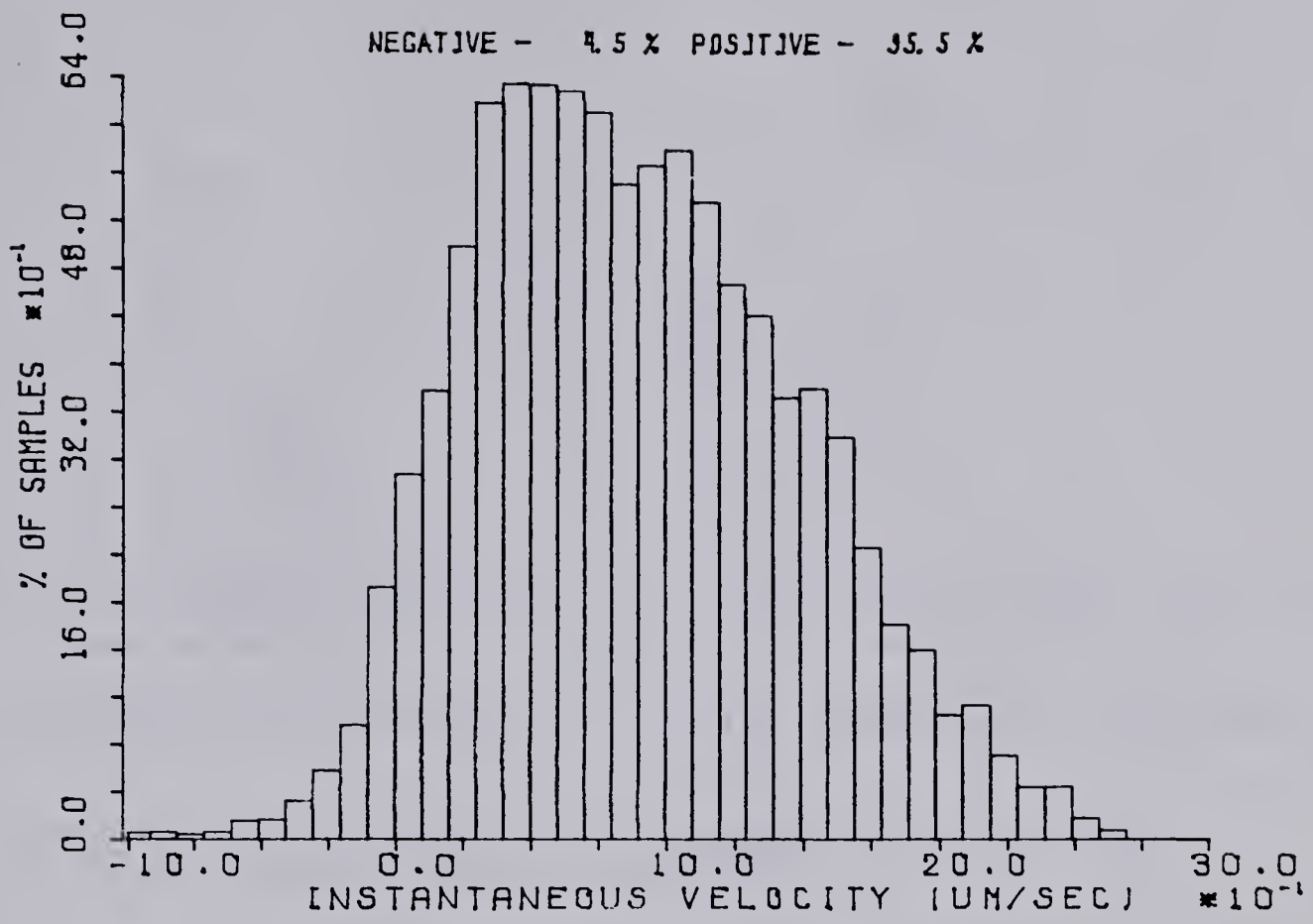

(a) Distribution of instantaneous velocity for somatopetal trajectories

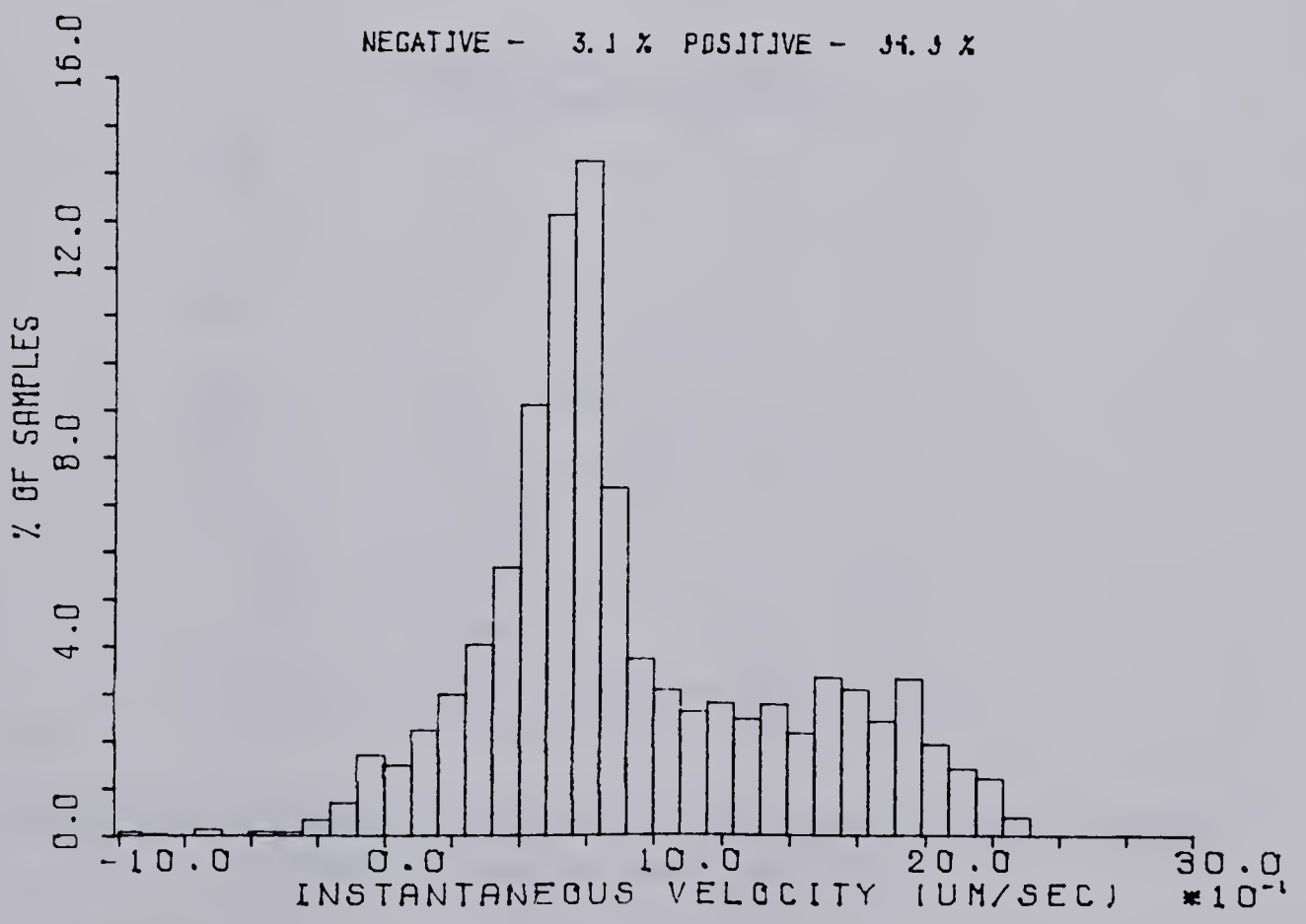

(b) Distribution of instantaneous velocity for somatofugal trajectories

Figure 6.4

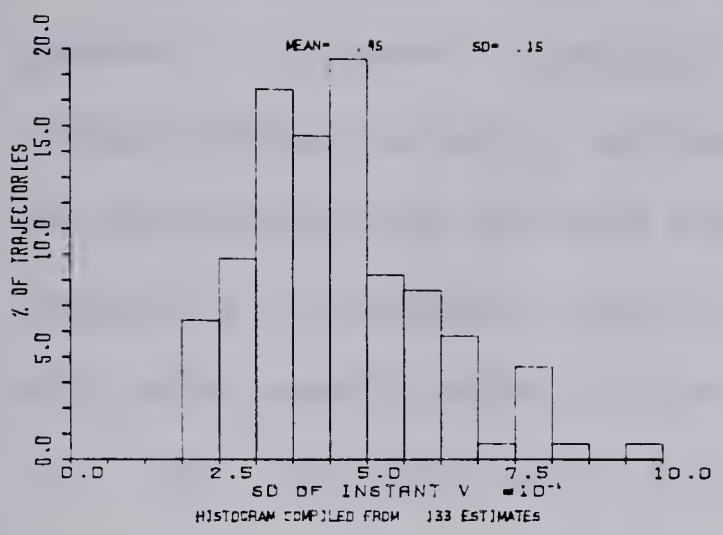

(a) Somatopetal trajectories

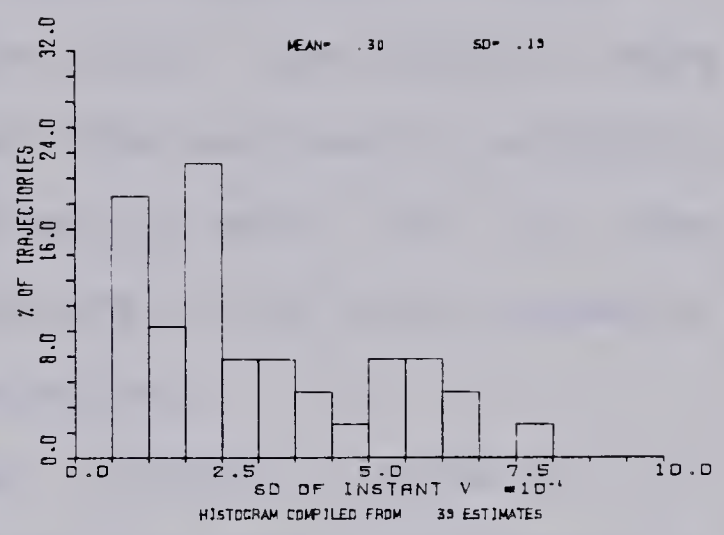

(b) Somatofugal trajectories

Figure 6.5 Distribution of the standard deviation of the instantaneous velocity.

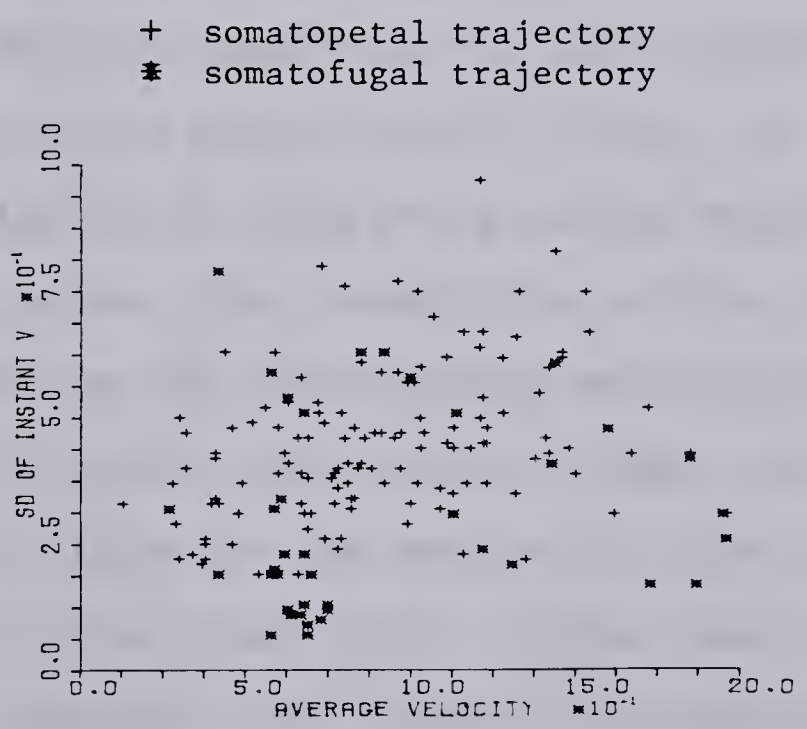

Figure 6.6 Standard deviation of the instantaneous velocity plotted versus the mean velocity.

velocity for each was computed (figure 6.4). It was necessary when computing the composite distributions to normalize the contributions of each trajectory, since in general slower moving particles contributed more instantaneous velocity estimates. This was done by weighting the contributions of each trajectory to each "bin" of the composite histogram by 1/N, where N is the total number of estimates contributed by the trajectory.

The distribution of the standard deviation of instantaneous velocity of each particle about its respective mean value for the two populations may be seen in figure 6.5. The mean of the somatopetal distribution is substantially greater than that of the somatofugal distribution, implying that on the average instantaneous velocity of somatopetally moving particles varies more widely than that of somatofugally moving particles.

To examine the relationship, if any, of the amount by which the velocity of a particle varied about its mean value to that mean value, the standard deviations of instantaneous velocity for the 172 trajectories were plotted versus their mean values (fig 6.6). The line of linear regression of the standard deviations on the mean velocities was computed, as was the correlation coefficient. These results indicated no correlation between the amount by which the instantaneous velocity of particles varied about their mean values and those mean values.

In the search for patterns or groupings in the movement

of particles it was essential to quantify their motion and to extract from the vast quantity of instantaneous velocity data available a small number of descriptive parameters.

An index of the net progress of particles, known as the vector-scalar ratio (VSR), has been defined by Breuer (Breuer et al.,1975). The VSR is the ratio of the net distance a particle moves divided by its total path length. The VSR may be considered as a measure of "efficiency" of particle movement. For example, a particle which never reversed its direction of movement would have a VSR of 1; at the other extreme, a particle which made no net movement would have a VSR of 0.

The VSR was calculated for each of the 133 somatopetal and 39 somatofugal trajectories. Histograms of the VSR's are plotted in figure 6.7. In figure 6.8 the trajectory VSRs are plotted versus the trajectory mean velocities, for the two populations. The line of linear regression of the trajectory VSR's on the mean velocities was computed, as was the correlation coefficient. Correlation was significant at the 99% level, and it was concluded that the smaller the average velocity of a given particle, the smaller its VSR.

Another parameter of interest was the percentage of time a particle spent moving in the minor direction (i.e. the percentage of velocity estimates which were negative for a given trajectory). Figure 6.9 illustrates the distribution of this parameter for the two trajectory populations. In figure 6.10 the percentages of time

(a) Distribution of VSR for somatopetal trajectories.

(b) Distribution of VSR for somatofugal trajectories.

Figure 6.7

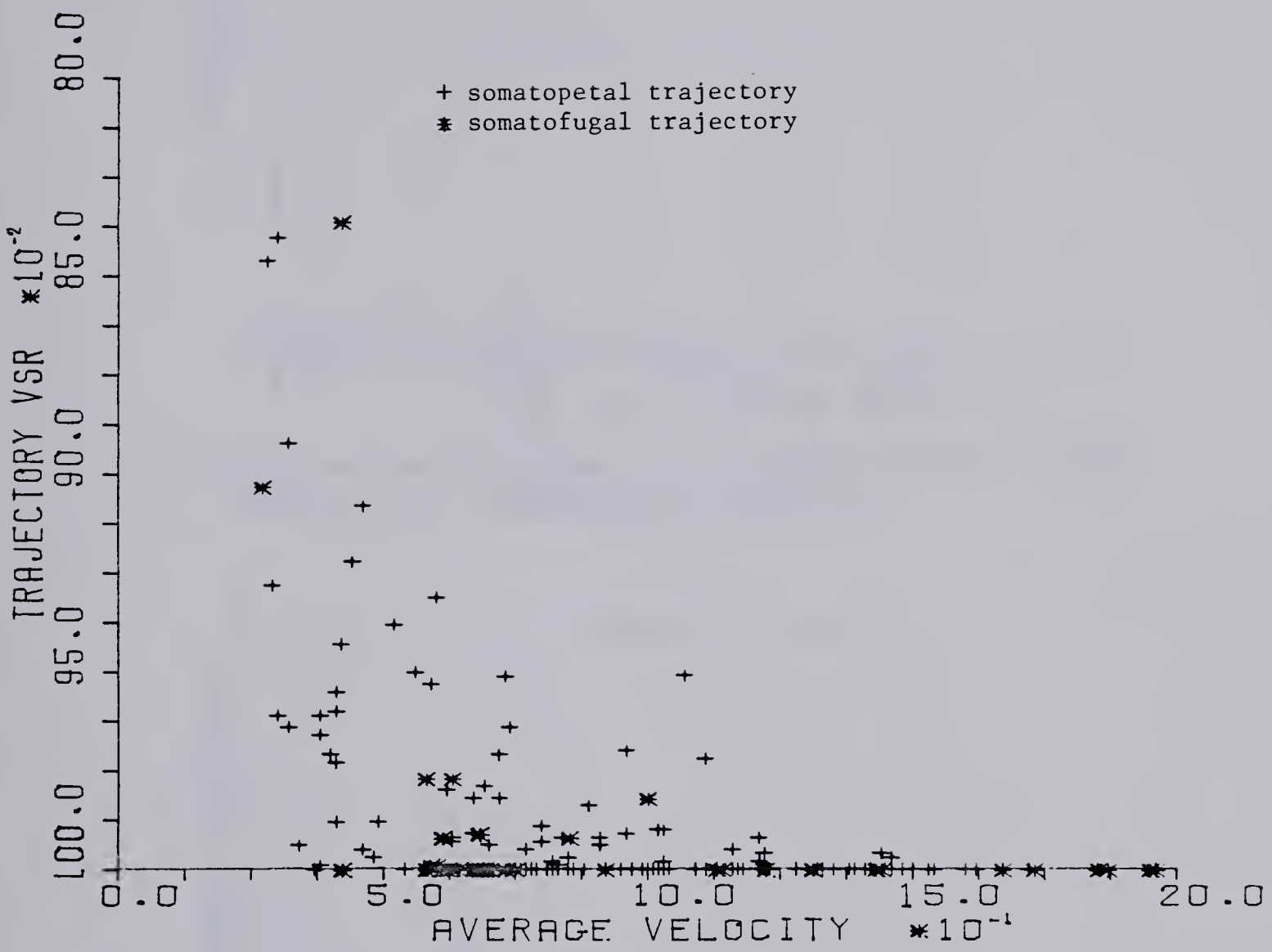

Figure 6.8 Relationship of trajectory VSR to average velocity.

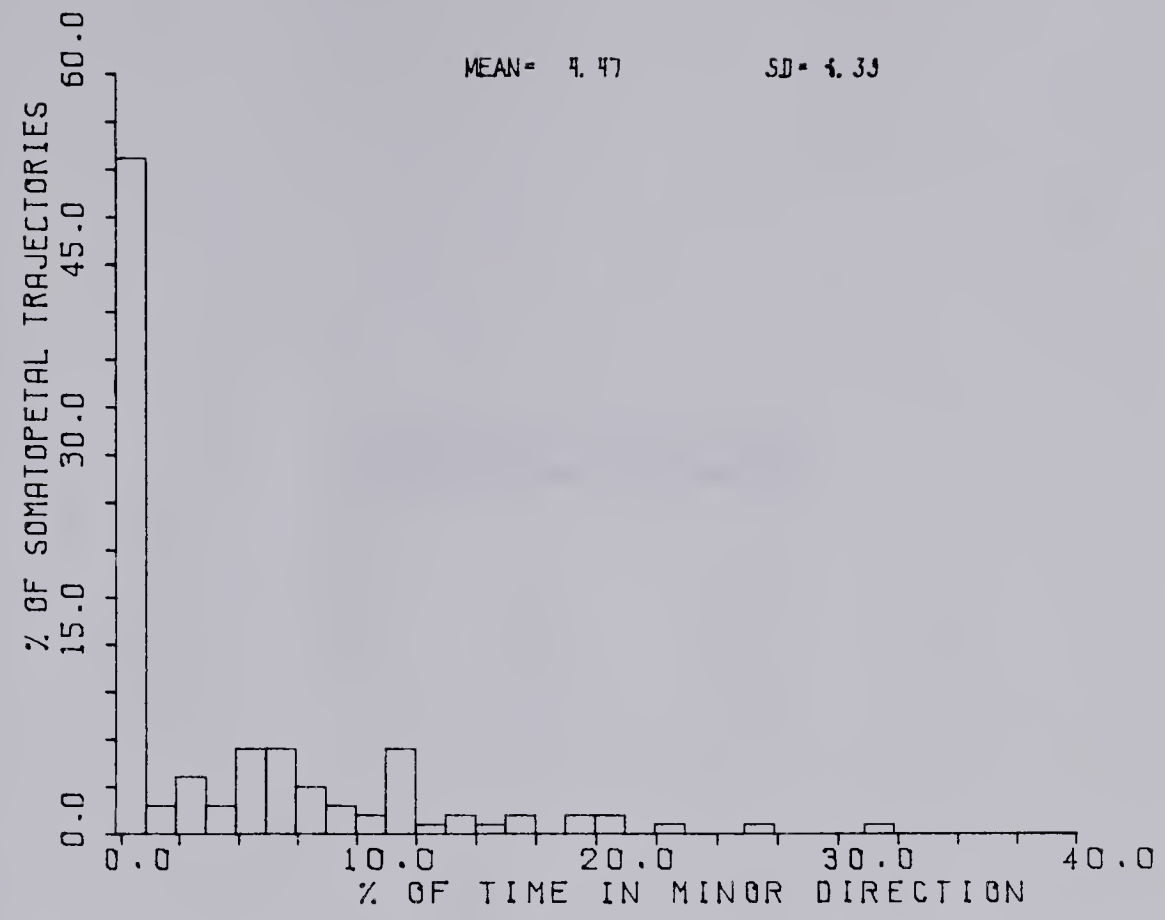

(a) Distribution of percent of time spent moving in minor direction for somatopetal trajectories.

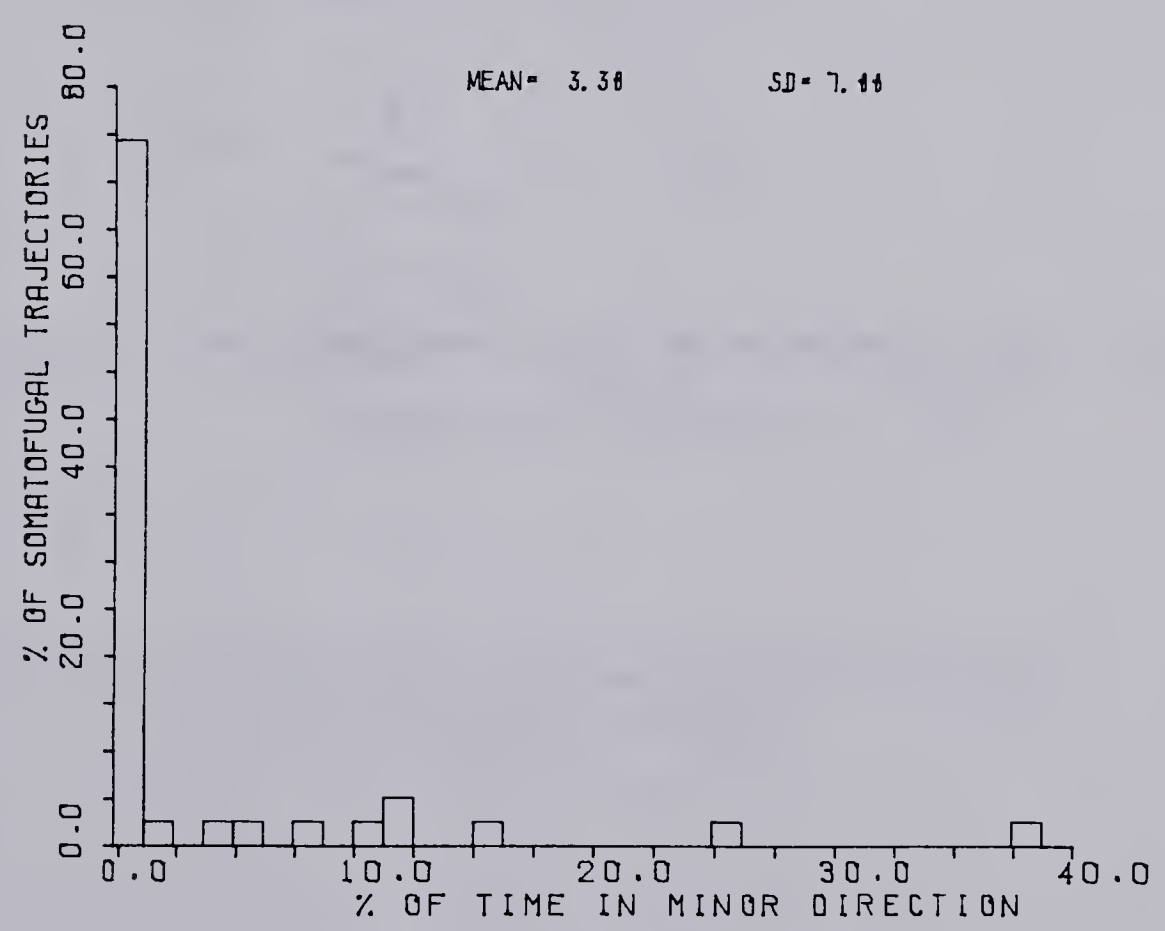

(b) Distribution of percent of time spent moving in minor direction for somatofugal trajectories.

Figure 6.9

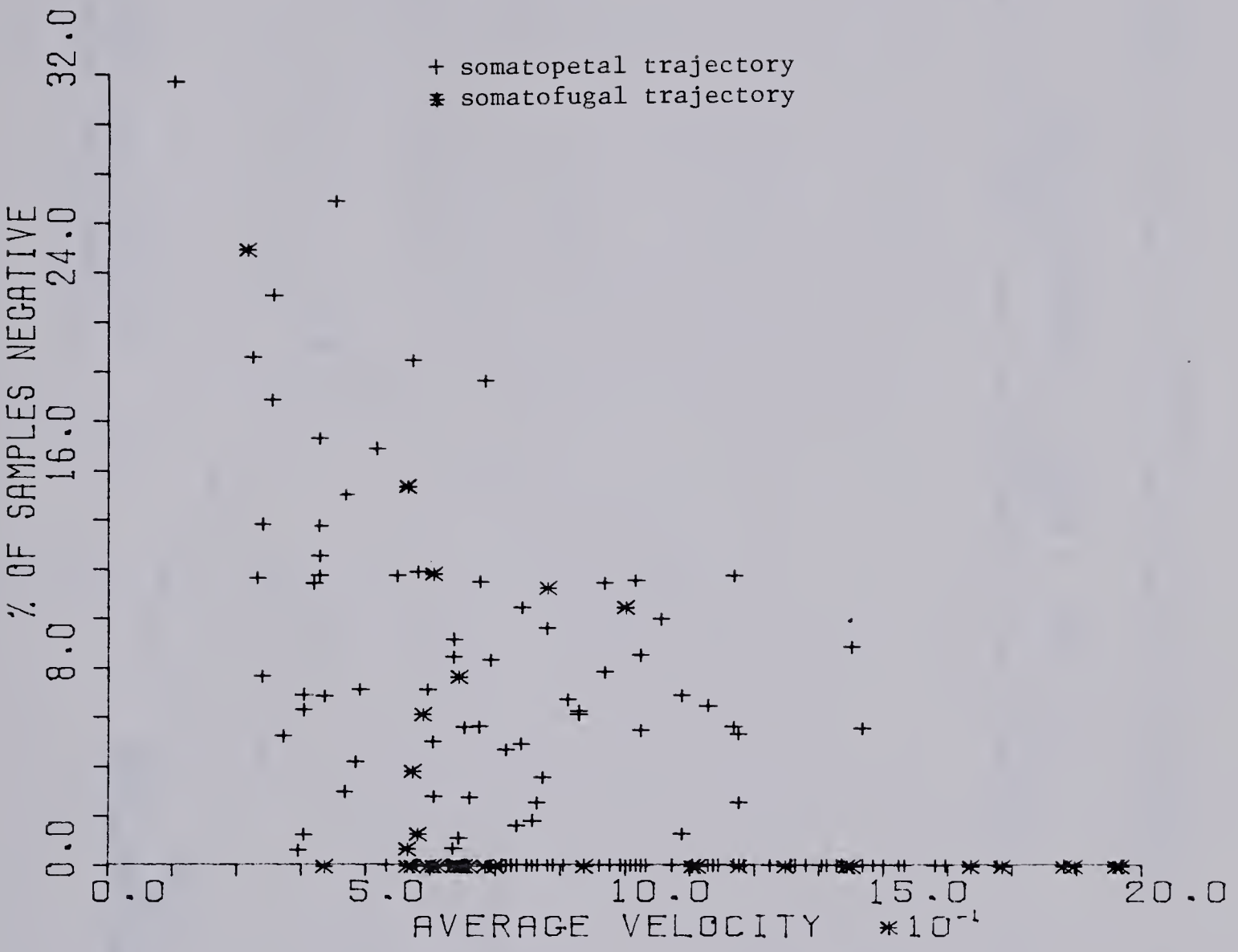

Figure 6.10 Relationship of time spent travelling in minor direction to average velocity.

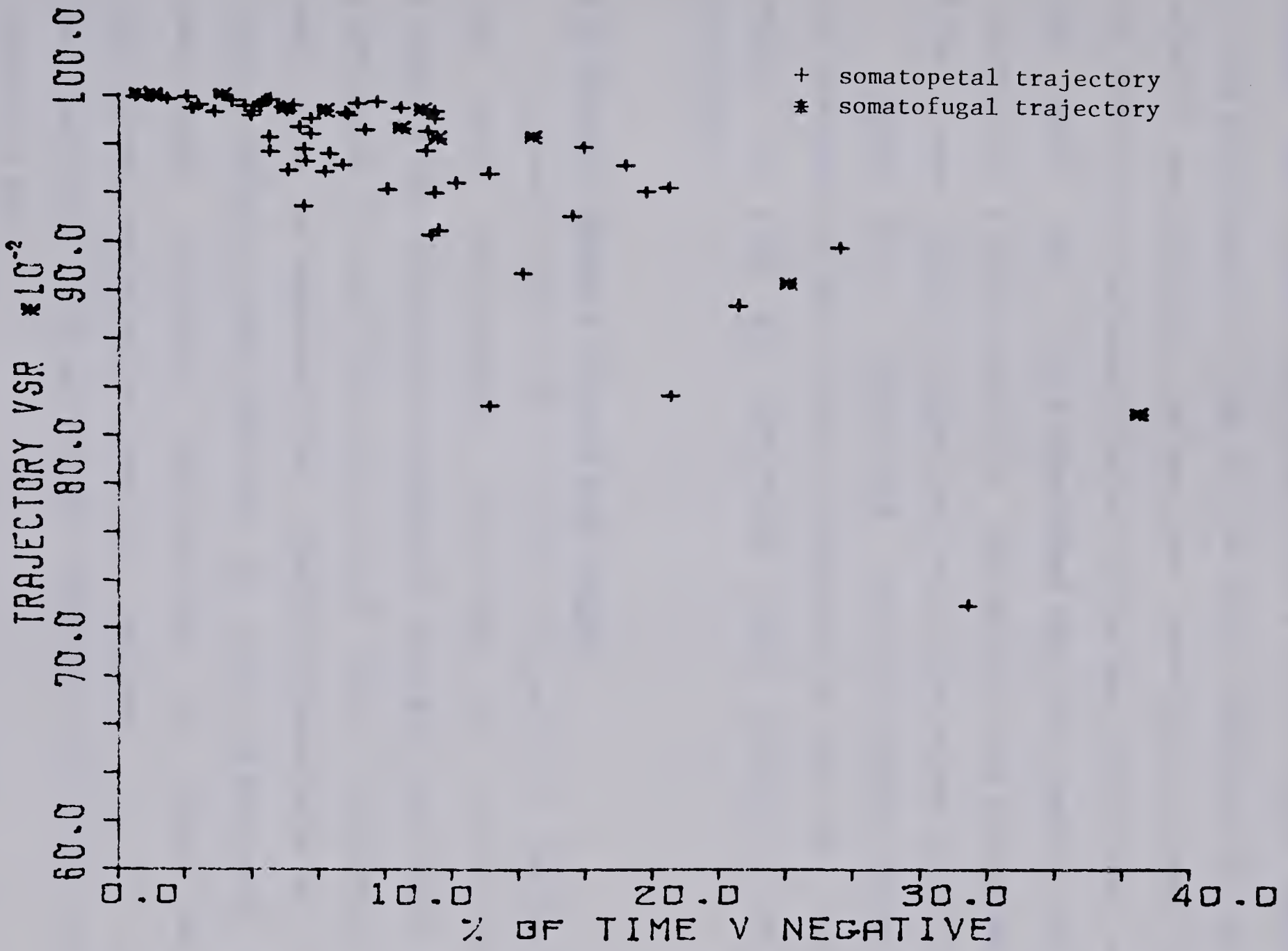

Figure 6.11 Relationship of trajectory VSR to the amount of time spent travelling in the minor direction

particles spent moving in the minor direction were plotted versus their mean velocities. The line of linear regression of the percentage of time in the minor direction on the mean velocity was computed, as was the correlation coefficient. The correlation between the variables was significant at the 99% level, and it was concluded that the smaller the mean velocity of a given particle, the greater the percentage of time it was likely to spend moving in the minor direction.

Figure 6.11 illustrates the relationship between the net movement of particles (as measured by the VSR), and the amount of time the particles spent moving in the minor direction.

6.4 Spatial aspects of particle motion

Figures 6.12(a)-(d) are plots of particle trajectories and their corresponding velocities for four pairs of trajectories. Each pair represents two particles whose paths overlapped in space for a portion of their trajectories. In each pair of observations a similarity was apparent in the velocities over those portions of the trajectories which overlapped. Although similarities in velocities of overlapping trajectories were not apparent in all cases, they occurred with sufficient frequency to warrant further investigation.

It can be hypothesized that particles in the same spatial location in the axon move with similar velocities. This would be expected if the force generating mechanism

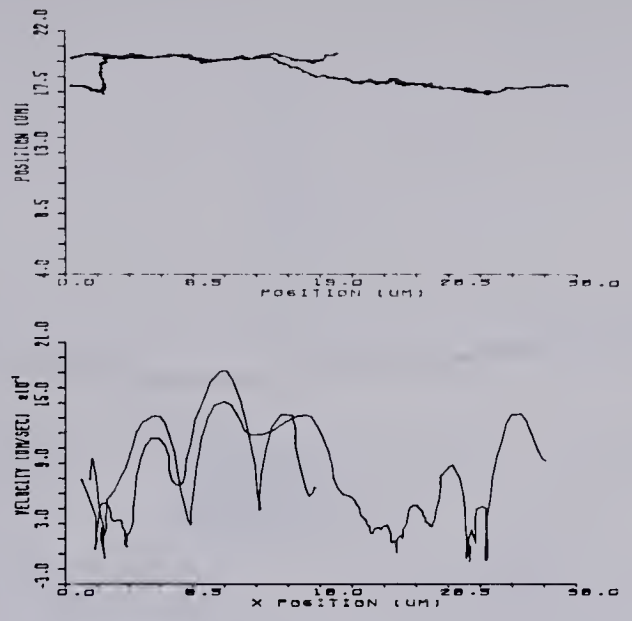

(a) Pair 1

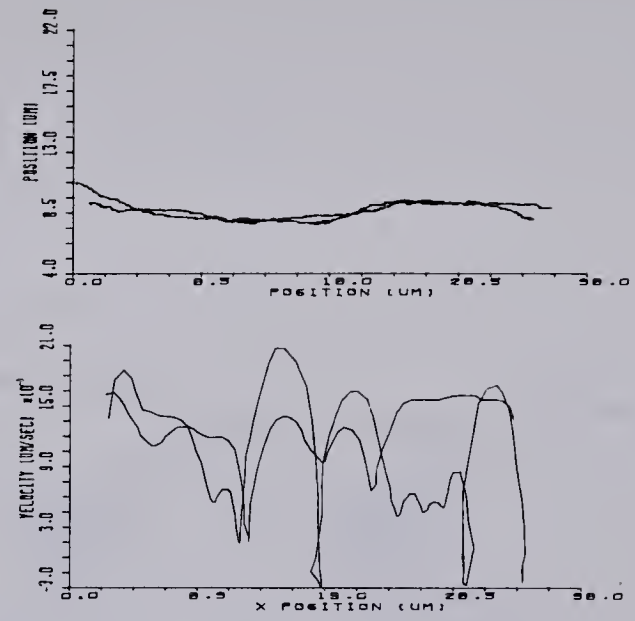

(b) Pair 2

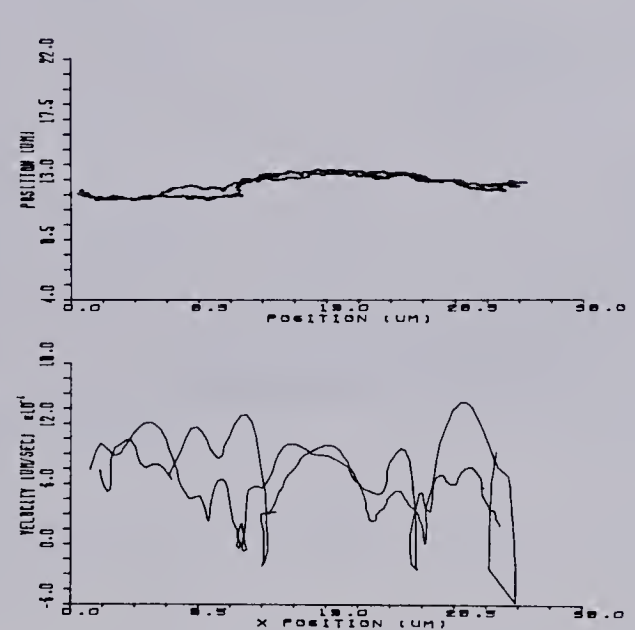

(c) Pair 3

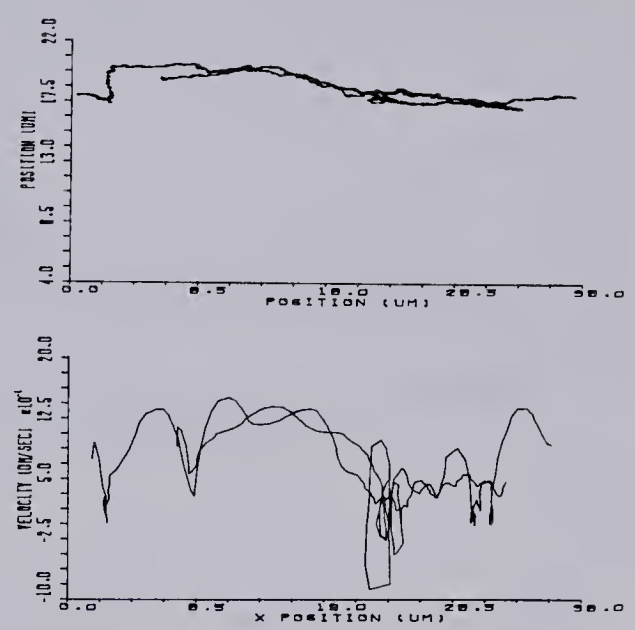

(d) Pair 4

Figure 6.12 Overlapping trajectory pairs and their corresponding instantaneous velocities.

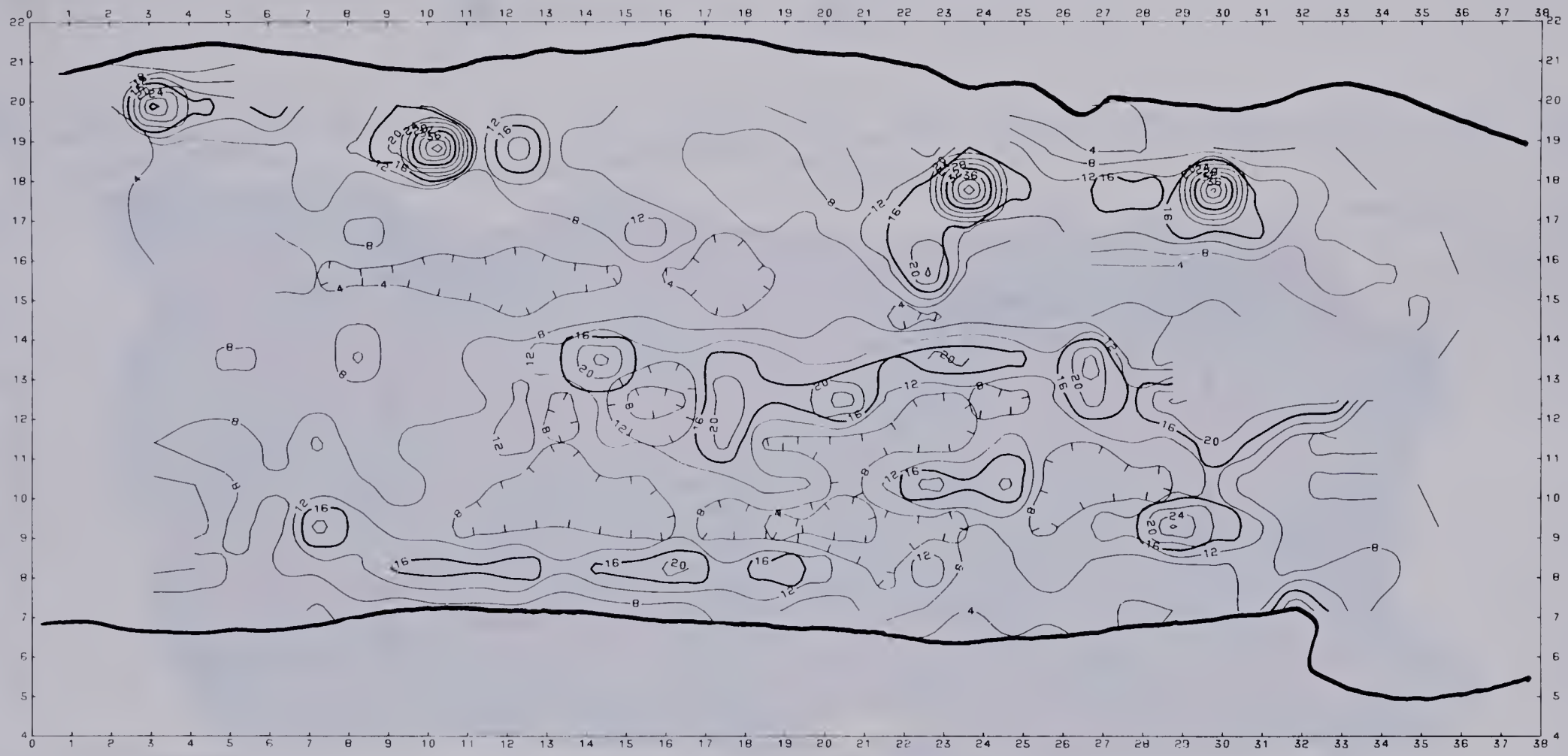

Figure 6.13 Contour map representing spatial distribution of particle position measurements and corresponding instantaneous velocity estimates.

Velocity Legend

	.00-.25 um/sec		1.00-1.25 um/sec
	.25-.50 "		1.25-1.50 "
	.50-.75 "		1.50-1.75 "
	.75-1.00 "		1.75-2.00 "

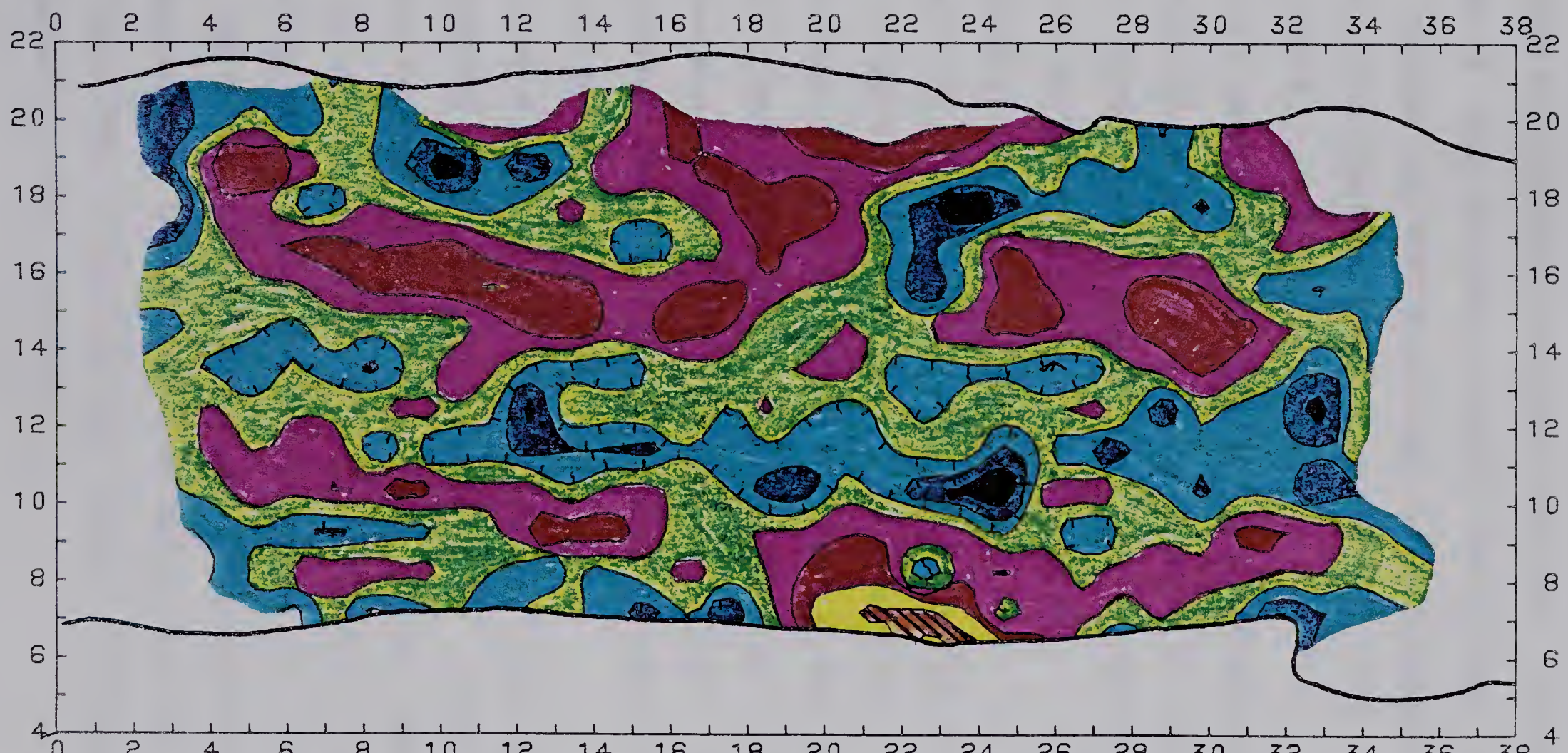

Figure 6.14 Contour map representing the spatial distribution of particle instantaneous velocities.

responsible for particle motion consisted of discrete, "stationary" sites distributed throughout the axon. It would also be the case if the particle axonal velocities were significantly related to local variations in the properties of the axoplasm. This hypothesis was investigated with the use of contour plots.

Figures 6.13 and 6.14 were obtained by analyzing 4375 estimates of velocity obtained from 42 somatopetally moving particles in axon 'I'. Figure 6.13 is a graphical representation of the distribution of data points, i.e the geographical density of the velocity estimates. It was obtained by computing the number of velocity estimates lying within .707 um of each grid node, and then computing and plotting a contour map of the number of points around each grid node versus x and y position. The search radius for the density estimates was chosen to be .707 um to ensure that all the area between the grid nodes (spaced 1 um apart) was covered, with minimal overlap.

The velocity-position contour plot shown in figure 6.14 attempts to display graphically the combined velocity results for forty two somatopetally moving particles. Should the velocity of each particle be totally unrelated to that of other particles moving in the same region in the axon, the velocity estimates at the grid nodes should be quite similar. The contour plot would therefore consist of only a few contour lines. This is not the case however, implying a correlation between position and velocity.

As can be seen from figure 6.14, the velocities of particles averaged in various regions of the axon, ranged from 0.0 um/sec to 2.0 um/sec. Areas of similar velocities varied considerably in size, and were longitudinally arranged with respect to the axon. There were no obvious relationships between these areas and optically discernible axonal structures such as the rod shaped mitochondria.

A similar examination of spatial aspects of somatofugal particle motion could not be conducted since insufficient measurements were available in individual axons.

CHAPTER VII

DISCUSSION AND CONCLUSIONS

7.1 Introduction

The preceding chapters have outlined the analysis of axonal particle movement by a variety of methods. This chapter shall compare the results thus obtained with those of other workers in the field, and shall attempt to draw some conclusions on the nature of axonal particle motion.

7.2 Spectral analysis

In their analysis of axonal particle movement, Forman's group (Forman et al,1977a) searched for periodicity in the instantaneous velocity estimates of 61 individual particles by means of autocorrelation and spectral analysis. They reported that the results were inconclusive, with no conspicuous or consistent patterns emerging. In retrospect this is not suprising, since the instantaneous velocity estimates had been obtained with the incremental distance method, and hence contained considerably amplified noise. The power at higher frequencies due to the noise in the velocity estimates could be at least as great as that at lower frequencies due to both noise and actual particle motion. Any underlying periodic components at low frequencies would not be obvious.

In this work the power spectra of 172 particle trajectories were analyzed. Any consistent periodic

component in the motion of the particles would be evidenced by peaks in the autopower spectra of the trajectory and velocity estimates. The trajectory power spectra were estimated in the manner previously described.

The considerable differences in the spectral estimates obtained with the two different methods (i.e. Forman's vs McLeod's) may be seen for two trajectories in figures 7.1(a)-(d). Figures 7.1(a) and (b) are spectral estimates obtained by analyzing two trajectories. Figures 7.1(c) and (d) were obtained by estimating the instantaneous velocities of the same two trajectories using the incremental distance method, and then analyzing the velocity estimates. The power at higher frequencies due to the accentuated noise in the velocity estimates is evident.

The trajectory power spectra suggested a general pattern in the motion of particles. Particle motion was consistently composed of low frequency components, typically in the range of from 0 to .2 Hz. Above .2 Hz the magnitude of the frequency components was much smaller. Thus it was concluded that the particles moved with an underlying low frequency periodic motion, whose period, although varying from particle to particle, was consistently longer than 5 seconds. It was also evident that a filming rate of 3 fps was more than sufficient to record the major details of particle motion.

The peak power of the averaged power spectra of the somatopetal trajectories was found to be somewhat more than

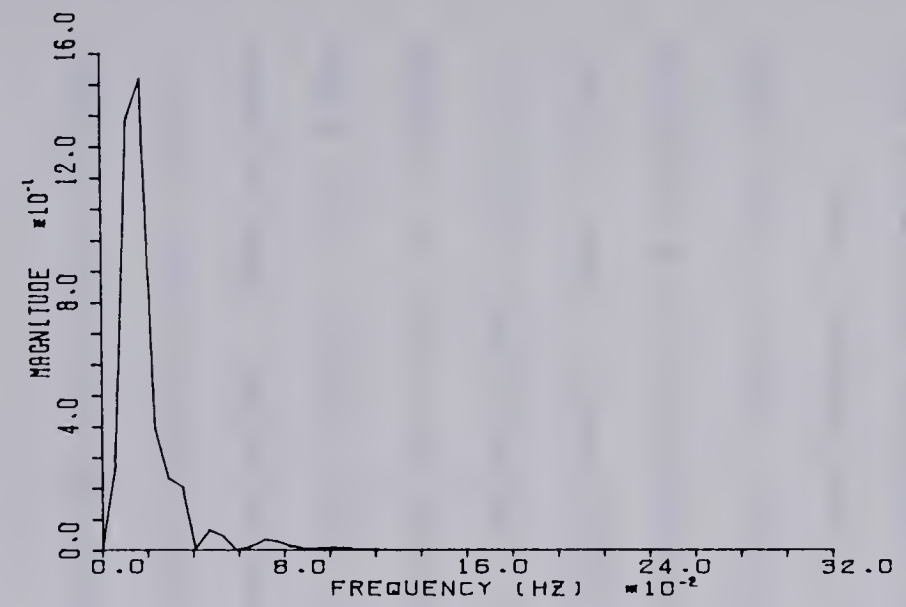

(a) Trajectory 1 - Displacement power spectrum obtained with procedure developed in thesis.

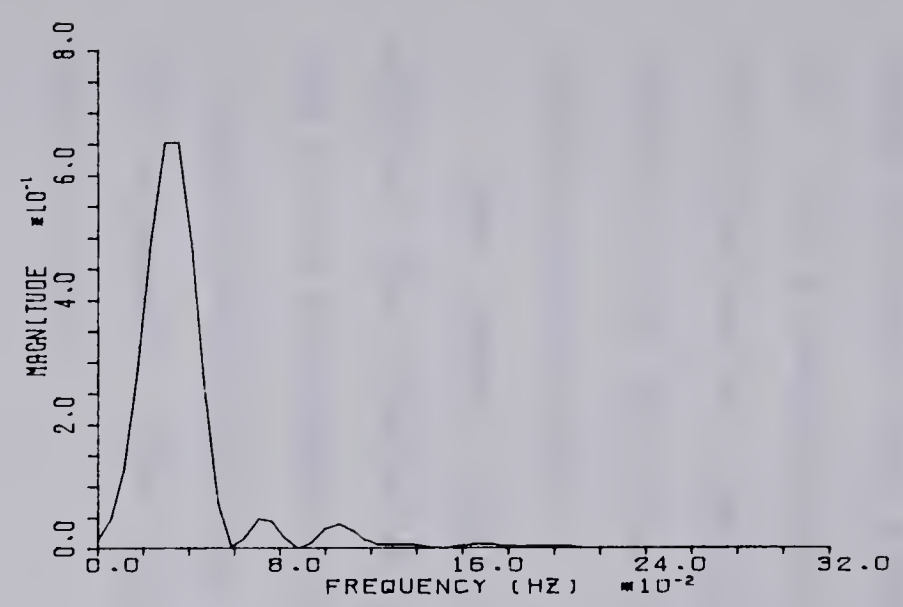

(b) Trajectory 2 - Displacement power spectrum obtained with procedure developed in thesis.

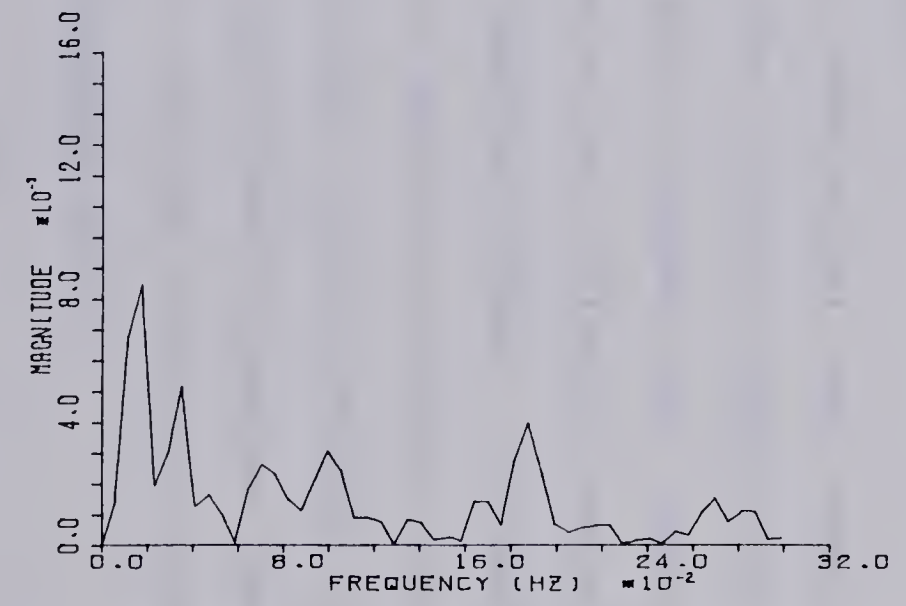

(c) Trajectory 1 - Velocity power spectrum as obtained with Forman's procedure.

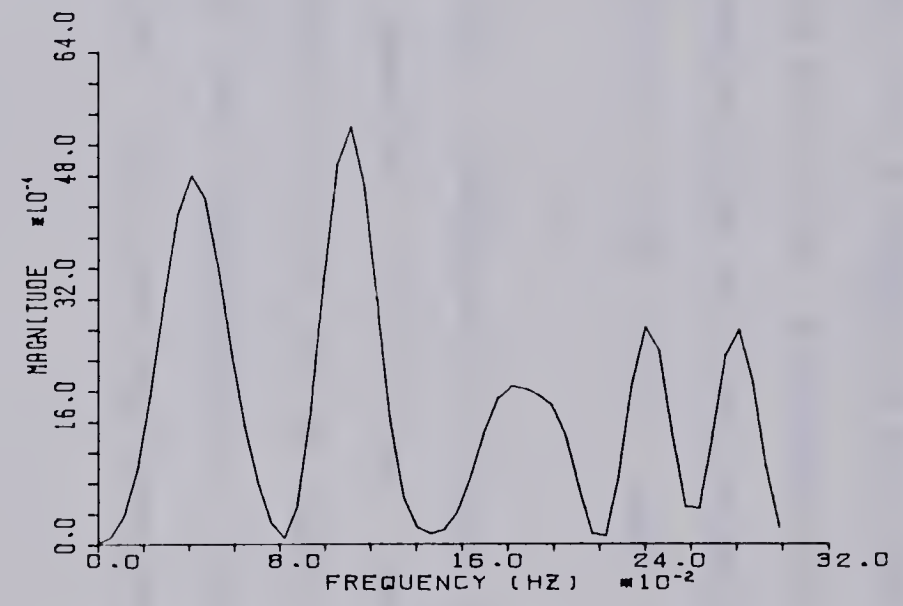

(d) Trajectory 2 - Velocity power spectrum as obtained with Forman's procedure.

Figure 7.1

twice that of the somatofugal trajectories. This implies that the instantaneous velocity of a somatopetal particle tends to vary more widely about its average value than does that of a somatofugally moving particle. Examination of the distribution of the standard deviations of the instantaneous velocity for the two populations (fig 6.5) leads to a similar conclusion.

The power spectra of the x component of position was used as the "trajectory power spectra". Since the power in the y and presumably the z components was two or more orders of magnitude less than that in the x component in the region of interest, the consequences of ignoring them were not significant.

7.3 Particle average velocities

The average velocities of somatofugal and somatopetal particles were similar to the values reported by other workers with similar preparations (Cooper and Smith,1974; Smith and Koles,1976; Forman et. al.,1977a,b) and observed in intact myelinated axons (Hammond,1977a). Although the means of the two populations of particle average velocities were not significantly different, the variance of the somatofugal population was significantly greater than that of the somatopetal population. This was consistent with the results reported by Hammond (Hammond,1977a).

7.4 Velocity estimation method

Analyses of both simulated and actual particle trajectories have clearly shown the advantages of the method developed in this thesis for the estimation of particle instantaneous velocity over the method found in the literature. It was felt that the reduction of the estimation error by at least one order of magnitude more than compensated for the loss with this method of approximately 10% of the results. With more accurate estimation of instantaneous velocity can come more sophisticated and more comprehensive analysis of particle instantaneous velocity.

As discussed previously for practical reasons in this work the x component of velocity was used as the particle instantaneous velocity, and the y and z components were ignored. The error due to ignoring these components was found to be very small. This approach must be used with care however, since in a very small number of cases (2-4%) particles were observed to make substantial movements in the y direction. Workers in the future may wish to examine such trajectories as special cases using more detailed analysis. Substantial movement in the z direction was not a problem, as in such cases the particle would leave the thin focal plane of the filming apparatus (disappearing from view) and hence the trajectory record would end.

7.5 Particle instantaneous velocities

A primary objective of the study of axonal particle movement has been to understand the mechanisms responsible

for this motion. The relative magnitude of the inertial and viscous forces acting on a particle can be estimated with the Reynolds number, which gives the ratio between the inertial and viscous forces acting on a body.

$$R = \frac{LV\rho}{z} \qquad (7.1)$$

V - velocity of the object
z - dynamic viscosity of the medium
ρ - density of the surrounding medium
L - characteristic length of the object (particle diameter)

For an axonal particle, typical values used in the literature (Cooper and Smith,1974; Copeland,1976) are $L=2*10^{-7}$ m, $V=2*10^{-6}$ m/sec, $\rho=1*10^{3}$ kg/m^3, z=1 Pa sec. These values give a Reynolds number of $R=4*10^{-10}$, which implies that the inertial forces acting on a particle are very small when compared with the viscous forces. Unless there is a force acting on a particle it will remain at rest, and when moving, will come to rest almost immediately should the motive force cease. As the viscous force on an object is directly proportional to its velocity, the instantaneous velocity of a particle is hypothesized to be directly proportional to, and a measure of, the forces acting on it. Since examination of the instantaneous velocities of a considerable number of particles has consistently shown that particle velocities vary smoothly with time, it is

hypothesized that the net motive force behaves in a similar manner. The temporal relationship may be related to some periodicity (with a period of more than 5 seconds) in the force generating mechanism which propels each particle.

The "noisy" appearance of the instantaneous velocity estimates as obtained with the incremental distance method and reported in the literature (Breuer et al.,1975;Forman et al.,1977a;Leestma et al.,1977) agrees closely with that predicted by simulation analysis in this work. As the errors in instantaneous velocity estimates obtained with this method have been shown to be considerable, extensive comparison of the instantaneous velocity results and associated parameters obtained in this work with those found in the literature is not appropriate.

Examination of the power spectra and instantaneous velocities both led to the conclusion that the instantaneous velocities of somatopetally moving particles tended to vary more widely about their mean values than did that of somatofugally moving particles. Results also indicated that the variation of a particle's instantaneous velocity was not related to its mean value.

7.6 Spatial analysis

Previous attempts to identify spatial patterns in particle motion have been crude. In their analysis of particle motion in neurites in tissue culture, Breuer's group plotted estimates of particles' instantaneous velocity

against distance along the neurite in an attempt to identify longitudinally separated zones of high or low velocity (Breuer et al.,1975). Their results revealed no such regions, and they concluded that if zones of high or low velocity do exist, they do not extend uniformly across the neurite. Leestma's group, using preparations and methods similar to Breuer, also concluded that zones of uniform velocity do not extend across the neurite (Leestma et al.,1977). They did, however, note different areas in which different particles exhibited similar "disturbances of motion" at different instants in time. This evidence led them to suggest that areas of disturbance are themselves moving along the axon.

It is the opinion of this author that these conclusions are largely unsubstantiated when the preparations and methods used are considered. The neurites in tissue culture used by both groups were so small that analysis of the details of motion must have been very difficult. Questions have also been raised as to whether behavior observed in cultured neurites can be considered typical of that in mature axons (Forman et al.,1977a). The considerable error in the instantaneous velocity estimation procedure used by both groups has been previously demonstrated. Leestma notes when discussing their preparation that scanning electron micrographs of the nerve fibres filmed indicated that rather than being single neurites they could in fact be composed of a number of neurites bound closely together. Hence particle

trajectories and "disturbances of motion" appearing on film to be in the same neurite could actually be in a number of adjacent neurites. Assuming regions of uniform velocity do exist, it seems unlikely that correspondingly located similar regions will be found in adjacent neurites.

In the preparations used in this work, all the trajectories filmed from a given preparation occurred within a single axon. In addition, the axons filmed were considerably larger than the cultured neurites used by Breuer and Leestma, and as a result more trajectories were tracked from a given segment, with a corresponding increase in the velocity estimates available for analysis.

Overlapping the trajectory plots of 42 somatopetal and 4 somatofugal particles recorded from a single segment of an axon (figure 4.2) failed to reveal the presence of tracks along which the particles moved.

The spatial relationship between microtubules and rod shaped mitochondria has been previously noted and discussed in the literature, as has the hypothesis that microtubules act as "tracks" along which particles move (Schmitt,1969; Smith,1973; Hammond and Smith,1976; Smith and McLeod,1979; Smith and McLeod,unpublished data). It has been also shown that a minimum level of ATP is required to maintain fast axoplasmic transport (Ochs,1974). As mitochondria are a source of intracellular ATP, it has been hypothesized that this energy source is used to "power" particle motion (Schmitt,1969). To investigate the possible positional

relationship between high particle velocity and mitochondria a transparency of the axonal structures and particle trajectories (figure 4.2) was overlaid on the contour plot of the velocity-position data (figure 6.14). Visual inspection of the two overlaid plots showed no apparent relationship between the rod-shaped mitochondria and regions of high particle velocity.

The contour plots of particle instantaneous velocity as a function of position have indicated a relationship between instantaneous velocities of particles and their spatial locations. The spatial relationship may be related to factors such as local variations in axoplasmic viscosity.

7.7 Conclusions

This thesis has outlined the development of a new method for the estimation of the instantaneous velocity of axonal particles. The superiority of the new method over that commonly used in the literature was demonstrated by comparison of the errors inherent in the use of each. The instantaneous velocities as estimated with the new method of one hundred and seventy-two particles were grouped, quantified, and compared using a number of techniques, in an attempt to identify patterns or relationships in particle motion. Although the results were at times inconclusive, further analysis of the instantaneous velocities was beyond the scope of this work.

The results support the hypothesis that the movement of

particles in axons is both time and position dependent. Although the mean velocities of the somatopetal and somatofugal populations were not significantly different, differences in the average power spectra of the two populations, and in the frequency distributions of the populations' instantaneous velocities indicate that there may be significant differences in the motive mechanisms acting on each.

Clearly considerable work remains to be done in the study of axonal particle motion. As the work of each researcher reveals additional details of the underlying mechanisms the overall process may be better understood. It is the hope of the author that the methods developed in this thesis will aid in this endeavor.

BIBLIOGRAPHY

ANTONIOU, A. (1979). Digital Filters: Analysis and Design. McGraw-Hill:New York.

BARONDES, S. H. and SAMPSON, F. E. (1967). Axoplasmic transport. Neurosci. Res. Prog. Bull. 5 :307-419.

BERGLAND, G. D. (1969). A guided tour of the Fast Fourier Transform. IEEE Spectrum 6 :41-52.

BERLINROOD, M. , MCGEE-RUSSELL, S. M. and ALLEN, R. D. (1972). Patterns of particle movement in nerve fibres in vitro - an analysis by photokymography and microscopy. J. Cell Science 11 :875-886.

BLOOMFIELD, PETER (1976). Fourier Analysis of Time Series: An Introduction. New York:Wiley.

BREUER, ANTHONY C. , CHRISTIAN, CLIFFORD N. , HENKART, MARYANNA , and NELSON, PHILLIP G. (1975). Computer analysis of organelle translocation in primary neuronal cultures and continuous cell lines. J. Cell Biol. 65 :562-576.

BRILLINGER, DAVID R. (1975). Time Series: Data Analysis and Theory. New York:Holt, Rinehart and Winston.

BURDWOOD, W. O. (1965). Rapid bidirectional particle movements in neurons. J. Cell Biol. 27 :215A.

CHILDERS, DONALD and DURLING, ALLEN (1975). Digital Filtering and Signal Processing. St. Paul:West.

COOLEY, J.W. and TUKEY, J.W. (1965). An algorithm for the machine calculation of complex Fourier series. Math. of Comput. 19 :297-301.

COOPER, P. D. and SMITH, R. S. (1974). The movement of optically detectable organelles in myelinated axons of Xenopus laevis. J. Physiol. 242 :77-97.

COPELAND, ARTHUR R. (1976). Axonal transport-I. Diffusion. Bul. Math. Biol. 38 :425-432.

COPELAND, ARTHUR R. (1976). Axonal transport-II. Convection. Bul. Math. Biol. 38 :435-444.

DAHLSTROM, A. (1967). The intraneuronal distribution of noradrenaline and the transport and life-span of amine storage granules in the sympathetic adenergic neuron. Naunyn-Schmiedebergs Arch. Exp. Path. Pharmak. 257

:93-115.

DANIELSON, G.C. and LANCZOS, C. (1942). Some improvements in practical Fourier analysis and their application to X-ray scattering from liquids. J. Franklin Inst. 233 :365-380,435-452.

FISHER, R. A. (1929). Tests of significance in harmonic analysis. Proc. R Soc., Ser. A 125 :54-59.

FORMAN, D.S., PADJEN, A.L., and SIGGINS, G.R. (1975). Intra-axonal organelle movements as studied by cinemicrography and computer analysis. Exp. Brain Res. 23, Suppl. 138A.

FORMAN, DAVID S. , PADJEN, ANTE L. and SIGGINS, GEORGE R. (1977a). Axonal transport of organelles visualized by light microscopy: cinemicrographic and computer analysis. Brain Res. 136 :197-213.

FORMAN, DAVID S. , PADJEN, ANTE L. and SIGGINS, GEORGE R. (1977b). Effect of temperature on the rapid retrograde transport of microscopically visible intra-axonal organelles. Brain Res. 136 :215-226.

GOLD, BERNARD and RADER, CHARLES M. (1969). Digital Processing of Signals. New York:McGraw-Hill.

HAMMOND, G. R. (1977a). The movement of optically detectable particles in intact myelinated axons. J. Physiol. 269 :74-76.

HAMMOND, G. R. and SMITH, R. S. (1977b). Inhibition of the rapid movement of optically detectable axonal particles by colchicine and vinblastine. Brain Res. 128 :227-242.

HAMMING, R. W. (1977). Digital Filters. Englewood Cliffs:Prentice-Hall.

HELMS, H. D. (1967). Fast Fourier transform method for computing difference equations and simulating filters. IEEE Trans. Audio and Electracoust. AU- 15 :85-90.

HELMS, H. D. (1968). Nonrecursive digital filters: design methods for achieving specifications on frequency response. IEEE Trans. Audio and Electracoust. AU- 16 :336-342.

HESPLOP, J. P. (1975). Axonal flow and fast transport in nerves. Adv. Comp. Physiol. Biochem. 6 :75-163.

HUGHES, A. (1953). The growth of embryonic neurites. A study on cultures of chick neural tissue. J. Anat. 87

:150-162.

JEFFREY, P.L. and AUSTIN, L. (1973). Axoplasmic transport. Progress in Neurobiol. 1 :205.

JENKINS, G.M. and WATTS, D.G. (1968). Spectral Analycis and Its Applications Holden-Day:San Fransisco.

KAISER, J.F. (1974). Nonrecursive digital filter design using the I -sinh window function. I974 Proc. IEEE Symp. On Circuits and Systems.

KATZ, BERNARD (1966). Nerve, Muscle, and Synapse. McGraw-Hill:New York.

KIRKPATRICK, JOEL B. , BRAY, JOHN J. and PALMER, SUE M. (1972). Visualization of axoplasmic flow in vitro by Nomarski microscopy. Comparison to rapid flow of radioactive proteins. Brain Res. 43 :1-10.

KIRKPATRICK, JOEL B. and STERN, LAWRENCE Z. (1973). Axoplasmic flow in human sural nerve. Arch. Neurol. 28 :308-312.

KOOPSMAN, L. H. (1974). The Spectral Analysis of Time Series. New York:Academic.

KUO, F. F. and KAISER, J. F. (1966). System Analysis by Digital Computer. New York:Wiley.

LASEK, R. J. (1968). Axoplasmic transport in cat dorsal root ganglion cells: as studied with ^{3}H-L-leucine. Brain Res. 7 :360-377.

LASEK, R. J. (1970). Protein transport in neurons. Int. Rev. Neurobiol. 13 :289-324.

LEESTMA, JAN E. (1976). Velocity measurements of particulate neuroplasmic flow in organized mammalian CNS tissue cultures. J. Neurobiol. 7 :173-183.

LEESTMA, JAN E. and FREEMAN, STEPHENNIE S. (1977). Computer-assisted analysis of particulate axoplasmic flow in organized CNS tissue cultures. J. Neurobiol. 8 :453-467.

LUBINSKA, L. (1964). Axoplasmic streaming in regenerating and in normal nerve fibres. Prog. Brain Res. 13 :1-66.

MATSUMOTO, T. (1920). The granules, vacuoles, and mitochondria in the sympathetic nerve fibres cultivated in vitro. John Hopkins Hosp. Bull. 31 :91-93.

MUNRO, D. M. (1971). Implementing the Fast Fourier Transform. Report No. 3,1971. Engineering in Medicine Laboratory, Imperial College of Science and Technology, London, S.W. England.

NATIONAL PHYSICAL LABORATORY (1961). Modern Computing Methods. Bristol, England:Wright .

NEVILLE, A. M. and KENNEDY, J. B. (1970). Basic Statistical Methods for Engineers and Scientists. Scranton:International.

OCHS, S. and JOHNSON, J. (1969). Fast and slow phases of axoplasmic flow in ventral root nerve fibres. J. Neurochem. 16 :845-853.

OCHS, S. (1971). Local supply of energy to the fast axoplasmic transport mechanism. Proc. Natn. Acad. Sci. U.S.A. 68 :1279-1282.

OCHS, SIDNEY (1974). Systems of material transport in nerve fibres (axoplasmic transport) related to nerve function and trophic control. An. N.Y. Acad. Sci. 228 :202-223.

OCHS, SIDNEY (1975). Axonal transport- a basis for neuronal pathology. ch.12 in Peripheral Neuropathy Vol. I ed. by DYCK, THOMAS, and LAMBERT Philadelphia:Saunders.

OPPENHEIM, ALAN V. and SCHAFER, RONALD W. (1975). Digital Signal Processing. Englewood Cliffs:Prentice-Hall.

OTNES, R. K. (1968). An elementary design procedure for digital filters. IEEE Trans. Audio and Electracoust. AU- 16 :330-335.

POMERAT, C. M., HENDLEMAN, W. J., RAIBORN, C. W. and MASSEY, J. F. (1967). Dynamic activities of nervous tissue in vitro. In The Neuron (ed. H. Hyden), pp 119-178. New York:Elsevier.

RABINER, LAWRENCE R. , GOLD, BERNARD and MCGONEGAL, C. A. (1970). An approach to the approximation problem for nonrecursive digital filters. IEEE Trans. Audio Electracoust. AU- 18 :83-106.

RABINER, LAWRENCE R. (1971). Techniques for designing finite-duration impulse-response digital filters. IEEE Trans. Commun. Technol. COM- 19 :188-195.

RAYNER, J. N. (1971). An Introduction to Spectral Analysis. London:Pion.

SAMPSON, ROBERT J. (1975). SURFACE II Graphics System. Kansas Geological Survey:Lawrence.

SCHMITT, F. O. (1969). Fibrous proteins and neuronal dynamics. In Cellular Dynamics of the Neuron (ed. S. H. Barondes), pp 95-111. New York: Academic Press.

SCHWARTZ, JAMES H. (1979). Axonal transport: components, mechanisms, and specificity. Ann. Rev. Neurosci. 2 :467-504.

SCHWARTZ, MISCHA and SHAW, LEONARD (1975). Signal Processing: Discrete Spectral Analysis, Estimation, and Detection. New York:McGraw-Hill.

SHANNON, CLAUDE E. and WEAVER, WARREN (1969). The Mathematical Theory of Communication. The University of Illinois Press.

SHIMSHONI, M. (1971). On Fisher's test of significance in harmonic analysis. Geophys. J. R. Astron. Soc. 23 :373-377.

SLEPIAN, D. , POLLAK, H. O. , and LANDAU, H. J.. (1961). Prolate spheroidal wave functions, Fourier analysis and uncertainty. I & II, Bell Systems Tech. J. 40 :43-83.

SMITH, R.S. (1971). Centripetal movement of particles in myelinated axons. Cytobios. 3 :259-262.

SMITH, R. S. (1972). Detection of organelles in myelinated nerve fibres by dark-field microscopy. Can. J. Physiol Pharmacol. 50 :467-469.

SMITH, R. S. (1973). Microtubules and neurofilament densities in amphibian spinal root nerve fibres: relationship to axoplasmic transport. Can. J. Physiol. Pharmacol. 51 :798-806.

SMITH, R. S. and KOLES, Z. J. (1976). Mean velocity of optically detectable intra-axonal particles measured by a cross-correlation method. Can. J. Physiol. Pharmacol. 54 :859-869.

SMITH, R. S. and MCLEOD, K. D. (1979a). Unusual particle trajectories and structural arrangements in myelinated nerve fibers. Can. J. Physiol. Pharmacol. 57 :1182-1186.

SMITH, R.S., KOLES, Z.J. and MCLEOD, K.D. (1979b). Analysis of particle motion in axons. Can. Physiol. 10 :192.

STOCKHAM, THOMAS G. (1966). High speed convolution and

correlation. Spring Joint Computer Conf. AFIPS Conf. Proc. 28 :229-233.

WEISS, P. and HISCOE, H. B. (1948). Experiments on the mechanism of nerve growth. J. Exp. Zool. 107 :315-395.

WELCH, PETER D. (1967). The use of Fast Fourier Transform for the estimation of power spectra: A method based on time averaging over short, modified periodograms. IEEE Trans. Audio Electroacoust. AU- 15 :70-73.